CIRCULATION AND ASSOCIATED VARIABILITY IN THE INTRA-AMERICAS SEA: THE ROLE OF LOOP CURRENT INTRUSION AND CARIBBEAN EDDIES

by

Yuehua Lin

SUBMITTED IN PARTIAL FULFILMENT OF THE REQUIREMENTS
FOR THE DEGREE OF DOCTOR OF PHILOSOPHY

at

DALHOUSIE UNIVERSITY
HALIFAX, NOVA SCOTIA
AUGUST 2010

DALHOUSIE UNIVERSITY

DEPARTMENT of OCEANOGRAPHY

The undersigned hereby certify that they have read and recommend to the Faculty of Graduate Studies for acceptance a thesis entitled "CIRCULATION AND ASSOCIATED VARIABILITY IN THE INTRA-AMERICAS SEA: THE ROLE OF LOOP CURRENT INTRUSION AND CARIBBEAN EDDIES" by Yuehua Lin in partial fulfillment of the requirements for the degree of Doctor of Philosophy.

Dated: August 3, 2010

External Examiner: _____

Research Co-Supervisor: _____

_____

Examining Committee: _____

_____

Department Representative: _____

DALHOUSIE UNIVERSITY

DATE: August 3, 2010

AUTHOR: Yuehua Lin

TITLE: CIRCULATION AND ASSOCIATED VARIABILITY IN THE INTRA-AMERICAS SEA: THE ROLE OF LOOP CURRENT INTRUSION AND CARIBBEAN EDDIES

DEPARTMENT: Department of Oceanography

DEGREE: Ph.D. CONVOCATION: October YEAR: 2010

Table of Contents

List of Tables

List of Figures

Abstract

Circulation and associated variability in the Intra-Americas Sea (IAS) are examined using observations and numerical models. Vertically integrated transport variations through the Yucatan Channel in the model are found to be related to the intrusion of the Loop Current into the Gulf of Mexico. We argue that the transport variations are part of a "compensation effect" by which transport variations through the Yucatan Channel are at least partly compensated by flow around Cuba. Numerical experiments show that the transport variations result from the interaction between the density anomalies associated with the Loop Current intrusion and the variable bottom topography. The compensation effect is found to be associated with baroclinic (2-layer) flow through the Yucatan Channel at timescales longer than a month, while at shorter timescales (less than a month) the vertical structure of the flow is barotropic.

An index, that can be computed from satellite data, is proposed for measuring the impact of the Loop Current intrusion on the transport variability through the Yucatan Channel. This index is shown to be significantly correlated at low frequencies (cutoff 120 days) with the cable estimates of transport between Florida and the Bahamas. We argue that it is the geometric connectivity between the Yucatan Channel and the Straits of Florida between Florida and the Bahamas that accounts for the relationship.

A three-dimensional, data-assimilative, ocean circulation model is developed in order to simulate circulation, hydrography and associated variability in the IAS from 1999 to 2002. The model performance is assessed by comparing model results with various observations made in the IAS during this period. Model results are used to study the role played by Caribbean eddies in the dynamics of monthly to seasonal (with timescales of 30-120 days) circulation variability in the IAS. It is shown that the variations in vertically integrated transport between Nicaragua and Jamaica are linked to the interaction of Caribbean eddies with the Nicaraguan Rise. The mechanism can be explained in terms of the form drag effect acting across the Nicaraguan Rise.

List of Abbreviations Used

CEOF	Complex Empirical Orthogonal Function
EOF	Empirical Orthogonal Function
FC	Florida Current
GOM	Gulf of Mexico
IAS	Intra-Americas Sea
LC	Loop Current
NWP	Northwest Providence
OB	Old Bahama
YC	Yucatan Current

Acknowledgements

First and foremost, I would like to thank my supervisors Jinyu Sheng and Richard Greatbatch for their guidance, encouragement, patience and generousity. Thanks to my thesis committee members Youyu Lu and Kumiko Azetsu-Scott, as well as to my thesis external examiner Lars Petter Røed and proposal external examiner Helmuth Thomas for their helpful comments. I appreciate Carsten Eden for providing the transport and sea surface height calculated from the FLAME model, Julio Sheinbaum for providing the observations taken during the CANEK program, and Greg Smith for providing the reanalysis data produced by the British Atmospheric Data Centre. Thanks are due to faculty members Alex Hay, Keith Thompson, and Dan Kelly for teaching. I am grateful to Bo Yang, Li Zhai, Xiaoming Zhai, Liang Wang, Liqun Tang, Daisuke Hasegawa, Jorge Urrego Blanco, Fred Woslyng, Faez Bakalian, Eric Oliver, and others for their useful discussions and suggestions. I thank Jackie Hurst, Tamara Cantrill, and Pamela Larivee for all kinds of help. Thank Daniel Morrison for responding to my email requests during weekends and solving computer problems. Finally I would thank my wife for her support and motivation along the way.

Chapter 1

Introduction

The Intra-Americas Sea (IAS, Figure 1.1) is a geographic region comprising the Caribbean Sea, the Gulf of Mexico (GOM), the Straits of Florida, and the adjacent western North Atlantic. A better understanding of the physical processes of the waters that flow in and through the IAS, especially its circulation variability, is important for a number of reasons.

First, the IAS plays an important role as a conduit for mass, heat, salt and other tracers in the Atlantic circulation system. In particular, the circulation system in the IAS comprising the Yucatan and Florida currents is the major feeder for the Gulf Stream. Not only is the Florida Current thought to be part of the wind-driven circulation of the subtropical gyre (Schmitz et al., 1992), but it is also thought to be part of the upper limb of the North Atlantic Meridional Overturning Circulation (AMOC: Schmitz and Richardson, 1991) important for climate change.

Second, the IAS contains the second largest body of very warm ($\geq 28.5°$) water on Earth: the western hemisphere warm pool (Wang and Enfield, 2001), which is a significant heat source for the atmosphere. On average, four tropical storms reach hurricane intensity in the IAS each year between June and November (Mooers and Maul, 1998). Understanding the air-sea interaction process for generating and maintaining tropical cyclones and their propagation is crucial for the coastal communities in the IAS region which are heavily populated and depend on tourism as the backbone of their economies.

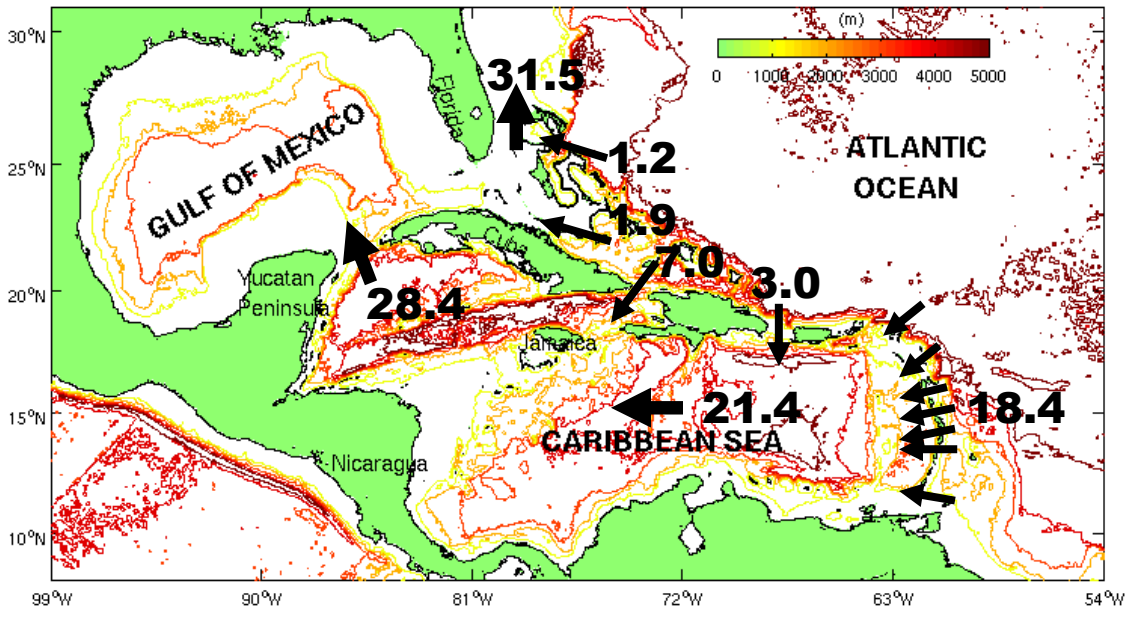

Figure 1.1. Topographic map (with depth contours in meters) of the Intra-Americas Sea based on 2-min gridded world elevations (contour interval is 1000 m). Mean transports through major passages based on Johns et al. (2002) are presented by arrows and numbers (in Sv).

Third, the waters of the IAS also support rich commercial fisheries and a major oil and gas industry. Physical processes in the IAS affect the ecosystems in the region (e.g., Tang et al., 2006). The ocean currents in the IAS, especially in coastal zones, are important for spawning, larva transport, growth, and feeding behavior for many fishes and invertebrates. For instance the strength of upwelling along the southern coast of the Caribbean Sea in response to wind forcing (Tang et al., 2006) influences the variability of biomass (e.g., plankton population) and organic material recycling, which is expected to be important for primary production.

1.1 Circulation Features in the IAS

The circulation in the IAS (Figure 1.1) is dominated by the throughflow (Mooers and Maul, 1998) associated with the North Atlantic western boundary current system. The strong westward Caribbean Current flows through the islands of the southern Lesser Antilles. Water then flows as the Yucatan Current through the Yucatan Channel, which connects the Caribbean Sea and the GOM, and forms the Loop Current in the GOM. Water exits the IAS through the Straits of Florida as the Florida Current between Florida and the Bahamas.

The Florida Current between Florida and the Bahamas has been monitored almost continuously since the early 1980's, beginning with the Subtropical Atlantic Climate Studies (STACS) program (Schott and Zantopp, 1985) and subsequently using submarine cables (Larsen, 1992; Baringer and Larsen, 2001). More recently, monitoring of the Florida Current between Florida and the Bahamas has become an essential part of the Research with Adaptive Particle Imaging Detectors/Meridional Overturning Circulation (RAPID/ MOCHA) array for monitoring the North Atlantic Meridional Overturning Circulation (Cunningham et al., 2007; Kanzow et al., 2007).

In their pioneering study of the Florida Current between Florida and the Bahamas, Niiler and Richardson (1973) showed that the Florida Current had a mean transport of about 30 Sv and a seasonal cycle with a maximum in summer and a minimum in fall (Figure 1.2). The character of the annual cycle was confirmed by STACS results observed from April 1982 to June 1984 (Schott et al., 1988). However, the Sverdrup

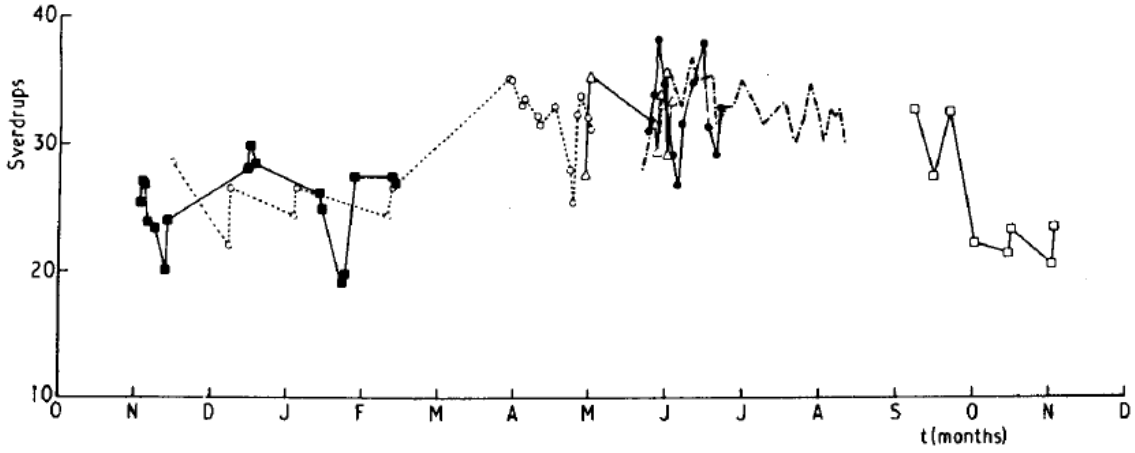

Figure 1.2. A plot of the Brooks (1979) data (the dot-dash line) and the Niiler and Richardson (1973) data (symbols correspond to data sequences) adapted from Anderson and Corry (1985), showing the observed transports through the Florida-Bahamas section.

transport, obtained by integrating the wind stress curl westwards along a line of latitude from the eastern boundary of the North Atlantic to Florida, gives a seasonal variation of transport of ±15 Sv with a maximum in winter (Anderson and Corry, 1985). The difference can be explained by the fact that on the seasonal timescale and for large horizontal scales, the barotropic response in the ocean interior at midlatitudes is described by the topographic Sverdrup relation. The observed phase of the seasonal fluctuations in transport through the Straits of Florida was successfully reproduced by a two-layer model by Anderson and Corry (1985) and a linear barotropic model by Greatbatch and Goulding (1989), although the amplitude was underestimated. These studies note the importance of wind forcing along the continental slope north of the Straits of Florida. Fanning et al. (1994) found that the amplitude produced by the model is dependent on the choice of seasonal wind stress climatology used to drive a model. Greatbatch et al. (1995) used a barotropic, uniform density model with realistic bottom topography driven by twice daily wind forcing to show that the daily transport variability between Florida and the Bahamas, as estimated using the submarine cable (Larsen, 1992; Baringer and Larsen, 2001), can be partially explained by wind forcing. Their numerical simulations were successful in capturing the seasonal cycle of transport.

As the two passageways providing the entry and exit routes for transport in and out of the GOM, flow through the Yucatan Channel and that part of the Straits of Florida between Florida and Cuba are intimately connected. Since runoff and the volume transport due to precipitation minus evaporation in the GOM make small contribution to volume change, on the order of 0.1 percent of transport of the Yucatan Current (Etter, 1983), the transport into the GOM through the Yucatan Current is expected to be balanced by the transport out through the Straits of Florida between Florida and Cuba on timescales longer than a few days.

A mean transport of ~25 Sv was observed by Hamilton et al. (2005) for the flow between Florida and Cuba during an 11-month period from December 1990 to November 1991, which agrees well with the estimates of 23.8 ± 1 Sv entering the GOM from the CANEK program (Ochoa et al., 2001; Sheinbaum et al., 2002) started in December 1996 and completed in June 2001. CANEK used a combination of shipboard Acoustic Doppler Current Profiler (ADCP) measurements, hydrographic/velocity surveys using CTD's,

Lowered-ADCP measurements and a current meter mooring array to monitor the transport through the Yucatan Channel. Compared to 32.3 ± 3.2 Sv based on long-term mean voltage-derived transports at 27˚N between Florida and the Bahamas for the Florida Current (Larsen 1992; Baringer and Larsen, 2001), it is suggested that in the mean, roughly 8 Sv passes north of Cuba and through the Bahama Island chain and joins the Florida Current upstream. On the other hand, the mean flow through the Old Bahama (OB) and Northwest Providence (NWP) channels has been thought to be relatively small (see Figure 1.1; Atkinson et al., 1995; Leaman et al., 1995). In particular, Atkinson et al. (1995) found that the transport through the OB Channel varied from -2.4 to +6.6 Sv based on current meter observations. Hamilton et al. (2005) found that the estimated transport of the flow through the OB Channel (approximately) varied from -3.1 to 11.1 Sv with a mean transport of 2.4 Sv during the 11-month period, and that the estimated transport through the NWP Channel varied from -4.5 to 3.9 Sv with a mean transport of 0.9 Sv, making ~3.3 Sv total in the mean.

The Loop Current is highly variable in position and strength with time, and can intrude northward into the northeastern GOM, forming an intense clockwise flow even as far northward as the Mississippi river delta or the Florida continental shelf (Wiseman and Dinnel, 1988; Huh et al., 1981). The Loop Current can retreat to have an almost direct path to the Straits of Florida (port-to-port configuration) after shedding a Loop Current eddy. The Loop Current eddy is an anti-cyclonic warm-core ring, which is formed and pinched off from the Loop Current, and then propagates westward at speeds of ~2-5 km day^{-1} (Coats, 1992; Elliott, 1982). The formation of cyclones in the vicinity of the Loop Current ring during the separation stage is also observed and has been analyzed (e.g., Vukovich and Maul, 1985; Cherubin et al., 2006).

The interval between Loop Current eddy shedding varies in the range of 6 to 17 months (Molinari, 1980), with primary periods of 6 and 11 months (Sturges and Leben, 2000). The mechanism supporting ring shedding has been widely studied, notably by Hurlburt and Thompson (1980), and more recently interpreted using the "momentum imbalance paradox" idea of Pichevin and Nof (1997) (see also Nof and Pichevin, 2001; Nof, 2005). These studies showed that the ring shedding can be captured by a single layer

reduced gravity (1 ½) layer model without the need to consider the interaction with the variable bottom topography.

The Loop Current's variability, including its extension, retraction, and eddy shedding, is also influenced by external dynamics. The Gulf-Caribbean connectivity is explored in Murphy et al. (1999), who show that Caribbean eddies that squeeze through the Yucatan Channel can affect the timing of Loop Current shedding. Sturges (1992) demonstrated interactions of the natural shedding frequency with the frequencies of variability of other oceanographic forcing fields, such as the Yucatan Channel inflow, the Florida Current and the North Brazil Current variability, as well as the synoptic meteorological forcing variability. Oey et al. (2003) concluded that wind-induced transport fluctuations through the Greater Antilles Passages cause shedding at shorter periods, while Caribbean eddies (anticyclones) cause shedding at longer periods. Oey (2004) argued that the potential vorticity flux anomaly at the Yucatan Channel may serve as a determining factor. Oey et al. (2005) reviewed the progress in recent numerical studies of the Loop Current, rings, and related circulation in the GOM.

Many efforts have been made in the past to connect the intrusion of the Loop Current into the GOM and the associated eddy shedding with the flow structure and transport through the Yucatan Channel (Maul et al., 1985; Candela et al., 2003; Bunge et al., 2002; Oey, 1996; Ezer et al., 2003), while the variability in the Loop Current system, including the Yucatan Current and Florida Current associated with eddy shedding remains poorly understood.

The intrusion of the Loop Current into the GOM is measured differently in different studies. For example, Vukovich (1995) used monthly averaged distance between the northern boundary of the Loop Current and the 30˚N latitude line to study the Loop Current eddy shedding frequency. Bunge et al. (2002) evaluated the variability of the Loop Current by the surface extension of the Loop Current, which was inferred from a series of radiometer images using graphic software to manually define the boundaries of the current. Ezer et al. (2003) generated a time series of variations of the Loop Current extension defined as the area averaged sea surface elevation over the region of the Loop Current (89˚W to 83˚W, 21˚N to 27˚N).

Detached Loop Current eddies may have a measurable impact on the heat budget of the GOM since a Loop Current eddy can extend to a depth of 1500 m and the volume of a Loop Current eddy has been estimated to be as much as 7% of the total volume of the Gulf of Mexico (Elliot, 1982). The heat and freshwater budgets of the GOM have been studied and reviewed by Etter (1983). The rate of heat loss to the atmosphere was found to intensify over the axis of the Loop Current (Etter, 1983). In the more recent study by Rivas et al. (2005), it was indicated that the deepest flows between the Caribbean Sea and the GOM through the Yucatan Channel, those that take place below the sill level at the Straits of Florida, have zero mean net mass transport but carry significant amounts of heat.

On the other hand, the mesoscale variability in the Caribbean Sea, known as "eddy waves", can be traced upstream to the North Brazil Current Retroflection (Johns et al., 1990). Eddies propagate along the Caribbean Current and then squeeze through the Yucatan Channel. In general, eddy activity is eroded after the Nicaraguan Rise through interaction with the bottom topography. Some eddies also enter the Cayman Sea from outside the Caribbean through the Windward Passage (Andrade and Barton, 2000). These Caribbean eddies can significantly affect the Loop Current's intrusion and shedding behavior of warm-core rings. Anticyclonic eddies cause shedding at longer periods (14-16 months) (Oey et al., 2003). Murphy et al. (1999) found there is a significant correlation between the Loop Current eddy shedding and the eddies near the Lesser Antilles with a time lag of 11 months. The potential explanation is that Loop Current eddy shedding exhibits correlation to the flux of potential vorticity through the Yucatan Channel (Candela et al., 2003). This potential vorticity flux is apparently driven by the eddies and meanders in the Caribbean Sea.

Caribbean eddies are quite regular, appearing at near 90-day intervals west of the southern Lesser Antille (Carton and Chao, 1999). Eddies can be spun up locally by the wind stress curl with a timescale about 100 days to the south of Hispaniola (Oey et al., 2003). Jouanno et al. (2008b) found the main frequency peaks for the mesoscale variability exhibit a westward shift from roughly 50 days near the Lesser Antilles to 100 days in the Cayman Basin. The shift has been associated with the growth and merging of

eddies. However, the effect of Caribbean eddies on the circulation variability in the Caribbean Sea is not fully understood.

1.2 Thesis Outline

The main objective of my thesis research is to use numerical ocean circulation models and available observations to investigate the main physical processes responsible for the transport variability and interconnection in the IAS. The influence of the Loop Current intrusion and propagation of Caribbean eddies on the circulation variability are also investigated in the thesis. Physical processes, such as eddy dynamics, wind forcing, baroclinic effects, topographic effects, and density driven currents are studied based on model results to improve our understanding of hydrodynamics of the observed flow and associated variability. In particular, my thesis research comprises (1) to use a three-dimensional ocean circulation model to simulate circulation, hydrography and associated variability in the IAS, and assess the model's behavior, and (2) to analyze observational data (such as current observations and satellite altimeter fields) and model results (e.g., regression analysis, spectrum analysis, empirical orthogonal function (EOF) analysis, and Complex EOF analysis).

The material of the thesis is laid out as follows: Chapter 2 presents a model study of the vertically integrated transport variability through the Yucatan Channel, focusing on the role of Loop Current evolution and flow compensation around Cuba. Chapter 3 examines the influence of Gulf of Mexico Loop Current intrusion on the transport of the Florida Current between the Florida and Bahamas and the associated variability of the Yucatan Current at timescales longer than 120 days. Chapter 4 presents the three-dimensional, data-assimilative, ocean circulation model used for simulating circulation, hydrography and associated variability in the IAS. Chapter 5 examines the monthly to seasonal variability in the Intra-Americas Sea, with an emphasis on the role played by Caribbean Eddies. An overall summary is given in Chapter 6.

It should be noted that Chapters 2 to 5 are based on four independent manuscripts, in which some figures and material in the introductions and model descriptions are similar. More specifically, Chapter 2 is the paper entitled "A model study of the vertically

integrated transport variability through the Yucatan Channel: Role of Loop Current evolution and flow compensation around Cuba" by Lin, Greatbatch, and Sheng (*Journal of Geophysical Research*, 2009). Chapter 3 is the paper entitled "The influence of Gulf of Mexico Loop Current intrusion on the transport of the Florida Current" by Lin, Greatbatch, and Sheng (*Ocean Dynamics*, 2010, in press). Chapter 4 is the paper entitled "A numerical study of circulation and associated variability in the Intra-Americas Sea" by Lin, Sheng, and Greatbatch (*Proceedings of the Eleventh International on Estuarine and Coastal Modelling*, 2010, in press). Chapter 5 is the manuscript entitled "A numerical study of monthly to seasonal variability of circulation in the Intra-Americas Sea: the role of Caribbean eddies" by Lin, Sheng, and Greatbatch (to be submitted shortly to *Continental Shelf Research*).

Chapter 2

A Model Study of the Vertically Integrated Transport Variability through the Yucatan Channel: the Role of Loop Current Evolution and Flow Compensation around Cuba[1]

2.1 Introduction

The current system flowing through the Yucatan Channel and Straits of Florida (see Figure 2.1) is important because it is the major feeder for the Gulf Stream. Not only is this current system thought to be part of the wind-driven circulation of the subtropical gyre (Schmitz et al., 1992) but it is also thought to be part of the upper limb of the North Atlantic meridional overturning circulation (Schmitz and Richardson, 1991) important for climate change. The Yucatan Channel has been the subject of an intensive monitoring study (CANEK program) (Ochoa et al., 2001; Sheinbaum et al., 2002) using shipboard acoustic Doppler current profiler (ADCP) measurements, hydrographic/velocity surveys using conductivity-temperature-depth and lowered ADCP measurements, and a current meter mooring array. The CANEK program was initiated in December 1996 and completed in June 2001. On the other hand, the Florida Current between Florida and the

[1] Lin, Y., R. J. Greatbatch, and J. Sheng (2009), A model study of the vertically integrated transport variability through the Yucatan Channel: Role of Loop Current evolution and flow compensation around Cuba, *J. Geophys. Res.*, 114, C08003.

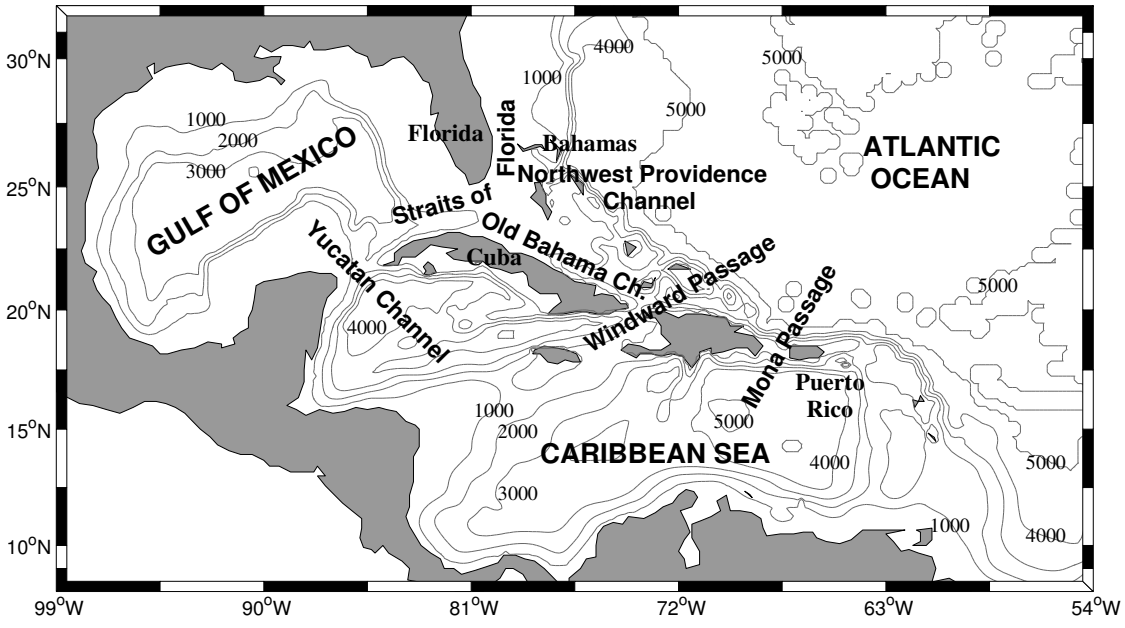

Figure 2.1. The model domain and major topographic features based on ETOPO-5 (contour interval is 1000 m).

Bahamas has been monitored almost continuously since the early 1980's, beginning with the Subtropical Atlantic Climate Studies (STACS) program (Schott and Zantopp, 1985) and subsequently using submarine cables (Larsen, 1992; Baringer and Larsen, 2001). More recently, monitoring of the Florida Current between Florida and the Bahamas has become an essential part of the Research with Adaptive Particle Imaging Detectors/Meridional Overturning Circulation (RAPID/ MOCHA) array for monitoring the North Atlantic Meridional Overturning Circulation (Cunningham et al., 2007; Kanzow et al., 2007).

A distinctive feature of the Gulf of Mexico is the intrusion of the Loop Current, connecting the Yucatan Channel with the Straits of Florida, and the associated ring shedding (see, e.g., Hurlburt and Thompson, 1980; Oey et al., 2005). The Loop Current can extend northward into the Gulf of Mexico, even as far as the Mississippi River delta and the Florida continental shelf (Huh et al., 1981; Wiseman and Dinnel, 1988). On the other hand, after shedding a ring, the Loop Current typically has a much more direct path from the Yucatan Channel to the Straits of Florida (port-to-port configuration). The mechanism supporting ring shedding has been widely studied, notably by Hurlburt and Thompson (1980), and more recently studied using the "momentum imbalance paradox" of Pichevin and Nof (1997) (see also Nof and Pichevin, 2001; Nof, 2005). These studies showed that the ring shedding can be captured by a single layer reduced gravity (1 ½) layer model without the need to consider the interaction with the variable bottom topography.

In this chapter we are not concerned with the mechanism of ring shedding but rather with the fluctuations in the vertically integrated transport that accompany Loop Current intrusion and ring shedding. Some previous studies have concentrated on the connection between deep flow variations in the Yucatan Channel and ring shedding (e.g., Maul et al., 1985; Bunge et al., 2002; Ezer et al., 2003; Oey et al., 2005). Others like Maul and Vukovich (1993) used monthly mean data to examine the relationship between variations in the Loop Current and the sea level difference between Cuba and Florida, but found no clear relationship. As noted in Chapter 1, there has also been much emphasis on the possible impact that changes in the flow conditions through the Yucatan Channel (e.g., flow velocity and the vorticity distribution) might play in preconditioning Loop Current

intrusion and ring shedding (e.g., Sheinbaum et al., 2002; Ezer et al., 2003; Oey et al., 2005; Oey, 2004). Here the focus is the variation in the vertically integrated transport through the Yucatan Channel that accompanies Loop Current intrusion and ring shedding. We view these transport variations as being a consequence of Loop Current intrusion, rather than the cause of the Loop Current intrusion itself (any possible feedback from the transport variations on the Loop Current intrusion is beyond the scope of this chapter). Such fluctuations are clearly evident in the high-resolution model analyzed by Cherubin et al. (2005) and are also present in the 1/12° eddy-permitting Family of Linked Atlantic Model Experiments (FLAME) model of the Atlantic Ocean between 20°S and 70°N driven by climatological, seasonally varying forcing (see Eden et al. (2007) for a description of this model). Figure 2.2a shows time series of the vertically integrated transport through the Yucatan Channel and also between Florida and the Bahamas in the FLAME model (3-day average), and Figure 2.2b shows the result of correlating the model sea surface height against the Yucatan Channel time series. The relationship between Loop Current intrusion and Yucatan Channel transport variability in the model is evident from the large negative correlation extending northward from the Yucatan Peninsula and the related region of positive correlation immediately to the west (correlations greater than 0.12 are significantly different from zero at the 99% level). It is also clear from the region of positive correlation around Cuba that fluctuations in transport through the Yucatan Channel in the model are at least partly compensated by flow around Cuba, another issue we investigate in this Chapter.

The arrangement of the Chapter is as follows. In Section 2.2 we describe the ocean model used in our study. In Section 2.3 we describe results from a specific experiment in which the relationship between Loop Current intrusion and transport variations through the Yucatan Channel is isolated. In Section 2.4 we discuss a more complete model run, including synoptic wind forcing. In Section 2.5 we elucidate the mechanism connecting Loop Current intrusion and the transport variability using two diagnostic model runs. In Section 2.6 we discuss the evidence for the compensation effect from the available observations, and in section 2.7 we provide a summary and discussion.

2.2 Model Setup and External Forcing

The three-dimensional numerical model used in this study is the primitive-equation ocean circulation model known as CANDIE (the Canadian version of DieCAST, Sheng et al., 1998). CANDIE has been successfully applied to address various modeling problems including the seasonal circulation in the northwestern Atlantic Ocean (Sheng et al., 2001) and the general circulation over the western Caribbean Sea (Sheng and Tang, 2003 and 2004; Tang et al., 2006).

The model domain covers the Intra-Americas Sea (IAS: 99˚W to 54˚W, 8˚N to 32˚N, Figure 2.1) with a horizontal resolution in both latitude and longitude of 1/6˚. The topographic dataset used in the model is ETOPO-5 (5-min gridded world elevations) from the National Geophysical Data Center. The temperature and salinity climatology is taken from the World Ocean Atlas Data 2001 of the National Oceanographic Data Center in the United States, and interpolated to the model grid.

The model uses fourth-order numerics (Dietrich, 1998) and Thuburn's (1996) flux limiter for the nonlinear advection terms. The subgrid scale mixing scheme of Smagorinsky (1963) is used for the horizontal eddy viscosity and diffusivity coefficients with the minimum value set to 15 m^2 s^{-1}, except where otherwise stated. The parameterization of Large et al. (1994) is used for the vertical eddy viscosity and diffusivity coefficients.

The following boundary conditions are used. At lateral solid (or closed) boundaries, the normal flow, tangential stress, and normal fluxes of potential temperature and salinity are set to zero (free-slip and insulating boundary conditions). Along the model open boundaries, the normal flow, temperature and salinity fields are adjusted using a method similar to the adaptive open boundary conditions suggested by Marchesiello et al. (2001). It first uses an explicit Orlanski radiation condition (Orlanski 1976) to determine whether the open boundary is passive (outward propagation) or active (inward propagation). If the open boundary is passive, the model prognostic variables are radiated outward to allow any perturbation generated inside the model domain to propagate outward as freely as possible. If the open boundary is active, the model prognostic variables at the open boundary are restored to the monthly mean climatologies at each z level with a timescale

of 20 days. Furthermore, the depth-mean normal flows across the open boundaries are interpolated from the seasonally varying mean transports from the 1/12˚ version of the FLAME Atlantic Ocean model used to produce Figure 2.2.

The results from four numerical experiments are described:

1. The control run (Exp-CR) model is forced by 6-hourly National Centers for Environmental Prediction (NCEP) wind fields from 1996 to 2001 (converted to wind stress using the formula of Large and Pond, 1981) and monthly mean surface heat flux (da Silva et al., 1994) using the method of Barnier et al. (1995). The model sea surface salinity is restored to the monthly mean climatology with a restoring timescale of 20 days. The model is initialized using January climatology for potential temperature and salinity.
2. The experiment Mean model is forced by annual mean (steady) wind stress and surface heat flux, and annual mean volume transports through the open boundaries are taken, as before, from the FLAME Atlantic Ocean model. The model sea surface salinity is restored to the annual mean climatology with a restoring timescale of 20 days. In this experiment, the background horizontal eddy viscosity and diffusivity coefficients are increased to 1.5×10^3 m^2 s^{-1} everywhere except for the region of the Gulf of Mexico and the adjacent area around Cuba in order to eliminate eddy activity outside the Gulf of Mexico. The model run in experiment Mean is purely prognostic.
3. In two diagnostic model runs, the time-independent potential temperature and salinity fields are specified in the model (the details are described in section 2.5). In these experiments there is no external forcing applied at the sea surface, and transports through open boundaries are set to zero. The model is integrated for 120 days to achieve a quasi-steady state.

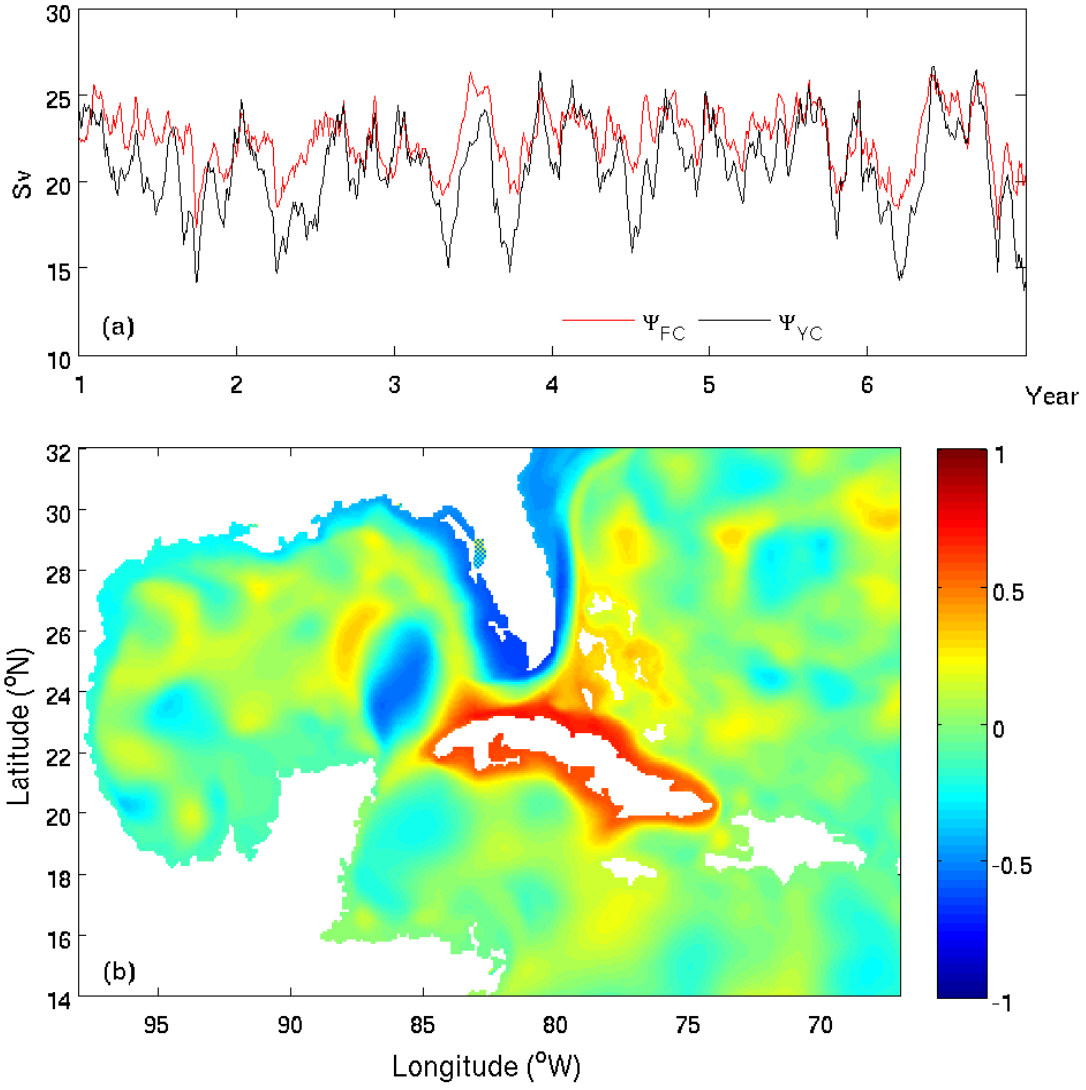

Figure 2.2. (a) Time series of the transport between Florida and the Bahamas (Ψ_{FC}) and through the Yucatan Channel (Ψ_{YC}) in the FLAME model (3-day average), both positive northward. (b) Distribution of the correlation coefficient between the sea surface height anomalies and transport anomalies through the Yucatan Channel calculated from FLAME model results.

2.3 Experiment Mean: A Link Between Transport Variability Through the Yucatan Channel and Loop Current Intrusion Into the Gulf of Mexico

We begin with experiment Mean. This experiment was integrated for 6 years and the model results (3-day average) from day 360 to 2160 (i.e. from year 2 to 6) are used for analysis. Since the forcing in this experiment is time-independent, and eddy activity outside the Gulf of Mexico is eliminated by using a large horizontal eddy viscosity coefficient there, significant temporal variations in the model are due entirely to the internal variability associated with the Loop Current intrusion and ring shedding. Figure 2.3a shows time series of the transport between Florida and the Bahamas (Ψ_{FC}) and through the Yucatan Channel (Ψ_{YC}) (both positive northward). The time mean transports are 31.0 Sv and 27.3 Sv respectively and are similar to the estimates given by Johns et al. (2002) based on their transport budget for the region (there is a slight linear trend in the transport time series due to model drift). As can be seen from Figure 2.3a, Ψ_{YC} exhibits quasi-periodic oscillations of period around 5.5 months with the peak-to-peak transport difference reaching up to ~5 Sv. These quasi-periodic oscillations in transport are associated with quasi-regular Loop Current ring shedding events in the model with a period of around 5.5 months. It is notable that although the influence of ring shedding can be seen in the transport of the Florida Current between Florida and the Bahamas, Ψ_{FC}, the transport variability is much weaker than that through the Yucatan Channel. It should be noted that transport between Florida and the Bahamas is free to vary in the model despite the fact that transport through the northern boundary of the model domain is fixed in this experiment (flow can pass north of the Bahamas, as happens in the FLAME model and as is implied by the region of positive correlation centered over the Bahamas in Figure 2.2b). It should also be noted that the difference in transport between the two time series plotted in Figure 2.3a compares well with the corresponding difference in transports found in the FLAME model and shown in Figure 2.2a.

It is obvious from the geometry of the region (Figure 2.1) that if the transport through the Yucatan Channel and the transport of the Florida Current between Florida and the

Bahamas do not vary together with the same amplitude, then there must be a significant compensating transport to the north of Cuba; in particular through the Old Bahama and Northwest Providence channels. The transport time series through these channels are shown in Figures 2.3b and 2.3c (transport is measured positive northwestward). It is clear that the main player in this experiment is the Old Bahama Channel, with relatively little transport variation taking place through the Northwest Providence Channel. Furthermore, from the comparison (Figure 2.3d) of the model-calculated transport anomalies (i.e. differences from the time mean) for Ψ'_{YC}, $-\Psi'_{OB}$, and $-\Psi'_{WW}$ (Ψ_{WW} represents the transport through the Windward Passage, positive northeastward), the temporal variability in Ψ_{YC} in the model is closely matched by southwestward transport anomalies through the Windward Passage, as well as southeastward transport anomalies through the Old Bahama Channel.

It follows that, at least in this experiment, transport variations in the Yucatan Channel are associated with anomalous transport around Cuba, connecting the Yucatan Channel with the Old Bahama Channel and the Windward Passage. The above transport variations are an example of the "compensation effect" being introduced in this chapter, whereby fluctuations in transport through the Yucatan Channel can be compensated, at least partly, by flow north of Cuba.

The period of occurrence of the Loop Current ring shedding events in experiment Mean is about 5.5 month, which corresponds to the smaller of the two primary peaks in the distribution of observed periods noted by Sturges and Leben (2000). Since the model external forcing is time-invariant in this experiment, the shedding period of ~5.5 months can be considered as the natural period of the ring shedding in the model. In the real ocean, the shedding frequency is influenced by many (external) factors such as the variability of forcing fields (Sturges, 1992) and eddies that propagate westward across the Caribbean Sea towards the Yucatan Channel (e.g., Oey et al., 2003).

Figure 2.4 shows the relationship between Loop Current intrusion/ring shedding and the Yucatan Channel transport, Ψ_{YC}, in the model. As can be seen, the Yucatan Channel transport decreases as the Loop Current intrudes into the Gulf of Mexico (Figure 2.4a), reaching a minimum (Figure 2.4b) when the Loop Current intrudes strongly into the gulf (Figure 2.4b) just as a ring starts to be shed. During the ring shedding, the transport starts

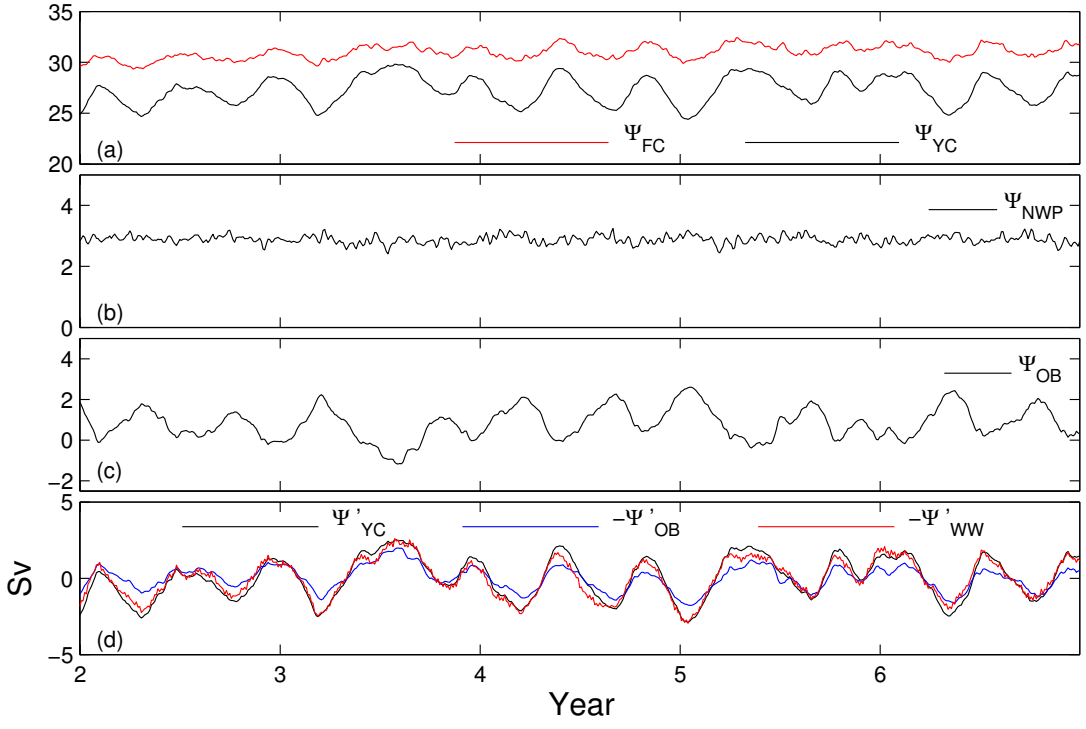

Figure 2.3. Time series of the model-calculated transports (3-day average) in experiment Mean from years 2 to 6 (a) between Florida and the Bahamas (Ψ_{FC}), and through the Yucatan Channel (Ψ_{YC}), (b) the transport through the Northwest Providence (Ψ_{NWP}) Channel, and (c) the transport through the Old Bahama Channel (Ψ_{OB}). (d) Comparison between model-calculated transport anomalies (time mean removed) Ψ'_{YC}, $-\Psi'_{OB}$, and $-\Psi'_{WW}$ (Ψ_{WW} is the transport through the Windward Passage).

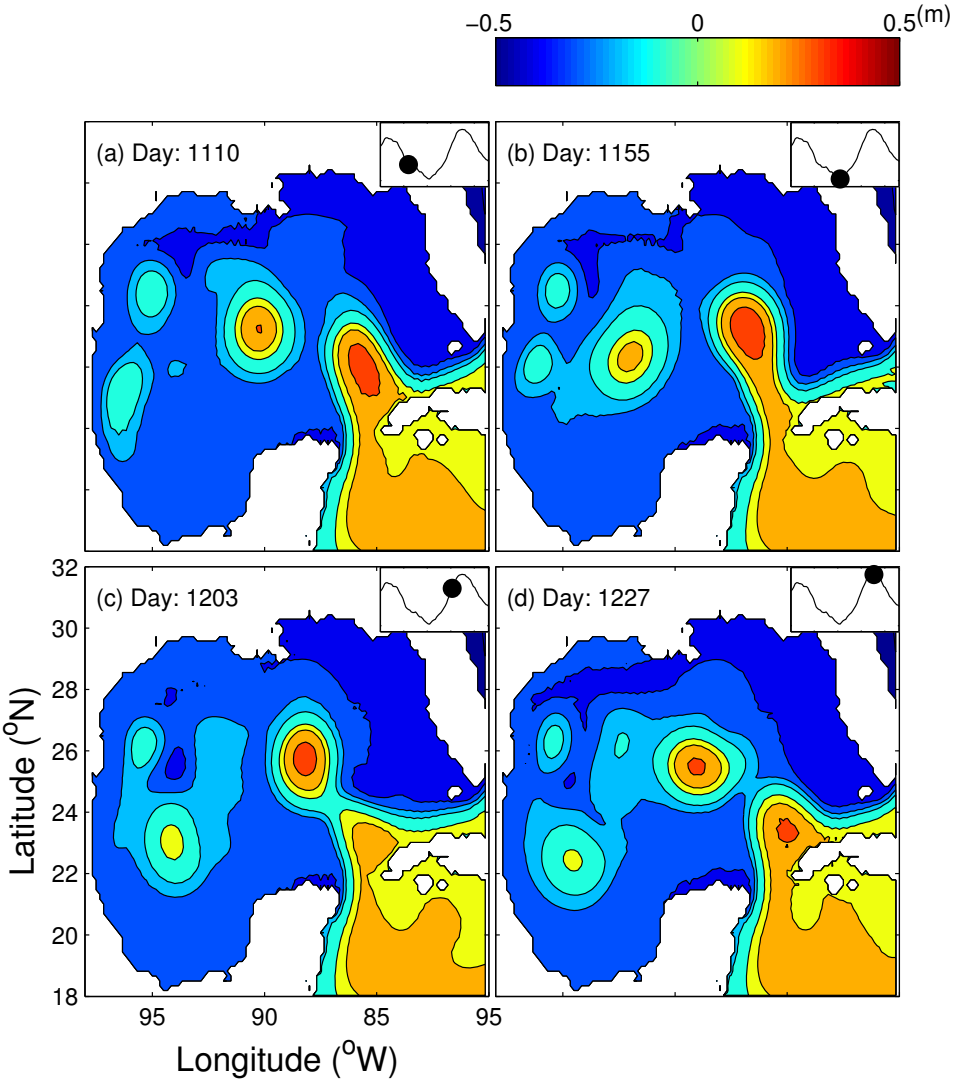

Figure 2.4. Snapshots of sea surface height fields (3-day average) produced by the model in experiment Mean and the corresponding transport variation through the Yucatan Channel (on the top right corner of Figures 2.4a-2.4d). Model time is marked by a solid dot on the time series of the transport through the Yucatan Channel.

to rise (Figure 2.4c) to reach a maximum soon after the ring is formed at which time a pool of anomalously warm water (anomalously high sea surface height) is found off the northwest coast of Cuba (Figure 2.4d). The transport variability documented here is consistent with the transport variability shown by Cherubin et al. (2005, figure 3d) as well as with that in the FLAME model. The different phases of Loop Current intrusion and ring shedding are associated with density anomalies (departures from the time mean) in the model and in section 2.5 we show that it is the interaction between these density anomalies and the underlying variable bottom topography that is responsible for the corresponding transport variations.

Experiment Mean has been repeated using a smaller domain for which the eastern boundary cuts through Cuba. In this experiment, transport through the Yucatan Channel is fixed in time by the time-invariant transport specified on the eastern boundary south of Cuba. Loop Current intrusion and ring shedding still occur, as one expects from the model study of Hurlburt and Thompson (1980) and the theoretical study of Pichevin and Nof (1997). However, the character of the Loop Current evolution is subtly different from that in Figure 2.4. In particular, the pool of warm water at the northwest corner of Cuba is a time-invariant feature, whereas in Figure 2.4, this feature varies as the transport varies. For example, in Figure 2.4, the Loop Current is strongly pinched to the north coast of Cuba when the transport is a minimum and the warm pool is absent (Figure 2.4b) but bulges away the coast when the transport is a maximum and the warm pool also reaches its maximum intensity (Figure 2.4d). As we show in section 2.5, the time variation of the warm pool is important for explaining the transport variations.

In an additional experiment, the Windward and Mona passages were closed, with everything else remaining as in experiment Mean. Loop Current intrusion and ring shedding was found, as before, as well as the associated transport changes through the Yucatan Channel, with very little difference in behavior from experiment Mean. Since, however, the Windward and Mona passages are closed in this experiment, the transport variations connect south of the island of Puerto Rico rather than around Cuba, as in experiment Mean. The experiment shows that the Windward and Mona passages do not play a fundamental role in the dynamics of the transport changes, consistent with the analysis to be presented in section 2.5.

2.4 Control Run (Exp-CR)

For a more general model set-up, we now turn to the control run (Exp-CR). This experiment was integrated for 6 years and the model results (3-day average) from days 360 to 2160 (i.e., from years 2 to 6) are used for analysis. We first describe the model validation and then move on to an analysis of the compensation effect in the model.

2.4.1 Model Validation

In the model, the time-mean transport between Florida and the Bahamas, $\Psi_{FC,}$ is 28.5 Sv, slightly less than the 32.3 ± 3.2 Sv estimated from the cable data (Larsen, 1992; Baringer and Larsen, 2001). The time-mean transport through the Yucatan Channel, $\Psi_{YC,}$ is 26.2 Sv, larger than the mean transport of 23.8 ± 1 Sv estimated from the CANEK array (Sheinbaum et al., 2002), but in keeping with the estimate for the Yucatan Channel transport given by Johns et al. (2002) by closing the transport budget for the Antilles passages (the mean transport of 26.2 Sv is also consistent with the high resolution model study of Cherubin et al. (2005)). The implied time-mean transport through the Old Bahama and Northwest Providence channels combined is 2.3 Sv and is similar to the observed estimates given by Atkinson et al. (1995) and Leaman et al. (1995). We note that the time-mean transport through the Windward Passage into the Caribbean Sea in the model is about 5.4 Sv, which is underestimated compared to the estimate of 7 Sv made by Johns et al. (2002) but closer to the more recent estimate of 3.5 Sv given by Johns et al. (2008).

There is a total of 10 eddy shedding events during the 5-year analysis period. The separation interval between shedding events varies between 5 and 8 months, which accords with the range of observed eddy separation intervals (e.g., Vukovich, 1995; Sturges and Leben, 2000). Overall, the model exhibits similar behavior to that found in previous numerical studies (Dietrich et al., 1997; Murphy et al., 1999; Oey et al., 2003).

The observed vertical structure of the time-mean flow through the Yucatan Channel can be characterized as an intense northward flow into the Gulf of Mexico in the western upper part of the channel and relatively weaker and southward flow on the eastern upper

and bottom layers (Figure 2.5a). A similar profile of the time-mean northward flow at the Yucatan Channel (~22 °N) is produced by the model (Figure 2.5b). The time-mean temperature distribution at the same section based on the model results compares well with the observations during the CANEK program, the isotherms being tilted to the surface in the western upper layer of the channel, as required by thermal wind to balance the intense northward flow. Furthermore, the location of the current maximum in the Yucatan Channel oscillates longitudinally associated with the Loop Current ring shedding events and the associated variations of the deep outflow (depth > 800 m) from the Gulf of Mexico, consistent with the Bunge et al. (2002) observations from CANEK, and the numerical simulations by Ezer et al. (2003) and Cherubin et al. (2005).

2.4.2 Compensation Effect in the Model

Figure 2.6a shows model-calculated transport time series for the Florida Current between Florida and the Bahamas, Ψ_{FC}, and for the Yucatan Channel, Ψ_{YC}. The correlation coefficient at zero lag between the two time series is 0.89, significantly different from zero at the 99% level (Figure 2.7). (The corresponding correlation between the daily mean transport estimates from the cable data and the CANEK data set is only 0.15, as an issue discussed further in section 2.6). Nevertheless, the two times series do not correspond exactly to each other, implying that some form of compensation effect must be operating in the model through the passageways north of Cuba. To examine this effect, Figures 2.6b and 2.6c show the transport time series from the model for the Northwest Providence (Ψ_{NWP}) and Old Bahama (Ψ_{OB}) channels. Correlation analysis (Figure 2.7) shows a significant negative correlation (0.85) between Ψ_{YC} and Ψ_{OB}, peaking near zero lag, indicative of the compensation effect, with only a very weak relationship between Ψ_{YC} and $\Psi_{NWP.}$ It follows that in the model it is the transport variations through the Old Bahama Channel that contribute to the compensation effect, with relatively little role for the Northwest Providence Channel, the same as we found when discussing experiment Mean in section 2.3. A comparison of the model-calculated transport anomalies (i.e. differences from the time mean) for Ψ'_{YC}, $-\Psi'_{OB}$, and $-\Psi'_{WW}$ is shown in Figure 2.6d. There is clearly a close relationship between all three time series. In particular, when Ψ_{YC}

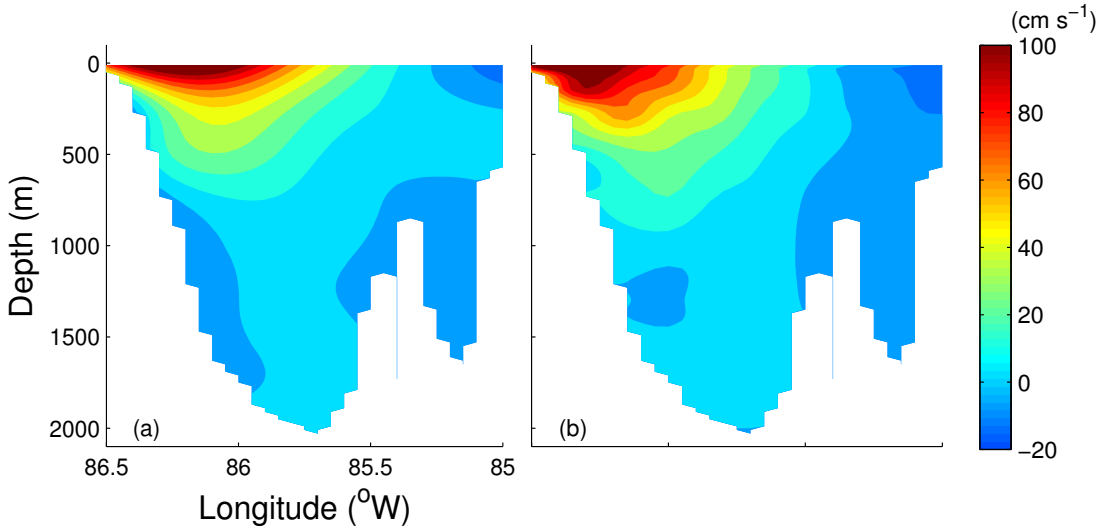

Figure 2.5. The time-mean northward normal velocity (cm s^{-1}) at the Yucatan Channel (a) observed by the CANEK program during 13 July 2000 to 31 May 2001, and (b) produced by the model in Exp-CR from years 2 to 6. Model results are interpolated and extrapolated to the same data grid as observation data.

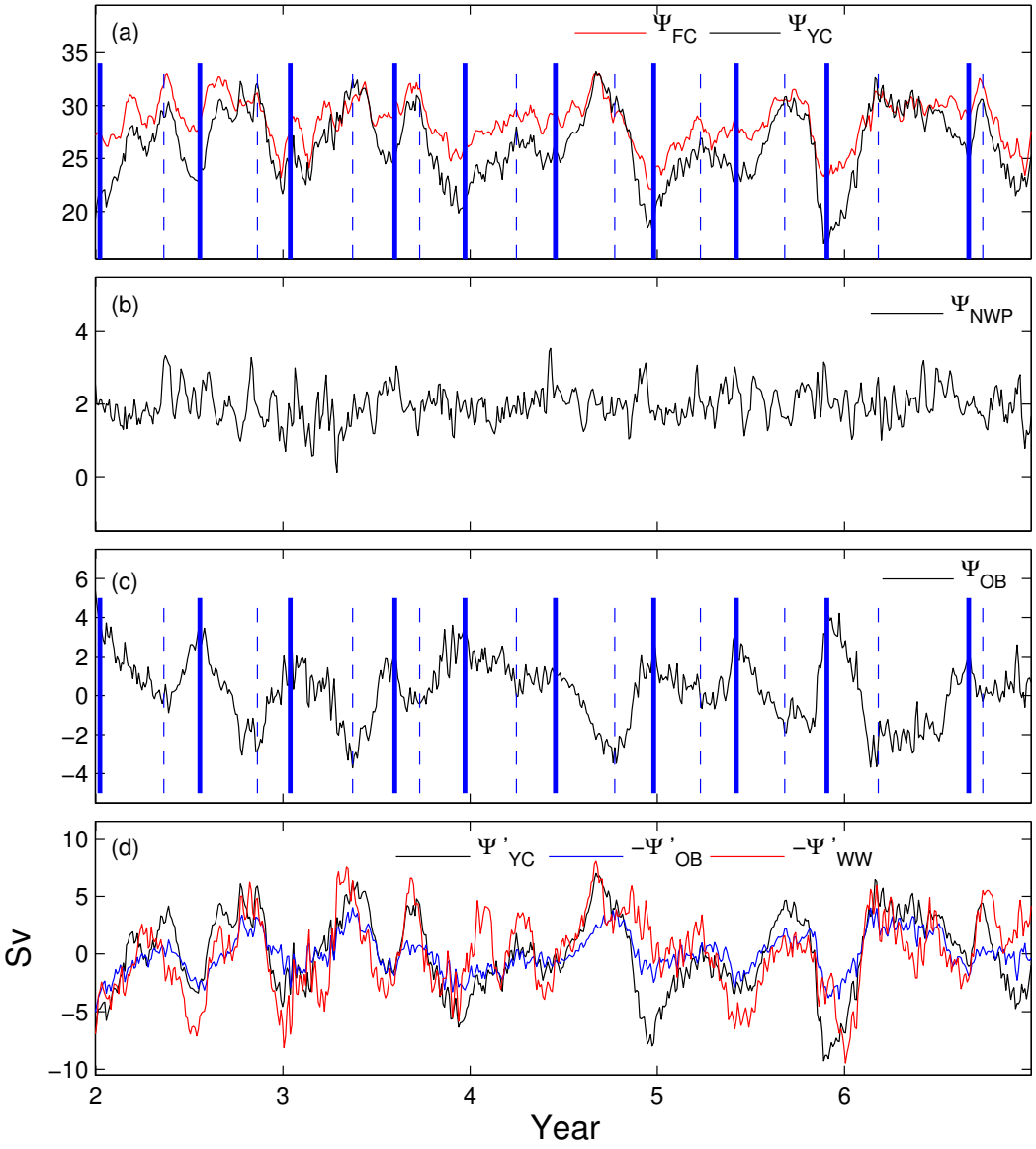

Figure 2.6. Time series of the model-calculated transports (3-day average) in Exp-CR from years 2 to 6 (a) between Florida and the Bahamas (Ψ_{FC}), and through the Yucatan Channel (Ψ_{YC}), (b) the transport through the Northwest Providence (Ψ_{NWP}) Channel, and (c) the transport through the Old Bahama Channel (Ψ_{OB}). (d) Comparison between model-calculated transport anomalies (time mean removed) of Ψ'_{YC}, $-\Psi'_{OB}$, and $-\Psi'_{WW}$ (Ψ_{WW} presents the transport through the Windward Passage). The solid blue vertical lines mark the events corresponding to maxima of Ψ_{OB} and corresponding minima of Ψ_{YC} produced by the model in Exp-CR. The dashed vertical lines mark the events corresponding to minima of Ψ_{OB} and corresponding to maxima of Ψ_{YC}.

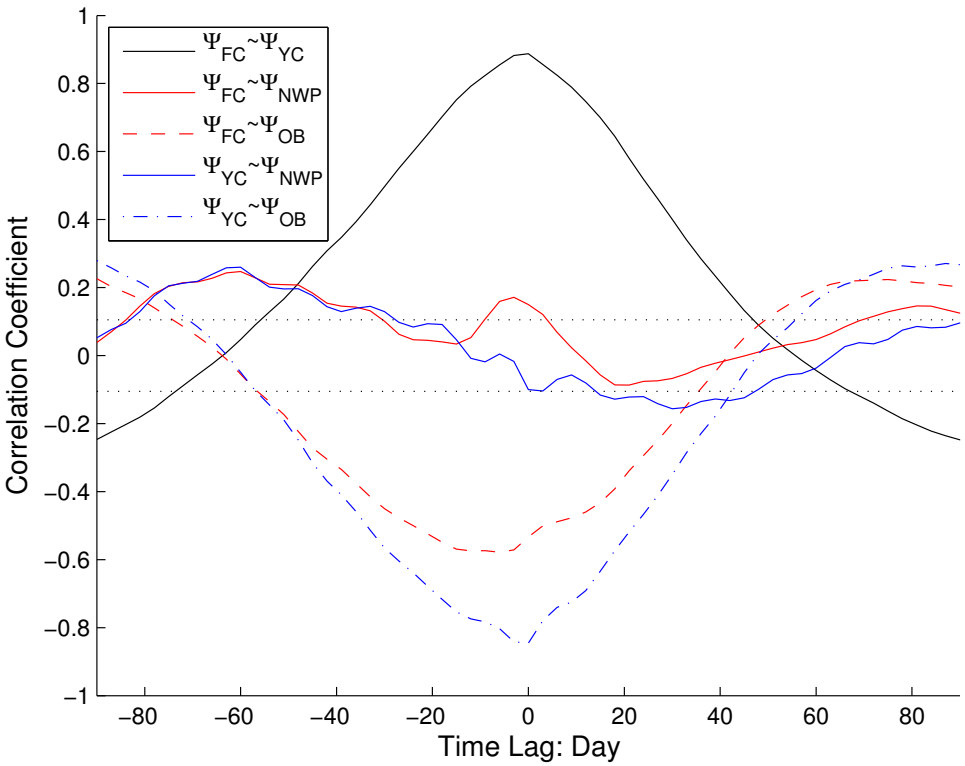

Figure 2.7. Correlation coefficients between transports of the Florida Current (Ψ_{FC}), the Yucatan Current (Ψ_{YC}), the flow through the Northwest Providence Channel (Ψ_{NWP}), and the flow through the Old Bahama Channel (Ψ_{OB}) calculated from model results (3-day average) in Exp-CR from years 2 to 6. Correlations outside the dotted lines are significantly different from zero at the 99% level.

increases, there is a corresponding increase in the southeastward flow through the Old Bahama Channel and also increased southwestward flow through the Windward Passage, implying an anomalous clockwise circulation around Cuba, with the opposite situation applying when Ψ_{YC} is decreased, exactly as we found in experiment Mean.

The connection between the large transport events in Figure 2.6 and the Loop Current intrusion is shown in Figures 2.8 and 2.9. Figure 2.8 shows the model sea surface height for all the events marked by the solid blue vertical lines in Figure 2.6 corresponding roughly to maxima in the northwestward transport through the Old Bahama Channel and corresponding minima in the northward transport through the Yucatan Channel. In each case, we see that the Loop Current intrudes strongly into the Gulf of Mexico, while at the same time it is pinched close to the northwest coast of Cuba, as in Figure 2.4b. Figure 2.9, on the other hand, shows the sea surface height corresponding roughly to minima (maxima) in the northwestward (northward) transport of the Old Bahama (Yucatan) Channel. This time we see the pool of warm water off the northwest coast of Cuba and an associated bulging of the Loop Current away from the coast, but no deep intrusion into the gulf as in Figure 2.8. A comparison with Figures 2.4b and 2.4d shows the same features in the sea surface height in association with the minima and maxima in northward transport through the Yucatan Channel in experiment Mean. It is also interesting that in Figures 2.8 and 2.9 we can see the presence of Caribbean eddies that squeeze through the Yucatan Channel (e.g., at day 1071 in Figure 2.8, and days 855, 1359, and 1866 in Figure 2.9).

We have also calculated the distribution of correlation coefficients between the model sea surface height anomalies and anomalies of the model-calculated transport through the Old Bahama Channel (positive northwestward). The result is shown in Figure 2.10a and is reassuringly similar to the correlation map computed using FLAME model output, based on Yucatan Channel transport (note the sign change) and shown in Figure 2.2b. The presence of flow compensation around Cuba is clearly evident, as implied by the high negative correlation all around Cuba. The connection between Loop Current intrusion and the transport variability is indicated by the elongated region of large positive anomaly to the north of the Yucatan Peninsula and the northward bulge in the region of negative correlation off the northwest coast of Cuba.

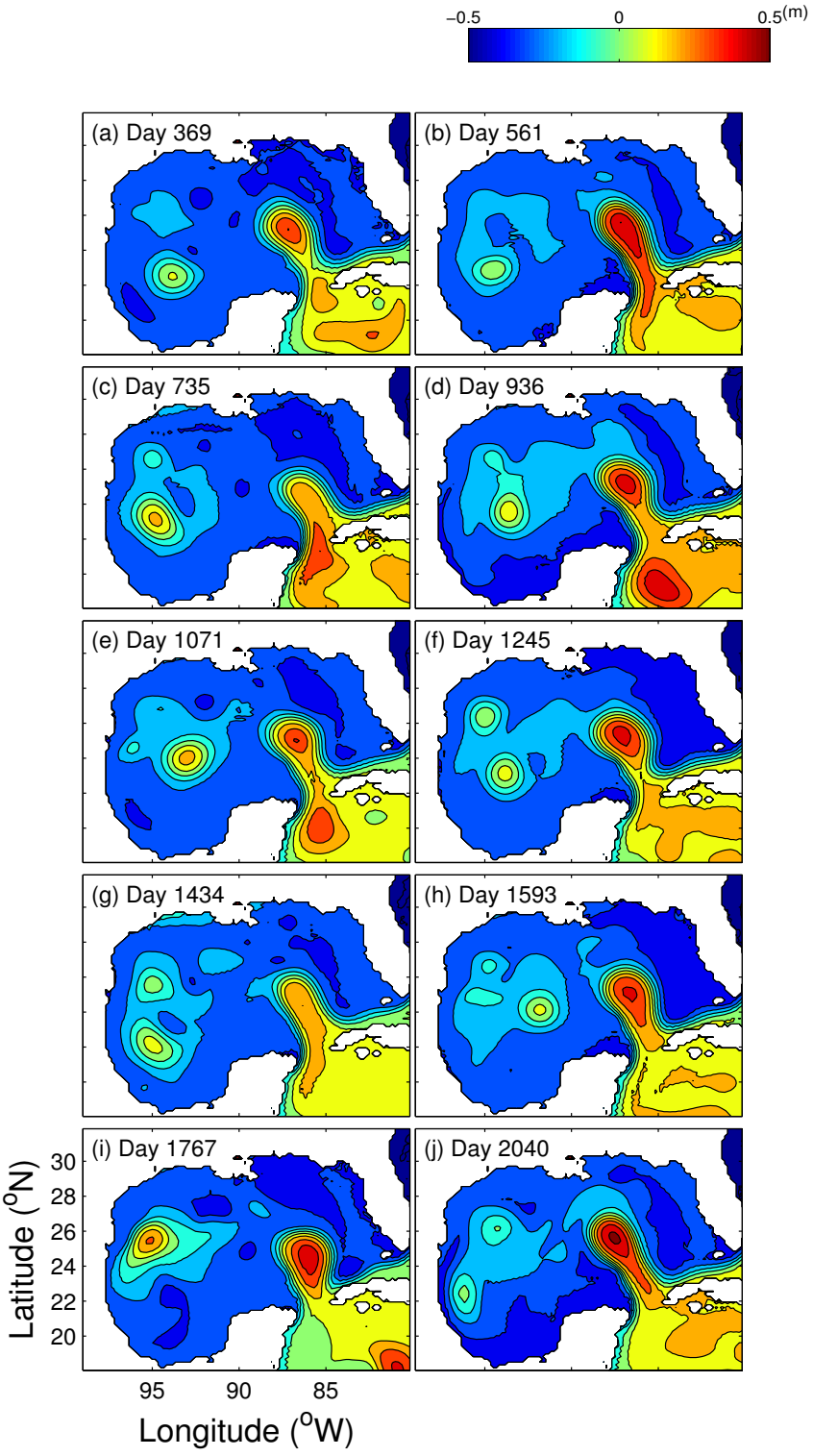

Figure 2.8. Snapshots of sea surface height fields (3-day average) for all the events marked by the solid blue vertical lines in Figure 2.6 produced by the model in Exp-CR.

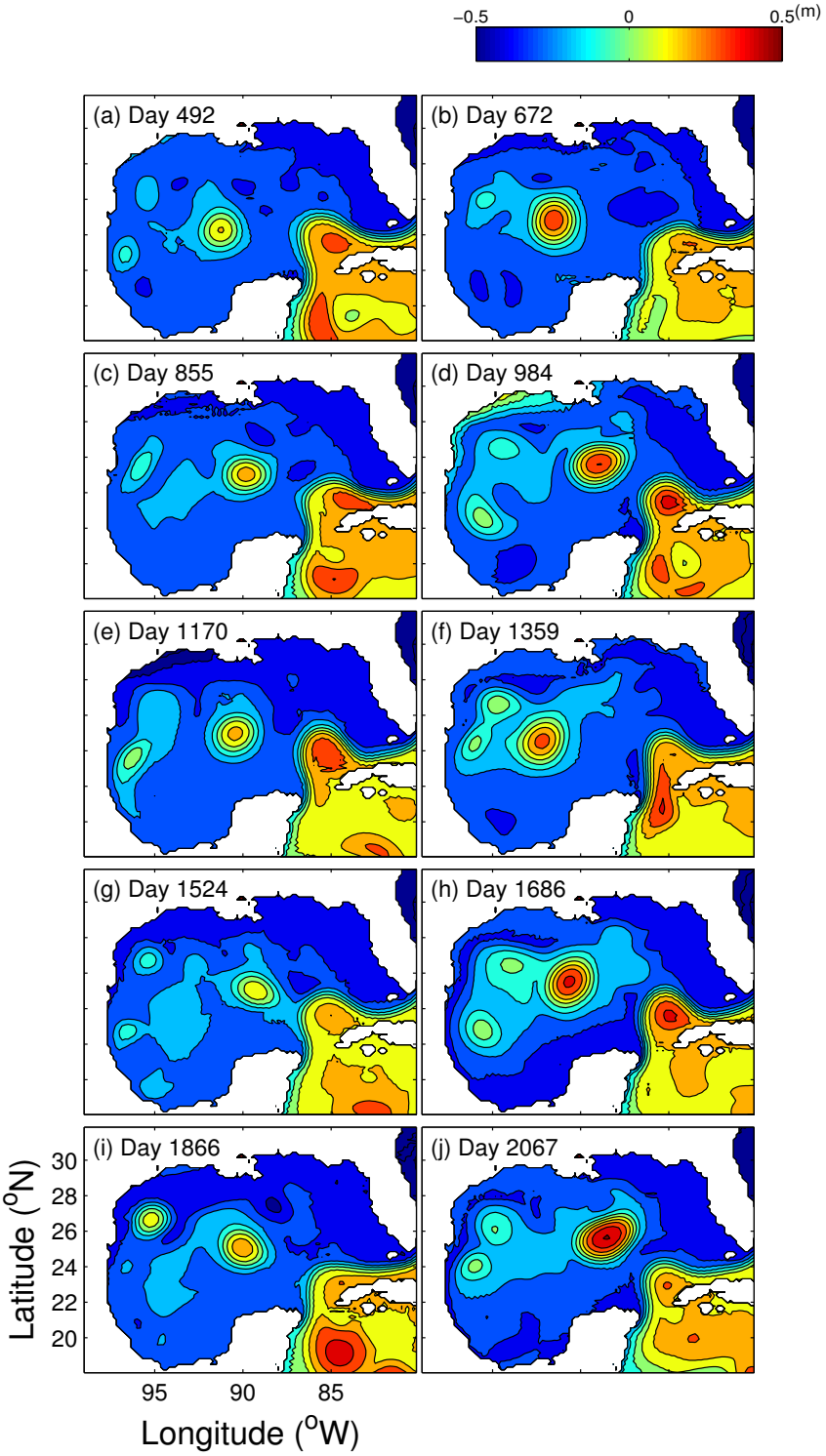

Figure 2.9. Snapshots of sea surface height fields (3-day average) for all the events marked by the dashed vertical lines in Figure 2.6 produced by the model in Exp-CR.

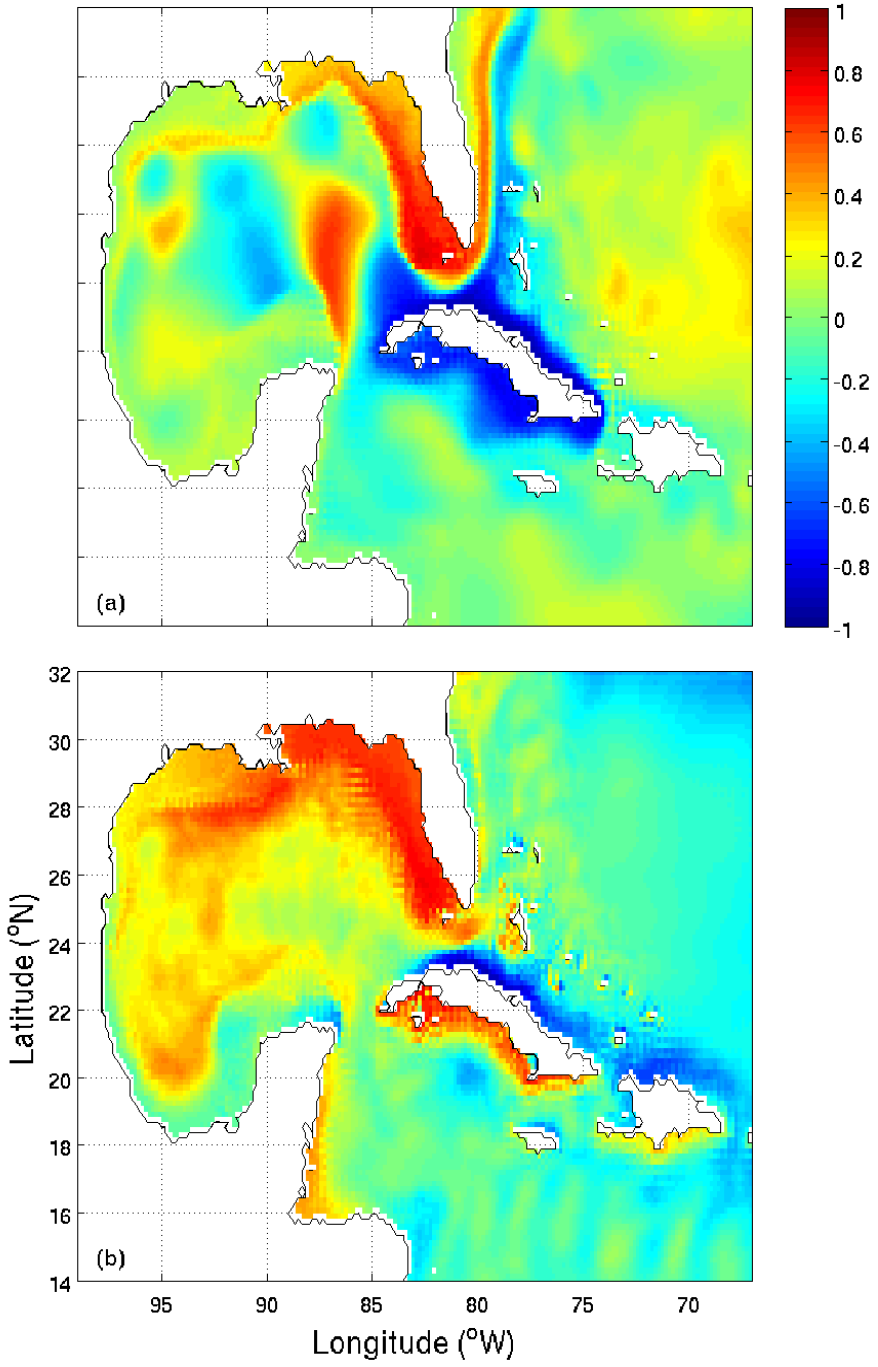

Figure 2.10. (a) Distribution of correlation coefficients between the sea surface height anomalies and transport anomalies through the Old Bahama Channel calculated from model results (3-day average) in Exp-CR from years 2 to 6. (b) Same as Figure 2.10a but for 30-day high-passfiltered results.

Flow compensation around Cuba is also a feature of the model results at higher frequency. (It should be noted that the model is driven by 6 hourly wind stress computed from NCEP wind fields.) Using model output that has been high-pass filtered with a cutoff timescale of 30 days, the correlation at zero lag between the northward transport through the Yucatan Channel and the northwestward transport through the Old Bahama Channel is -0.63 and is significantly different from zero at the 99% level. The amplitude of the high-frequency transport anomalies produced by the model varies from 0.5 to 2 Sv. Figure 2.10b shows the correlation of model sea surface height anomalies with northwestward transport anomalies through the Old Bahama Channel, again both high-pass filtered with a cutoff of 30 days. The pattern is quite different from that in Figure 2.10a, indicating that quite different dynamics are operating. In fact, at these high frequencies it is wind forcing that is important, the transport through the Old Bahama Channel being highly correlated with the along-channel wind stress. The influence of wind forcing is evident from Figure 2.10b with sea level anomalies of opposite sign on the north and south coast of Cuba indicative of Ekman divergence and convergence, respectively, in association with a westward wind stress.

2.5 Diagnostic Model Results: the Mechanism by Which Loop Current Intrusion Affects Transport Variations at the Yucatan Channel

To understand the dynamics responsible for the transport fluctuations through the Yucatan Channel, we have run the model in diagnostic mode in which the model potential temperature and salinity fields are specified and held time-independent and the model otherwise has no forcing. The diagnostic mode is constructed by adding potential temperature and salinity anomaly fields extracted from experiment Mean to the horizontal average of the annual mean climatology for the whole model domain. Surface forcing and transports through the model open boundaries are set to zero. Instead a simple linear friction in the horizontal momentum equations is used at each level, i.e. a term in vector notation, $-\varepsilon(u, v)$, where ε corresponds to a timescale of 15 days (i.e. $1/\varepsilon =$

15 days) and has no vertical dependence. The use of a linear friction eliminates the possibility that rectification effects from the friction term can drive vertically integrated transports.

The model is then integrated to reach a quasi-steady state. In the first run, the model uses potential temperature and salinity anomalies taken from day 1155 in experiment Mean, associated with a minimum of $\Psi_{YC,}$ and in the second run, the model uses potential temperature and salinity anomalies from day 1230, associated with a maximum of Ψ_{YC} (see Figure 2.4). The first/second model run gives a cyclonic/anticyclonic circulation around Cuba (and hence a southward/northward transport anomaly through the Yucatan Channel). The volume transport stream function difference, the second run minus the first run, is shown in Figure 2.11. There is 3.8 Sv transport difference generated for Ψ_{YC}, comparable to the peak-to-peak transport difference found in experiment Mean. Of this 3.8 Sv, 2.5 Sv is associated with compensating flow through the Old Bahama Channel with the remaining 1.3 Sv circulating round and through the Bahama Island archipelago. Importantly, the results show that the compensation effect associated with Loop Current intrusion and ring shedding can be understood as the result of the interaction of the density anomalies and the underlying variable bottom topography.

To identify the precise mechanism, we note that a feature of the geometry in this area is that the water depth in the Old Bahama Channel, and in the Straits of Florida between Florida and Cuba, is much less than that in the Yucatan Channel and the Gulf of Mexico to the west and in the North Atlantic Ocean to the east. As a consequence, pressure differences across the ridge connecting Florida and Cuba can affect the transport through the Straits of Florida between Cuba and Florida, and hence Ψ_{YC} by volume conservation, by means of the form drag effect. To illustrate the form drag effect we consider the vertically integrated zonal momentum balance:

$$-fV = -\frac{1}{\rho_0}\frac{\partial}{\partial x}\int_{-H}^{0} p\,dz + \frac{1}{\rho_0} p_b H_x - \varepsilon U \qquad (2.1)$$

where (U, V) is the vertically integrated transport vector, H is the water depth, p is the pressure perturbation from the undisturbed state, and p_b is the value of p at the bottom (corresponding to the bottom pressure). The second term on the right-hand side is the topographic form drag term associated with pressure differences across topographic

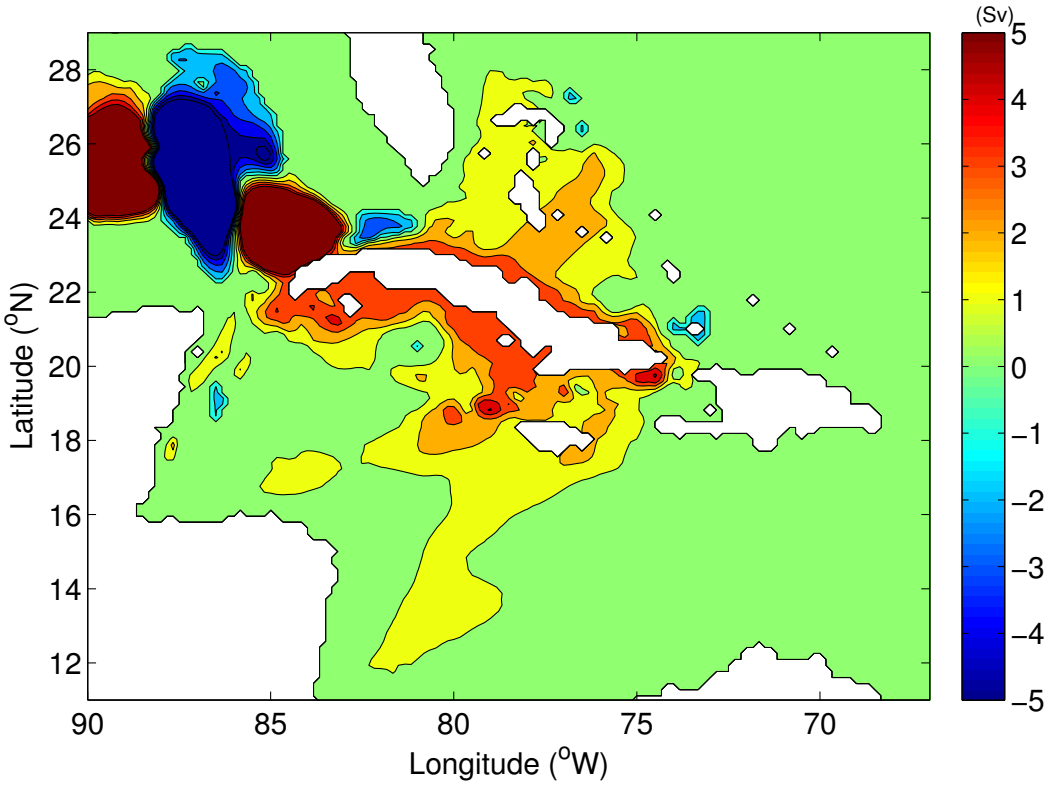

Figure 2.11. Differences in volume transport stream functions (color shading) between two diagnostic runs (in the steady state) driven by potential temperature and salinity anomalies extracted from model results in experiment Mean at day 1155 (corresponding to a minimum in transports through the Yucatan Channel) and day 1230 (corresponding to a maximum in transports through the Yucatan Channel).

ridges (see, for example, Hughes and de Cuevas, 2001). We use this equation to interpret the results from the diagnostic model. Integrating zonally across the model domain along a line of latitude passing between Florida and Cuba (i.e. passing through the Straits of Florida), the first term on the right-hand side goes to zero (it is zero at the western end of the section where the water depth, H, on the western side of the Gulf of Mexico goes to zero; and it is zero at the eastern end of the section where the transport variability is zero). Likewise, because no transport is allowed to pass through the boundaries of the diagnostic model, the net northward transport across the line of latitude (the zonal integral of the term on the left-hand side) is also zero, leaving a balance between the friction term and the topographic form drag. (Note that the argument is unchanged if the line of latitude is blocked by islands and also if the line of integration is curved in order to follow a water-only path.)

To illustrate the form drag mechanism, Figure 2.12 shows the correlation between the temperature field along 23.9˚N, at the Gulf of Mexico entrance to the Straits of Florida, and Ψ_{YC} in experiment Mean. It can be seen that increased Ψ_{YC} is associated with warmer (lighter) water over the slope (this is the warm pool near the northwest coast of Cuba noted when discussing Figure 2.4d). By contrast, the hydrographic conditions on the topographic slope east of the Bahama Islands do not change in experiment Mean in relation to Yucatan Channel transport variability. As a consequence, in the run with the diagnostic model corresponding to a maximum in Ψ_{YC}, the bottom pressure is lower on the Gulf of Mexico side of the ridge, where the water is anomalously warm, than on the Bahamas side. The resulting pressure difference across the ridge then drives enhanced eastward transport through the Straits of Florida by the form drag effect which, because of volume conservation, leads to the increased Ψ_{YC}.

It is interesting that the transport difference shown in Figure 2.11 mirrors quite closely the features seen in the sea surface height pattern implied by Figure 2.10a. In particular, we can see the (negative) transport anomaly associated with the elongated feature to the north of the Yucatan Peninsula and, importantly, the (positive) transport anomaly off the northwest coast of Cuba. When the transport through the Yucatan Channel is enhanced, the latter feature is associated with the pool of warm water off the northwest coast of Cuba, while the former feature indicates that when transport through

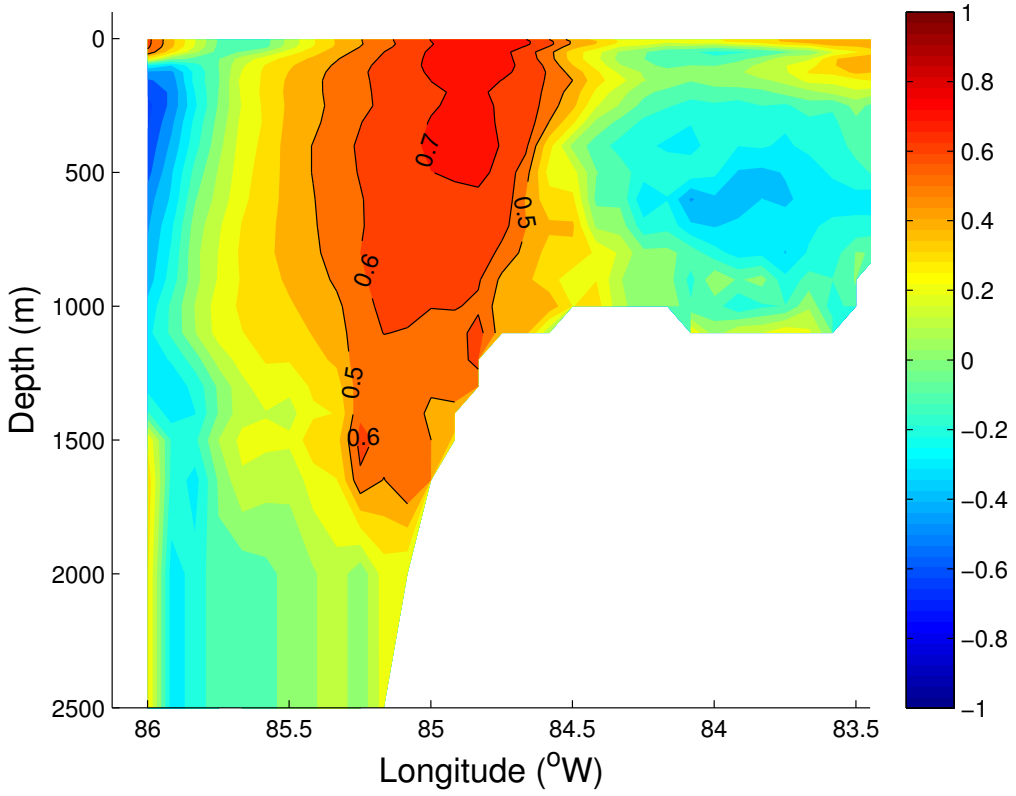

Figure 2.12. The vertical distribution of correlation coefficients along a transect at 23.9°N (the Straits of Florida between Florida and Cuba), between the model-calculated potential temperature field and the transport through the Yucatan Channel (positive northward) calculated from model results (3-day average) in experiment Mean from years 2 to 6.

the Yucatan Channel is enhanced, the deep intrusion by the Loop Current into the gulf is absent.

We argue, therefore, that it is the interaction between the Loop Current intrusion and the sloping topography at the Gulf of Mexico entrance to the Straits of Florida that is responsible for the link between Yucatan/Old Bahama Channel transport variability and the Loop Current intrusion and ring shedding. In particular, the evolution of the Loop Current, as it intrudes into the Gulf of Mexico, leads both to the pinching of the flow to the northwest of Cuba, as in Figure 2.4b, and the expansion of the warm pool northwest of Cuba, as in Figure 2.4d. It is the density anomalies associated with the fluctuations in the warm pool that, through interaction with the sloping bottom topography, drive the transport variations. This conclusion is consistent with the two additional experiments described in section 2.3. In one, the Windward and Mona passages were closed, yet the transport variations were found as before. In the other, the transport through the Yucatan Channel was specified to be time-invariant by the model set-up, and the warm pool northwest of Cuba became a steady, time-invariant feature of the model results.

2.6 Evidence for the Compensation Effect from Observations

Two oceanographic data sets are of particular importance. The first is the daily mean transport of the Florida Current inferred from voltage differences across the Florida-Bahamas submarine cable at 27˚N (Baringer and Larsen, 2001). The second is the set of daily mean transport estimates from the 2-year observation array in the Yucatan Current during the CANEK program (Ochoa et al., 2001; Bunge et al., 2002; Sheinbaum et al., 2002; Candela et al., 2003; Abascal et al., 2003). The data come from two periods: 10 September 1999 to 15 June 2000, and 13 July 2000 to 31 May 2001. For comparison, the observed transport estimates during the period 13 July 2000 to 31 May 2001 (when both observational data sets are available simultaneously) are shown in Figure 2.13. During this period, the cable-estimated transport of the Florida Current varied between 22.7 and 39.6 Sv and the CANEK estimates of the Yucatan Channel transport between 12.8 and 31.7 Sv. Although there are events common to both time series (e.g., during

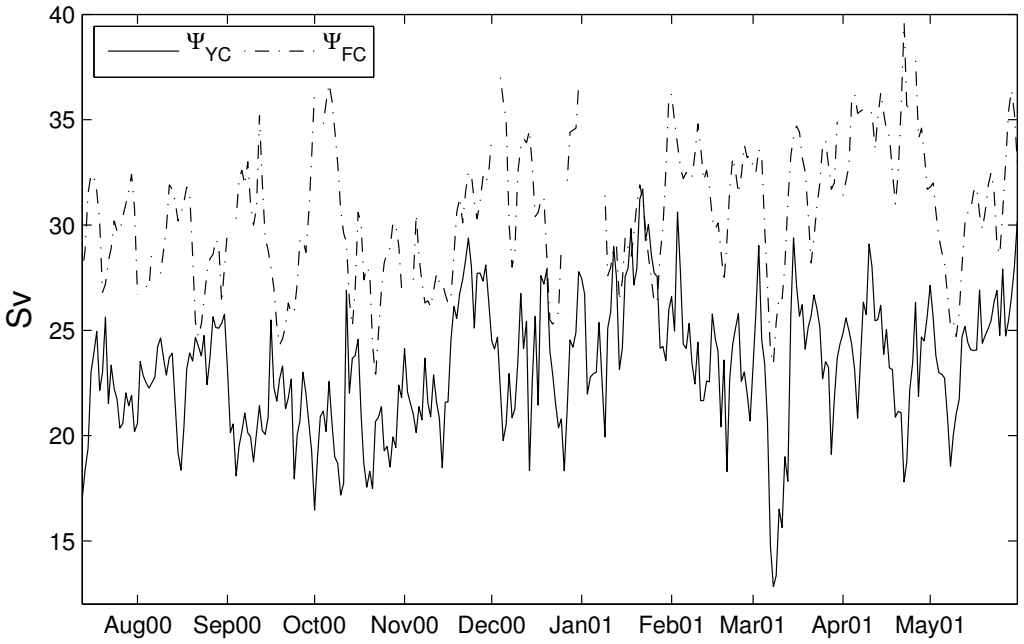

Figure 2.13. Time series of transports of the Florida Current from the cable data (Ψ_{FC}, dot-dashed line) and through the Yucatan Channel based on the CANEK program (Ψ_{YC}, solid line) from 13 July 2000 to 31 May 2001.

March of 2001) a visual inspection suggests that there is no clear relationship between the two measured transport estimates. Indeed, the correlation at zero lag is only 0.15. As noted in section 2.4, the relationship between the two transport time series is very much stronger in the model (correlation at zero lag of 0.89). It should be noted, however, that we have less than one year of data with which to make the comparison, which is not long enough to properly assess the impact of Loop Current intrusion in the two transport times series, whereas the Loop Current intrusion effect dominates the transport variability in the model. (In an attempt to assess the correlation at low frequency, we have low-pass filtered both the CANEK and cable transport time series with a cutoff of 120 days. The correlation between the two time series then rises to 0.5 and is more in keeping with the model. However, given the shortness of the time series we can use for the comparison, one cannot draw a firm conclusion). In addition, in the model we are lacking transport variability on daily timescales through the boundary to the north of Straits of Florida due to the specification of a seasonally-only varying transport time series taken from the FLAME model (see section 2.2). Nevertheless, if the transport estimates from the cable and CANEK data sets are accurate, then in reality the compensation effect must operate to a much greater extent than we have found in the model. Of course, the low correlation between the CANEK- and cable-estimated daily transport estimates could be because of data problems. For example, the mean transport through the Yucatan Channel from the CANEK data set is 23.8 ± 1 Sv as given by Sheinbaum et al. (2002), is considerably less than the 32.3 ± 3.2 Sv for the Florida Current between Florida and the Bahamas given by Baringer and Larsen (2001) and verified over many years against mooring observations (e.g., the STACS program; Schott and Zantopp, 1985). The difference of more than 8 Sv is roughly double the transport estimated for the passages north of Cuba by Atkinson et al. (1995) and Leaman et al. (1995) (see also Johns et al, 2002). It is also possible that the model overestimates the link between the variations in transport of the Florida and Yucatan currents. We note, however, that the correlation between the transport time series shown in Figure 2.2a from the $1/12^{o}$ Atlantic Ocean FLAME model is 0.8 and is also considerably higher than is found between the CANEK and cable data sets. Only further detailed monitoring efforts, especially of the Yucatan Channel, which has been much less monitored than the Florida Current, will be able to clarify this issue.

Evidence for the compensation effect is also provided by Hamilton et al. (2005). They note that variations in the cable-estimated transport between Florida and the Bahamas are not necessarily an accurate indicator of the transport variability of the Loop Current as it exits the Gulf of Mexico (and by implication, the transport through the Yucatan Channel into the gulf), implying that, in their opinion, significant transport must pass through the passageways north of Cuba and south of the cable site at 27^{o}N. They base their conclusion on estimated transports from December 1990 to November 1991 based on moored arrays at several sections in the Straits of Florida extending both south and southeastwards from Key West, and between Florida and the Bahamas, including the side channels north of Cuba.

2.7 Summary and Discussion

Using a number of different model experiments, we have examined the link between variations in the vertically integrated transport through the Yucatan Channel and the intrusion of the Loop Current into the Gulf of Mexico in association with ring shedding. Such transport variations are a feature of the $1/12^{o}$ FLAME model of the Atlantic Ocean (Figure 2.2) and can also be seen in the model study of Cherubin et al. (2005). We have seen that in the models the transport of the Yucatan Channel reaches a minimum when the Loop Current intrusion into the Gulf of Mexico is at a maximum, typically just prior to ring shedding. Likewise, the maximum transport through the Yucatan Channel occurs typically soon after a ring has been shed and is associated with a bulging of the Loop Current away from the northwest coast of Cuba, in contrast to the pinching of the Loop Current close to the coast when there is a strong intrusion into the gulf. We argued that the transport variations associated with the Loop Current intrusion arise from the interaction between the density anomalies associated with the Loop Current evolution and the variable bottom topography, the mechanism being the form drag effect across the ridge connecting Florida and Cuba. We have also argued that transport variations through the Yucatan Channel are at least partly compensated by flow variations through the channels north of Cuba, notably the Old Bahama Channel (what we have called the compensation effect). Using a version of the model driven by 6 hourly wind stress

derived from NCEP wind data, we showed that in addition to the influence of the Loop Current intrusion, the compensation effect also operates on timescales shorter than 30 days, but in this case the dynamics are wind driven. We note that because of the compensation effect, transport through the Yucatan Channel and between Florida and the Bahamas (at the site of the submarine cable; Baringer and Larsen, 2001) does not vary in unison in either our model or the FLAME model, although in both models the corresponding transport time series are highly correlated (greater than 0.8). This contrasts with the very low correlation (0.15) between the transport times series measured during the CANEK program (Sheinbaum et al., 2002) and the cable estimate (Baringer and Larsen, 2002). It should be noted, however, that we have less than 1 year of data with which to compute the correlation of 0.15 and that 1 year is not long enough to allow sampling of the Loop Current intrusion events that dominate the model transport time series. Nevertheless, discrepancies of this kind argue the need for more detailed monitoring of the flow pathways entering and leaving the Gulf of Mexico and the Bahama Island chain.

Clearly, an improvement in the model would be to replace the seasonally varying transport on the northern boundary by a more realistic representation of the daily transport variability. A more realistic specification of the time varying transport on the northern boundary would also shed light on the mechanisms governing the daily transport variability seen in the cable data (see Greatbatch et al. (1995) who noted the importance in their model of forcing north of the Florida Straits for driving Florida Current transport variability). Another topic we have not addressed is whether the transport variations we have discussed can feedback and influence the intrusion of the Loop Current. As noted in the introduction, many authors have suggested that changes in the flow conditions through the Yucatan Channel (e.g., flow velocity and the vorticity distribution) might play a role in preconditioning Loop Current intrusion and ring shedding (e.g., Sheinbaum et al., 2002; Ezer et al., 2003; Oey et al., 2005; Oey, 2004). Clearly, further work is required on the general topic of Florida and Yucatan Current transport variability.

Chapter 3

The Influence of Gulf of Mexico Loop Current Intrusion on the Transport of the Florida Current[1]

3.1 Introduction

The current system flowing through the Yucatan Channel and the Straits of Florida (see Figure 3.1) forms part of the North Atlantic western boundary current system and is thought to carry not only part of the wind-driven return flow of the subtropical gyre but also the upper limb of the North Atlantic Meridional Overturning Circulation (Schmitz and Richardson, 1991; Schmitz et al., 1992). Monitoring of the Florida Current between Florida and the Bahamas has been almost continuous since the early 1980's, beginning with the STACS program (Schott and Zantopp, 1985), subsequently using submarine cables at 27°N (Figure 3.1b; Larsen, 1992; Baringer and Larsen, 2001), and also as part of the RAPID/MOCHA array for monitoring the overturning circulation (Cunningham et al., 2007; Kanzow et al., 2007). Understanding the observed variability of the Florida Current is a topic of continuing interest. Niiler and Richardson (1973) first identified the

[1] Lin, Y., R. J. Greatbatch, and J. Sheng (2010a), The influence of Gulf of Mexico Loop Current intrusion on the transport of the Florida Current, *Ocean Dynamics*, in press.

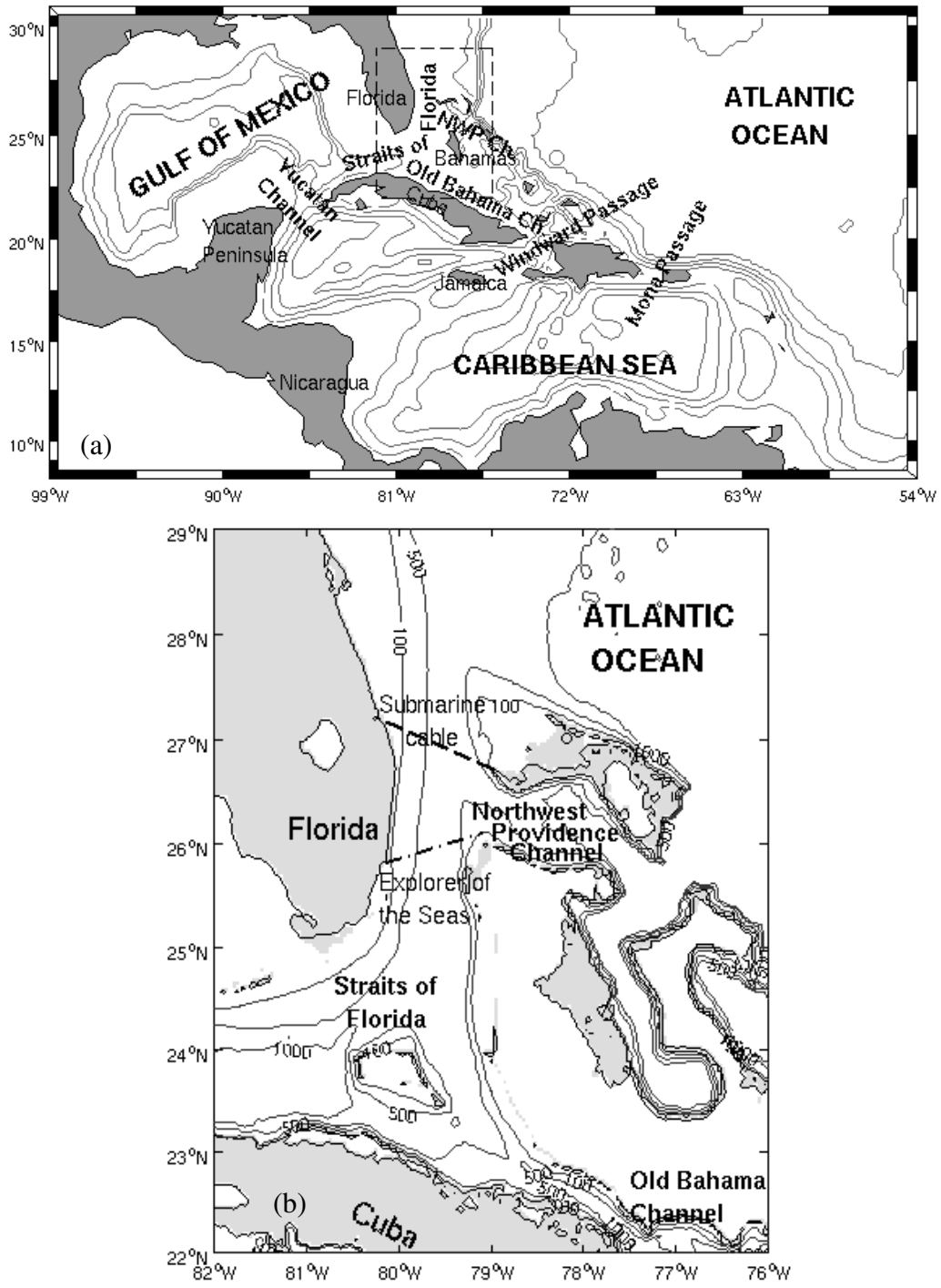

Figure 3.1. Major topography features in (a) the Intra-Americas Sea and (b) Straits of Florida and adjacent areas marked by dashed lines in (a). The contour lines show water depth with an interval of 1000 m in (a) and water depth at 100, 500, and 1000 m in (b). Dashed line and dot-dashed line in (b) show the approximate positions of the submarine cable and the "Explorer of the Seas" cruise track across the Straits of Florida.

seasonal cycle indicating a peak northward transport in the summer and a minimum in late autumn, at variance with expectations based on flat-bottomed Sverdrup theory. Anderson and Corry (1985) explained the discrepancy by noting that, on annual timescales, adjustment by baroclinic Rossby waves is too slow to compensate for the underlying variable bottom topography (see also Gill and Niiler, 1973) and that the phase of the seasonal cycle can be explained using the topographic Sverdrup relation with an additional contribution from baroclinic coastal processes. This idea was exploited in the studies by Greatbatch and Goulding (1989), Fanning et al. (1994), and Greatbatch et al. (1995). In the latter, it is shown that a uniform-density, single-layer barotropic model with realistic bottom topography and driven by realistic, twice-daily wind forcing can capture the seasonal cycle in the cable transports, as monitored up to that time. Baringer and Larsen (2001) noted a change in the annual cycle after about 1990. It remains to be seen if this change can be accounted for by wind forcing. The model is rather less successful, however, at capturing the daily variability in the transport and is also missing an interesting component of variability with roughly 8-month timescale that is present in the cable data in some years (see, in particular, 1986 in figure 3 in Greatbatch et al. (1995) and also figure 4 in that paper for a comparison between 60-day low-pass filtered model output and the cable data). Variability at the longer, interannual to decadal timescales has received less attention, although Baringer and Larsen (2001) have pointed out an apparent link between the interannual variability of the North Atlantic Oscillation index and the cable transports. Recently, DiNezio et al. (2009) have found evidence that interannual to decadal timescale variability in the cable transports is linked to wind stress curl variability further east at the same latitude, suggesting that long Rossby wave propagation from the east plays a role in determining the Florida Current transport variability on these timescales.

As implied by the importance of the variable bottom topography, propagation of coastal trapped waves southwards along the North American continental slope play an important role in the studies of Anderson and Corry (1985) and Greatbatch et al. (1995). On the other hand, westward propagating Rossby waves are emphasized on the longer, interannual to decadal timescales considered by DiNezio et al. (2009). In the present study, we ask whether the transport of the Florida Current between Florida and the

Bahamas is also influenced by variability upstream in the Gulf of Mexico. The geometry of the region (see Figure 3.1) implies that variations in transport through the Yucatan Channel must pass either through the passageways northeast of Cuba (e.g., the Old Bahama Channel) or through the Straits of Florida between Florida and the Bahamas, suggesting the possibility of such a link. Unfortunately, we know much less about the transport variability through the Yucatan Channel than we do about the transport variability between Florida and the Bahamas. The only available long-term transport estimates in the Yucatan Channel are from the CANEK program (Ochoa et al., 2001; Sheinbaum et al., 2002) initiated in December 1996 and completed in June 2001. CANEK used a combination of shipboard Acoustic Doppler Current Profiler (ADCP) measurements, hydrographic/velocity surveys using CTD's, lowered-ADCP measurements and a current meter mooring array to monitor the transport. As noted by Lin et al. (2009) (see also Chapter 2), the correlation between the CANEK derived daily transports of the Yucatan Current and the cable voltage inferred transports of the Florida Current is only 0.15, suggesting that a large part of the Yucatan transport variability passes northeast of Cuba and not between Florida and the Bahamas at the latitude of the submarine cable. A similar conclusion was reached by Hamilton et al. (2005) based on a monitoring program for the Straits of Florida carried out between December 1990 and November 1991.

Nevertheless, a distinctive feature of the circulation in the Gulf of Mexico is the intrusion of the Loop Current, connecting the Yucatan Channel with the Straits of Florida, and the associated eddy shedding (see, for example, Hurlburt and Thompson, 1980; Oey et al., 2005). The Loop Current can extend northward into the Gulf of Mexico, even as far as the Mississippi river delta and the Florida continental shelf (Huh et al., 1981; Wiseman and Dinnel, 1988). Maul and Vukovich (1993) tried to find a consistent relationship between the monthly position of the Loop Current and the monthly volume transport of Gulf of Mexico outflow, estimated from the sea level difference between Florida and Cuba, but were unsuccessful. However, a clear relation is found by Bunge et al. (2002) using CANEK observations between the Loop Current extension area into the Gulf of Mexico and deep flows at the Yucatan Channel. Recently, Lin et al. (2009) (see Chapter 2) have argued that the intrusion of the Loop Current into the Gulf of Mexico drives

vertically integrated transport variations through the Yucatan Channel through the interaction between the density anomalies associated with the Loop Current intrusion and the underlying variable bottom topography (in particular, the pressure difference across the ridge linking Florida to Cuba). This finding led us to re-examine the link between the Loop Current intrusion and the cable transport estimates. We find, for the first time, a statistically significant link at low frequencies (timescales longer than 120 days), suggesting that Loop Current intrusion does indeed influence the cable-estimated transports of the Florida Current.

An important issue is how the Loop Current intrusion into the Gulf of Mexico is measured. Maul and Vukovich (1993) used the northern boundary of the Loop Current estimated from satellite infra-red imagery. On the other hand, Bunge et al. (2002) used the extension area of the Loop Current estimated from radiometer images and Ezer et al. (2003) defined an index in terms of area-averaged sea surface elevations over the Loop Current region (89˚W to 83˚W, 21˚N to 27˚N) taken from their model. Here, we define a new index using satellite altimeter data (see section 3.2). The choice of this index is based on an empirical orthogonal function (EOF) analysis of sea surface height anomalies from altimeter observations, guidance from the numerical model of Lin et al. (2009), and the CANEK transport estimates for the Yucatan Channel, as described in detail below. The index is not intended to be a comprehensive index for measuring Loop Current intrusion but rather only the aspect of Loop Current intrusion that is responsible for driving variations in vertically integrated transport through the Yucatan Channel.

3.2 Connection Between Loop Current Intrusion and Transport Variability Through the Yucatan Channel

As shown in Lin et al. (2009) and in Chapter 2, the density anomalies associated with the intrusion of the Loop Current into the Gulf of Mexico can drive significant variations in the vertically integrated transport through the Yucatan Channel. Lin et al. (2009) (see also Chapter 2) have shown that the key feature for driving the vertically-transport variations is the development of anomalies in the pressure difference on the sloping topography between the two sides of the ridge connecting Cuba and Florida. Fluctuations

in this pressure difference drive vertically integrated transport variations between Cuba and Florida because of the topographic form drag effect, and these transport variations in turn lead to vertically integrated transport variations through the Yucatan Channel because of the geometry of the region. (See Figure 3.1 and note that for there to be no net accumulation of water in the Gulf of Mexico, variations in vertically integrated transport between Cuba and Florida must be exactly compensated by variations in vertically integrated transport through the Yucatan Channel.) The density anomalies associated with Loop Current intrusion and the underlying pressure anomalies are themselves associated with anomalies in sea surface height, raising the possibility of using an index based on altimeter data as a means of measuring this component of Yucatan Channel vertically integrated transport variability. In order to derive such an index, we begin by revisiting the relationship between Loop Current intrusion and variations in vertically integrated transport through the Yucatan Channel in the model of Lin et al. (2009), while noting that other higher resolution models (e.g., the model used by Cherubin et al. (2005) and the 1/12˚ North Atlantic model used by Eden et al. (2007)) exhibit very similar behavior.

The model domain used by Lin et al. (2009) covers the Intra-Americas Sea (see Figure 3.1a) with a horizontal resolution in both latitude and longitude of 1/6˚. The model is forced by six-hourly NCEP wind fields from 1996 to 2001. Readers are referred to Lin et al. (2009) (see also Chapter 2) for more details. The model was integrated for 6 years and the model results (3-day average) from year 2 to 6 are used for analysis. There are a total of 10 eddy shedding events during the 5-year period. The separation interval between shedding events varies between 5 and 8 months, which, while on the short side, nevertheless falls into the range of observed eddy separation intervals (e.g., Vukovich, 1995; Sturges and Leben, 2000). It should be noted, however, that it is not eddy shedding that is important for the model transport variations through the Yucatan Channel but rather the Loop Current intrusion itself and the interaction of the associated density anomalies with the underlying bottom topography (Lin et al., 2009). This is an important point because Loop Current intrusion does not always lead to the shedding of an eddy.

Figure 3.2a shows the time series of vertically integrated transport through the Yucatan Channel in the model (positive northward). Composites of sea surface height

(SSH; Figures 3.2b and 3.2d) and sea surface height anomaly from the model (Figures 3.2c and 3.2e) are made at the times of the transport maxima and minima shown by the vertical bars in Figure 3.2a. Here anomaly means departure from the average over the whole analysis period. (Noted that the composite plots are almost everywhere significantly different from zero at the 99% level). When the transport is at a minimum, the Loop Current intrudes strongly into the Gulf (Figures 3.2b and 3.2c), with a corresponding positive sea surface height anomaly centered at 25.0˚N and 86.5˚W, and a negative sea surface height anomaly centered at 23.5˚N and 84.0˚W off the northwest coast of Cuba. On the other hand, when the transport is a maximum, the Loop Current is in its port-to-port configuration (Figures 3.2d and 3.2e) and the pattern of sea surface height anomalies is reversed. In particular, at this time a negative sea surface height anomaly is found at 25.0˚N, 86.5˚W and there is now a positive sea surface height anomaly off the northwest coast of Cuba around 23.5˚N, 84.0˚W. It should be noted that when the sea surface height is anomalously high off the northwest coast of Cuba, there is a pool of anomalously warm water at the same location and, likewise, a pool of anomalously cold water at the same location when the sea surface height is anomalously low (see figure 12 in Lin et al. (2009) reproduced as Figure 2.12 in this thesis).

We now turn to the altimeter data and begin with the Merged Maps of Sea Level Anomalies (resolution 1/3˚×1/3˚) from Le Traon et al. (1998). The time series at each grid location are low-pass filtered with a cutoff timescale of 120 days to focus on the low-frequency variability. An EOF analysis is then carried out on the low-pass filtered data for the region 92˚W to 82˚W, 22.5˚N to 28˚N where the sea surface height anomalies in the model output are found. The analysis period is from 14 October 1992 to 23 January 2008. The first two EOF's explain 29.3% and 19.7% of the variance, respectively, and so, together, explain almost 50% of the variance. The spatial pattern of both EOF's (Figures 3.3a and 3.3b) is similar to the model anomaly pattern at the time of maximum transport through the Yucatan Channel (Figure 3.2e), be it with some displacement in the centres of action. However, as we shall see in the next paragraph, it is the second EOF whose principal component (PC) times series, at least during the CANEK period, is linked to the vertically integrated transport variability through the Yucatan Channel. The first EOF (Figure 3.3a), on the other hand, corresponds to the transition between transport maxima

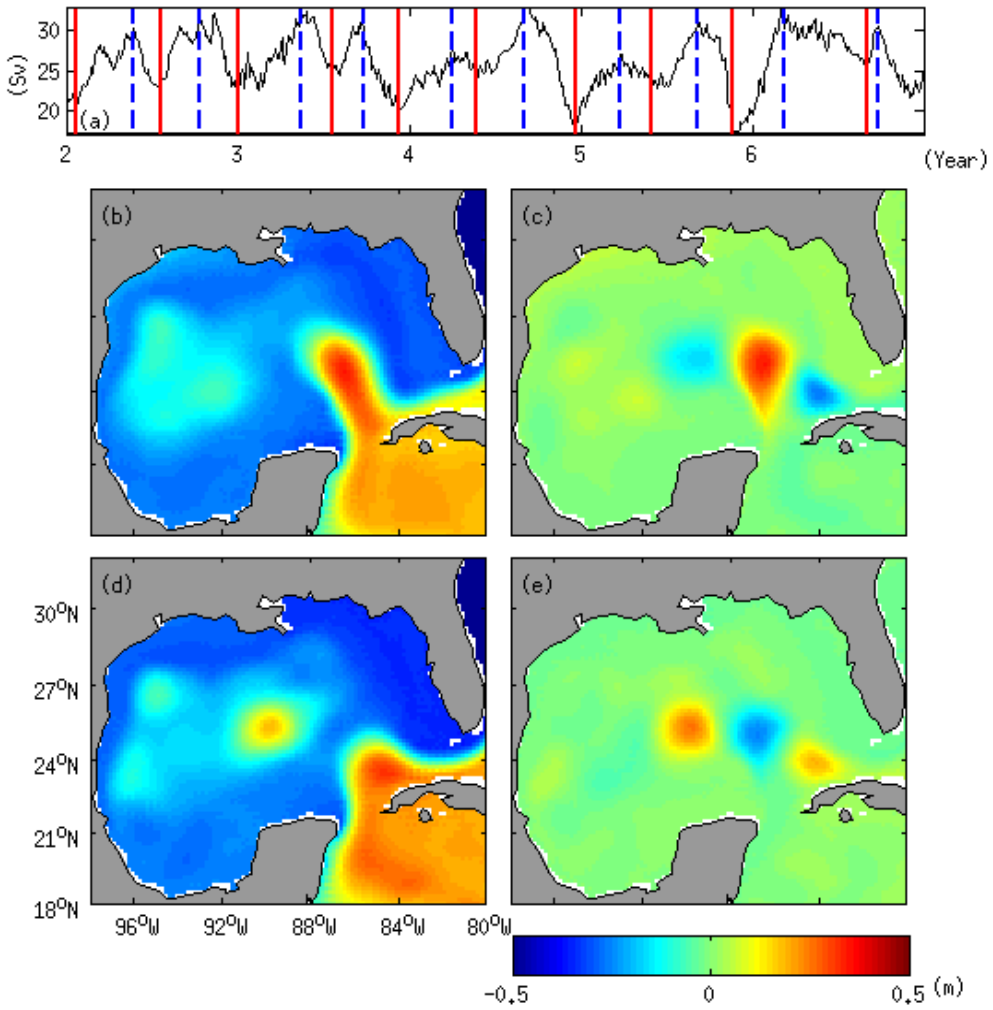

Figure 3.2. (a) Time series of the model-calculated transports (3-day average) through the Yucatan Channel from year 2 to 6, positive northward. Vertical dashed blue lines and solid red lines mark the transport maxima and minima through the Yucatan Channel respectively. (b) and (c) Composite plots of 3-day average sea surface height fields and associated anomalies calculated from model results corresponding to transport minima marked in (a). (d), (e) Similar to (b) and (c) but for the results corresponding to transport maxima marked in (a).

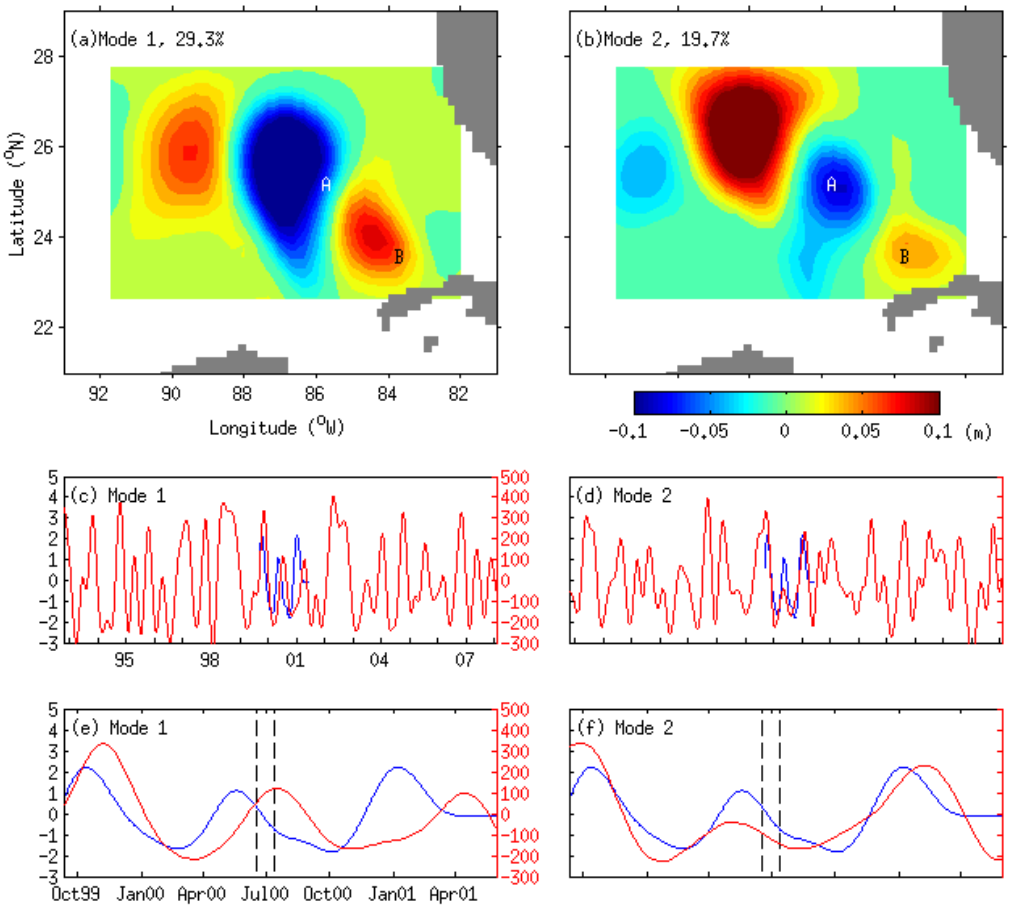

Figure 3.3. An empirical orthogonal function (EOF) analysis based on satellite altimeter data from 1992 to 2008 (low-pass filtered with a cutoff timescale of 120 days). Horizontal patterns of (a) the first EOF (29.3%) and (b) the second EOF (19.7%). Location A is at 25.0˚N, 86.0˚W and location B is at 23.5˚N, 84.0˚W. The corresponding principal component time series (red lines, units (non-dimensional) in red) for the first and second EOF's are shown in (c) and (d). Blue lines in (c) and (d) represent observed transport variations (low-pass filtered with a cutoff timescale of 120 days, in units of Sv (left hand axis)) of the Yucatan Current from the CANEK program. (e) and (f) are the same time series from (c) and (d) but shown only for the CANEK period. Observations of the Yucatan Current were not made over the period of about 1 month marked by vertical dashed lines in (e) and (f).

and minima and tends to vary in quadrature with the second mode. Indeed, the PC time series associated with the first two EOF's have a correlation of 0.6 (significant at the 99% level) with the first EOF lagging by 63 days (cf. Figures 3.3c and 3.3d).

Another data set available to us is the daily estimates of transport through the Yucatan Channel made during the CANEK program (Ochoa et al., 2001; Sheinbaum et al., 2002). The data come from two time periods: 10 September 1999 to 15 June 2000 and 13 July2000 to 31 May 2001. Since the gap between the two time periods is less than 1 month and we focus on low-frequency variations, we filled the gap with a linear interpolation and low-pass filtered the time series, as for the altimeter data, with a cutoff timescale of 120 days (see Figures 3.3e and 3.3f). We then compare the PC time series for the first two EOF's calculated from the satellite data with the vertically integrated transport through the Yucatan Channel (positive northward) estimated during the CANEK program. For the second satellite-based EOF mode (Figure 3.3d), going along with the sea surface height anomaly pattern shown in Figure 3.3b, the principal component time series varies synchronously with the observed transport time series (Figures 3.3d and 3.3f), consistent with what we noted earlier in the previous paragraph. The PC time series for the first satellite-based EOF mode also varies with the observed low-frequency transport variations through the Yucatan Channel, but lags the transport by about 50 days (Figures 3.3c and 3.3e). The lag is consistent with the previous discussion in which the first EOF mode corresponds to the transition phase during which transport is either increasing or decreasing.

We can now construct an index for measuring the influence of the Loop Current intrusion on Yucatan Channel vertically integrated transport variability. In particular, we take the difference between the sea surface height anomalies at locations B (23.5˚N, 84.0˚W) and A (25.0˚N, 86.0˚W) marked in Figure 3.3 ($\Delta SSH = SSHA_B - SSHA_A$). Rather than using the product of Le Traon et al. (1998), the sea surface height anomalies at B and A are calculated directly from the altimeter data. In particular, sea surface height anomaly variations at location B are calculated based on the satellite track crossing the location B southward about every 10 days, and sea surface height anomaly variations at location A are calculated based on the satellite track crossing the location A southward about 3 days later. Satellite altimeter data from Topex/Poseidon between 1992 and 2002

and data from JASON between 2002 and 2009 are used (both time series agree closely during the roughly 1-year period of overlap). The resulting difference (B – A) is then low-pass filtered, as before, with a cutoff timescale of 120 days. The satellite-based index (ΔSSH) is consistent with the low-frequency (low-pass filtered with a cutoff timescale of 120 days) transport estimates at the Yucatan Channel from CANEK from September 1999 to May 2001 (Figure 3.4). The correlation coefficient is 0.83. Unfortunately, given the shortness of the record from CANEK, the above comparison cannot conclusively demonstrate the existence of a link between Yucatan Channel transport variations and the Loop Current intrusion as measured by ΔSSH. Nevertheless, the above comparison is consistent with the existence of such a relationship and, as noted when discussing Figure 3.2, we know that such a relationship exists in models. In fact, although not shown here, the index calculated from the 5-year model results of Lin et al. (2009) can be used as an index for the low-frequency transport variations through the Yucatan Channel in that model. It should be noted, however, that factors other than Loop Current intrusion (e.g., wind forcing and Caribbean eddies; see Oey et al. (2003) and Chapter 5) can influence the vertically integrated transport through the Yucatan Channel so we do not expect an exact correspondence between the transport variations and ΔSSH. What ΔSSH approximates is the contribution to the Yucatan Channel vertically integrated transport variability that is driven by the interaction between the density anomalies arising from the Loop Current intrusion and the underlying variable bottom topography.

3.3 The Influence of Loop Current Intrusion on the Transport of the Florida Current

Based on 17 years of data, from 1992 to 2009, we can examine the relationship between the index, ΔSSH, defined above, and the transport of the Florida Current inferred from the Florida-Bahamas submarine cable at 27˚N (Baringer and Larsen, 2001). Synchronous cable data are used in the study (low-pass filtered with a cutoff timescale of 120 days, as for the altimeter data). The cable data are available for two periods, with the first period from 1992 to 1998 and the second period from 2000 to 2009.

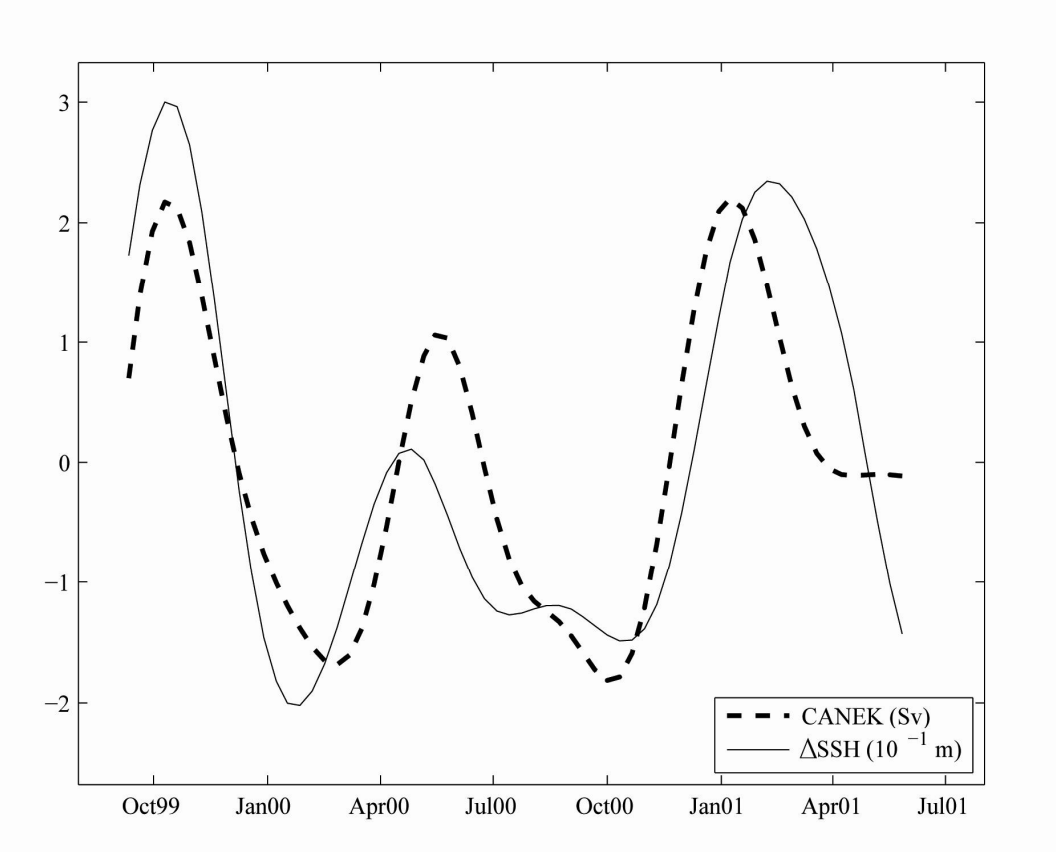

Figure 3.4. The index (ΔSSH, solid line) calculated from the sea surface height anomaly difference, location B minus location A, shown in Figure 3.3, based on the Topex/Poseidon sea surface height anomaly measurement (low-pass filtered with a cutoff timescale of 120 days). The dashed line represents transport anomaly estimates from CANEK (low-pass filtered with a cutoff timescale of 120 days) for the Yucatan Channel from 13 July 2000 to 31 May 2001, referenced to the long-term mean.

Figure 3.5 shows the 17-year time series of the index (ΔSSH) and the low-pass filtered cable transport estimates. Visual inspection suggests a relationship between ΔSSH and the transport variations of the Florida Current, although the relationship is clearly not exact. The correlation coefficient between the detrended time series for the whole period is 0.45 (significantly different from zero at the 99% level). During the first period of data overlap (1992 to 1998) the correlation is 0.41 and during the second period of data overlap (2001-2009), 0.5. We believe the physical basis for the relationship is as follows. The index ΔSSH has been chosen in such a way as to capture the signature in sea surface height anomaly of that part of the Yucatan Channel transport variability that is driven by the interaction between the density anomalies associated with Loop Current intrusion and the underlying variable bottom topography. Transport variability at the Yucatan Channel must, in turn, vary synchronously with the transport variability through the Straits of Florida between Cuba and Florida; otherwise, there will be an accumulation of water in the Gulf of Mexico which is not observed. In turn, transport variability through the Straits of Florida between Cuba and Florida must be compensated either through the channels north of Cuba or through the Straits of Florida between Florida and the Bahamas. It is the part through the latter that we believe is being picked up by our correlation analysis.

We can also use the time series of the sea surface height anomaly at location B alone (see Figure 3.3) to provide an index for comparison with the cable data. The motivation for using location B alone, rather than the difference in sea surface height anomaly between locations B and A, is that in the model of Lin et al. (2009) it is the fluctuations in density at the location B (see their figure 12, reproduced in this thesis as Figure 2.12) that are important for driving the associated vertically integrated transport anomalies through the Yucatan Channel. Figure 3.6a shows a comparison between the time series at location B and the difference B-A (i.e. ΔSSH) showing that, in fact, it is sea surface height anomaly at location B that dominates the difference B-A (the correlation is 0.86). Figure 3.6b compares the index time series calculated at location B alone and the cable data. The correlation over the whole time series is 0.37, and during the overlap periods 1992-1998 and 2001-2009 is 0.39 and 0.35, respectively. These correlations are lower than the corresponding correlations (0.45, 0.41, and 0.5, respectively) between the time series

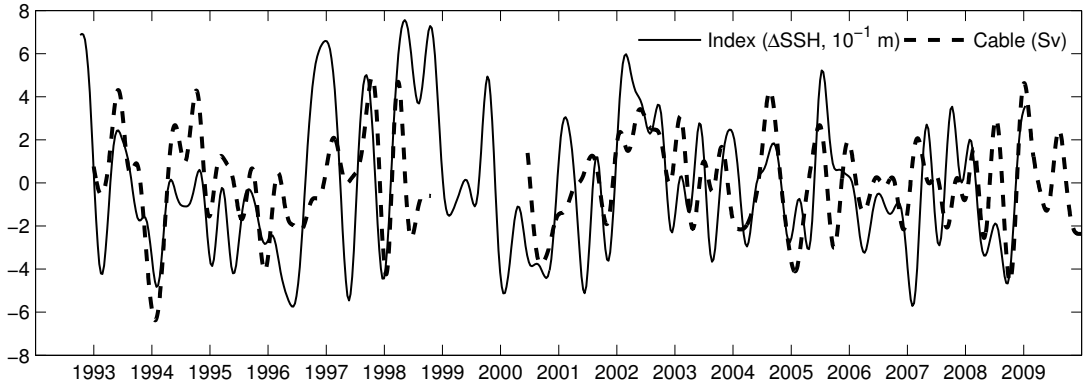

Figure 3.5. The sea surface height anomaly index, ΔSSH (solid line; units m), calculated for the period 1992 to 2009. Dashed lines (units: Sv) are the cable-estimated transport anomalies for the Florida Current and referenced to the long-term mean. All time series are low-pass filtered with a cutoff timescale of 120 days.

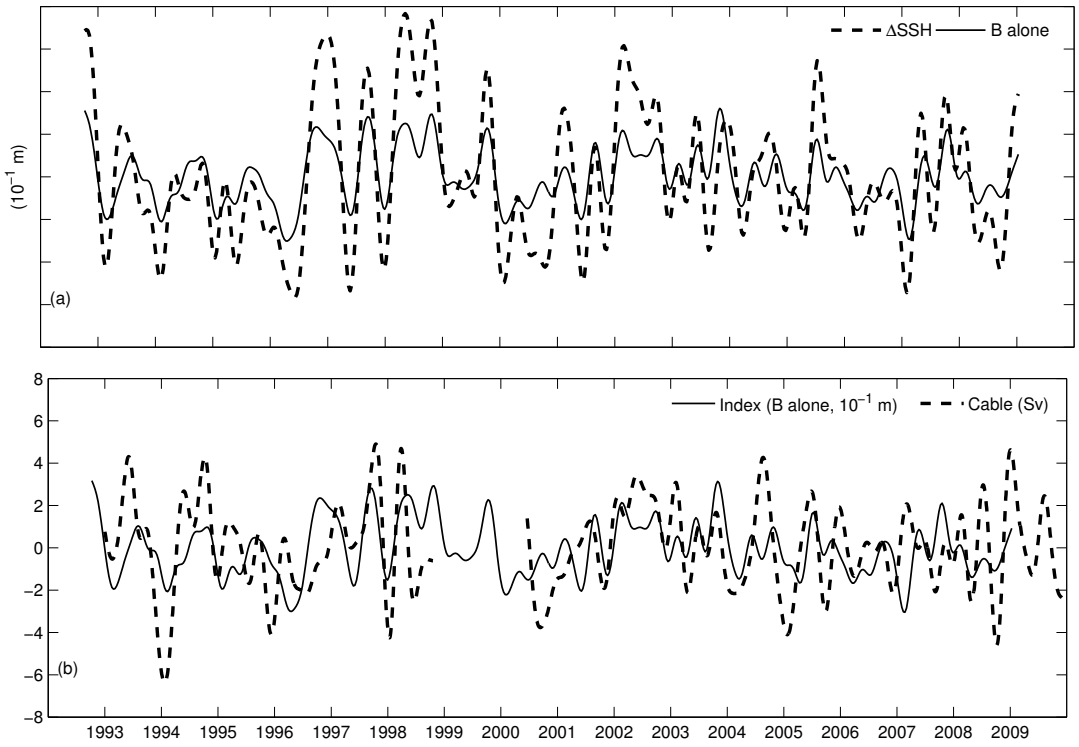

Figure 3.6. (a) Comparison between the time series of (1) the satellite-derived sea surface height anomalies at location B alone (solid line) and (2) the index ΔSSH that is the difference (B-A) in sea surface height anomalies between locations B and A in Figure 3.3 (dashed line) for the period 1992 to 2009. (b) Comparison between the sea surface height anomalies at location B alone (solid line; units m) and the cable-estimated transport anomalies (dashed lines; units Sv) for the Florida Current during the same time period, referenced to the long-term mean. All time series are low-pass filtered with a cutoff timescale of 120 days.

ΔSSH and the cable data found previously, suggesting that the full index, ΔSSH, is a better measure of Loop Current intrusion influence on vertically integrated transport variability between Florida and the Bahamas than the time series of sea surface height anomaly at location B alone.

Another data set available to use is the time series of transport estimates from the ship-of-opportunity platform "Explorer of the Seas" discussed by Beal et al. (2008) and available from 2002 onwards. These transport estimates are for the Florida Current at 26˚N just to the south of the entrance to the Northwest Providence Channel (see Figure 3.1b) and so are south of the location of the cable estimates but north of the Old Bahama Channel (the latter runs north of Cuba and in the model of Lin et al. (2009) is the main conduit for compensating transport variations at the Yucatan Channel). Figure 3.7a compares the index (ΔSSH) with the "Explorer of the Seas" transport estimates and also shows the cable data. A positive correlation between the index, ΔSSH, and the "Explorer of the Seas" time series (correlation 0.46 for detrended time series, significantly different from zero at the 99% level) can be seen from the beginning of 2003 onwards, although there are also times (e.g., earlier in 2002) when the two time series vary out-of-phase. The reasons for the out of phase behaviour are not known at this time but, clearly, there is the suggestion that other influences, perhaps local to the Straits of Florida, are at work. The correlation between the index, ΔSSH, and the cable data over the same time period is slightly lower (0.41), as we might expect given the presence of the Northwest Providence Channel between the location of the "Explorer of the Seas" cruise track and the submarine cable (see Figure 3.1b). Interestingly, sometimes out-of-phase behaviour can be seen (e.g., around January 2006) between the "Explorer of the Seas" and the cable data, suggesting an influence from the Northwest Providence Channel.

Figure 3.7b compares the time series of sea surface height anomaly from location B alone, rather than ΔSSH, with the "Explorer of the Seas" data. The results are quite similar. The correlation between the two detrended time series from 2003 onwards (0.33) is actually lower than when using ΔSSH (0.46). However, the correlation between the sea surface height anomaly from location B and the cable data over the same time period is very close (0.35).

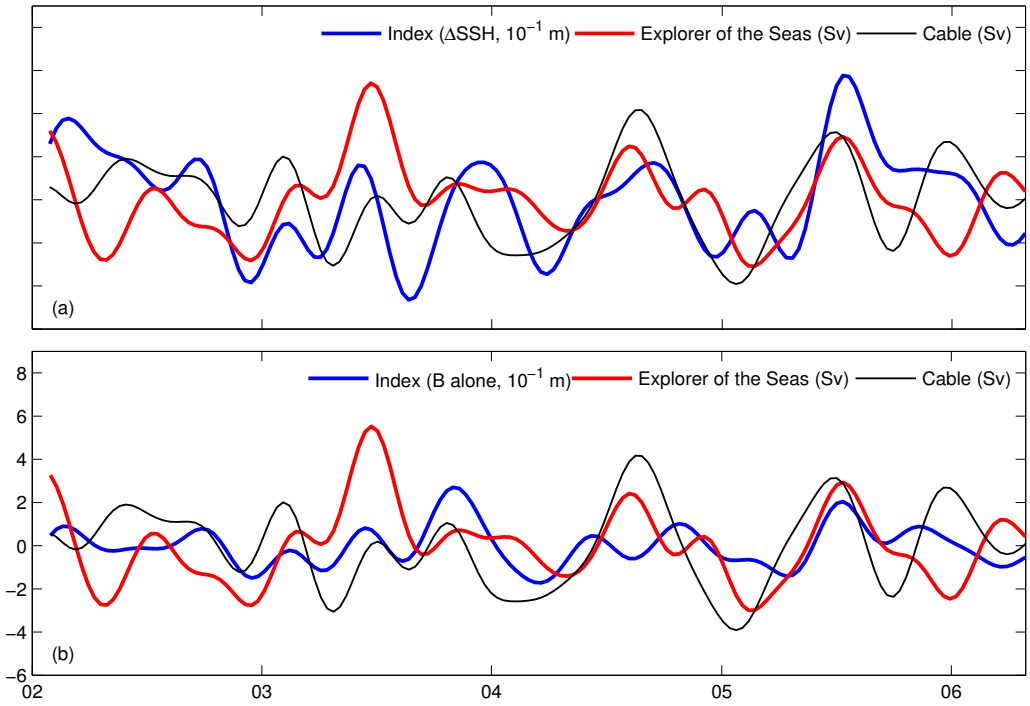

Figure 3.7. (a) Comparison between the index, ΔSSH (blue line; units m), and the estimates of the vertically integrated transport from the "Explorer of the Seas" data set for the period 2002 to 2006 (red line; units Sv), and referenced to the mean over the whole data set. The black line shows the cable-estimated transport anomalies in Sv for the Florida Current, referenced to the long-term mean. (b) Similar comparison but using the sea surface height anomalies at location B alone (blue line). All time series are low-pass filtered with a cutoff timescale of 120 days.

3.4 Summary and Discussion

The current system flowing through the Yucatan Channel and Straits of Florida is important because it is the major feeder for the Gulf Stream which, in turn, carries the upper limb of the North Atlantic Meridional Overturning Circulation, important for climate (e.g., Cunningham et al., 2007). We began by noting that many studies have emphasized the likely importance of either the continental slope north of the Straits (e.g., Anderson and Corry, 1985; Greatbatch et al., 1995) or westward propagation of long Rossby waves (DiNezio et al., 2009) for influencing the transport variations between Florida and the Bahamas, as estimated using submarine cables at 27˚N (see Figure 3.1; Larsen, 1992; Baringer and Larsen, 2001). Here, we have asked whether the cable transport estimates are affected by influences from upstream in the Gulf of Mexico and, in particular, the time-varying intrusion of the Loop Current into the Gulf of Mexico. We have introduced an index based on the difference in sea surface height anomalies between two locations in the southeastern Gulf of Mexico; one is centered at 25.0˚N, 86.0˚W and the other at 23.5˚N, 84.0˚W off the northwest coast of Cuba. These locations were chosen based on an EOF analysis of satellite altimeter data following guidance from a numerical model and comparison with the CANEK estimates of vertically integrated transport through the Yucatan Channel (although it should be noted that there are only 2 years of data from CANEK). The new index can be interpreted as a proxy for that part of the vertically integrated transport variations through the Yucatan Channel that are driven by the interaction between the density anomalies arising from the Loop Current intrusion and the underlying variable bottom topography, as discussed by Lin et al. (2009) and in Chapter 2. Given the geometric connectivity between the Yucatan Channel and the location of the submarine cable between Florida and the Bahamas, it is possible that intrusion-induced fluctuations in vertically integrated transport through the Yucatan Channel also have a signature in the cable-estimated transports of the Florida Current. We have presented evidence of such a link, in particular between the low-pass filtered sea surface height anomaly index (cutoff 120 days) based on satellite altimeter data and the low-pass filtered cable estimates of the vertically integrated transport variations between Florida and the Bahamas (see Figure 3.5). The correlation between the two detrended,

low-pass time series is 0.45 and is statistically significant at the 99% level, the first time such a relationship has been shown.

The physical basis for a connection between Loop Current intrusion and the transport through the Yucatan Channel is discussed in Lin et al. (2009) (see also Chapter 2), where it is shown that the transport is affected by the interaction between the density anomalies associated with Loop Current intrusion and the variable bottom topography between Florida and Cuba and, in particular, the associated pressure difference across the ridge connecting Cuba and Florida. For there to be no net accumulation of water in the Gulf of Mexico, the transport into the Gulf through the Yucatan Channel must be exactly balanced by the transport out through the Straits of Florida between the Florida and Cuba. However, not all the transport exiting the Gulf between Florida and Cuba has to pass between Florida and the Bahamas because of leakage through the Old Bahama and Northwest Providence Channels (Maul and Vukovich, 1993; Hamilton et al., 2005). It seems likely that significant transport variability does indeed take place through the channels north of Cuba. Only much more detailed field studies, such as presented by Hamilton et al. (2005), will be able to sort out exactly how the transport variations between the connecting channels are linked.

Chapter 4

A Numerical Study of Circulation and Associated Variability in the Intra-Americas Sea[1]

4.1 Introduction

The Intra-Americas Sea (IAS, Figure 4.1) plays a very important role as a conduit for mass, heat, salt and other tracers in the Atlantic circulation system. Circulation in the IAS is dominated by the throughflow that feeds the Gulf Stream (Mooers and Maul, 1998). The main flow (known as the Caribbean Current) from the Caribbean Sea passes through the Yucatan Channel as the Yucatan Current to form the Loop Current in the Gulf of Mexico (GOM). Water exits the IAS through the Straits of Florida between Florida and the Bahamas as the Florida Current. Although the mean general circulation in the IAS is reasonably understood, the main physical processes responsible for circulation variability in the IAS remains to be understood.

Circulation and hydrography at the Yucatan Channel were the subject of an intensive

---

[1] Lin, Y., J. Sheng, and R. J. Greatbatch, (2010b), A numerical study of circulation and associated variability in the Intra-Americas Sea, *Proceedings of the Eleventh International on Estuarine and Coastal Modelling*, published by American Society of Civil Engineers, Reston, VA, in press.

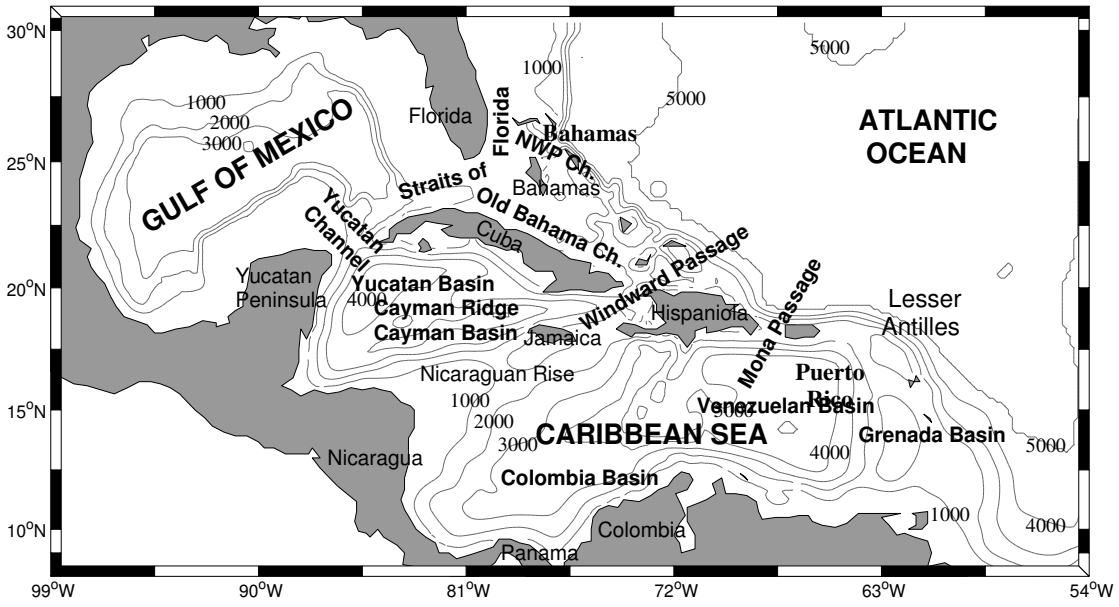

Figure 4.1. The domain and major topographic features of the circulation model for the Intra-Americas Sea. Depth contour interval is 1000 m. The model topography is based on 5-minute world topography and bathymetry (ETOPO5).

monitoring study during the CANEK field program (e.g., Sheinbaum et al., 2002) using shipboard Acoustic Doppler Current Profilers (ADCPs), hydrographic/velocity surveys using CTD and Lowered-ADCPs, and a current meter mooring array. The CANEK program was completed in June 2001. The Florida Current between Florida and the Bahamas has also been monitored almost continuously since the early 1980's using submarine cables (Baringer and Larsen, 2001).

The net accumulation of water in the GOM due to runoff and precipitation (or evaporation) is only on the order of 0.1 percent of the transports through the GOM (Etter, 1983). In addition, based on satellite altimetry measurements, the volume rate of change of the GOM is small (less than one percent of the transports through the GOM) (Bunge et al., 2002). As a result, the mean sea level rise in the GOM is ignored in the study, i.e. assuming of zero net accumulation of water in the GOM. Therefore the volume transport into the Gulf through the Yucatan Channel must be equal to the transport out through the Straits of Florida between the Florida and Cuba.

However, not all the volume transport exiting the GOM through the Straits of Florida between Florida and Cuba has to pass the transect between Florida and the Bahamas because of leakage through the Old Bahama (OB) and Northwest Providence (NWP) Channels to the north of Cuba (Hamilton et al., 2005). As discussed in Lin et al. (2009) and in Chapter 2, the correlation between the CANEK derived daily transports and the cable transport estimates (Figure 2.13) is only ~0.15 (a maximum correlation of about 0.28 with a lag of 14 days, Yucatan Channel transports leading). This suggests that a notable part of the Yucatan Channel transport variability passes northeast of Cuba and not between Florida and the Bahamas at the latitude of the submarine cable. A similar suggestion was also made previously by Hamilton et al. (2005) based on a monitoring program for the Straits of Florida carried out between December 1990 and November 1991. Lin et al. (2009) (see also Chapter 2) suggest that transport variations through the Yucatan Channel are partially compensated by flow variations through the channels north of Cuba (known as the "compensation effect").

Although the time-mean flow through the channels north of Cuba (the OB and NWP Channels) is small (Atkinson et al., 1995; Leaman et al., 1995), Hamilton et al. (2005) found that the estimated transport of the flow through the OB Channel (approximately)

varied significantly from -3.1 to 11.1 Sv during an 11-month period from December 1990 to November 1991. They also found that the estimated transport variations through the NWP Channel were between -4.5 and 3.9 Sv.

The Loop Current and its ring shedding phenomenon are important circulation features in the GOM. The detached Loop Current rings can extend up to a depth of 1500 m and the total volume of the ring can be up to ~7% of the total water volume in the GOM (Elliott, 1982). As a result, the detached rings should have a measurable impact on the heat budget on the GOM. At depths deeper than the sill depth of the Straits of Florida (~800 m), the GOM is only connected with the Caribbean Sea. The volume transport between the Caribbean Sea and the GOM is relatively small, but carries significant amounts of heat and oxygen (Rivas et al., 2005).

Lin et al. (2009) (see also Chapter 2) discussed the main physical process for a connection between Loop Current intrusion and the transport through the Yucatan Channel and demonstrated that the transport through the GOM is affected by the interaction between the density anomalies associated with Loop Current intrusion and the variable bottom topography between Florida and Cuba. This suggests that skills of a numerical model could be improved significantly by adjusting isopycnals over the Loop Current region using data assimilation. The main objectives of the study in this chapter are to (1) generate realistic circulation and associated variability in the IAS using a regional, three-dimensional, data-assimilative, ocean circulation model, and (2) improve our understanding of hydrodynamics of the observed flow and associated variability made by the CANEK program and the cable data during the period between 13 July 2000 and 31 May 2001 based on model results.

The remainder of this chapter is arranged as follows. Section 4.2 describes the regional ocean circulation model used in our study. Section 4.3 presents the comparison between model results and observations. Section 4.4 discusses the compensation effect between the Yucatan Channel and the channels north of Cuba. The final section is a summary.

4.2 Model Setup and External Forcing

The regional ocean circulation model used in this study is the primitive-equation ocean general circulation model known as CANDIE (the CANadian version of DIEcast, Sheng et al., 1998). CANDIE was earlier successfully applied to address various simulating problems including the seasonal circulation in the northwestern Atlantic Ocean (Sheng et al., 2001) and the general circulation over the western Caribbean Sea (Sheng and Tang, 2003 and 2004; Tang et al., 2006).

The model domain covers the Intra-Americas Sea between 99˚W and 54˚W and between 8˚N and 32˚N (Figure 4.1), with a horizontal resolution in both latitude and longitude of 1/6˚. The topographic data used in the model are 5-minute world topography and bathymetry dataset known as ETOPO-5. The model uses 32 z-levels in the vertical, with a vertical resolution of 5 m for the top z-level, gradually expanding resolutions from 10 - 100 m for the following 12 z-levels, 100 m for the following 11 z-levels, and coarser vertical resolutions (up to 500 m) for the last 8 z-levels. No partial cells are used in the model in this study.

The model uses fourth-order numerics (Dietrich, 1998) and Thuburn's (1996) flux limiter for the nonlinear advection terms (Thuburn, 1996). The Smagorinsky sub-grid scale mixing scheme is used for the horizontal eddy viscosity and diffusivity coefficients with the minimum value set to 1.5 m^2 s^{-1}. The parameterization of Large et al. (1994) is used for the vertical eddy viscosity and diffusivity coefficients.

The regional ocean circulation model of the IAS is forced by 6-hourly wind fields produced by the National Centers for Environmental Prediction (NCEP). The net heat flux at the sea surface is calculated using the bulk formulae taken from Gill (1982), including terms of the solar radiation into the ocean, the net upward flux of long-wave radiation from the ocean, the latent heat flux carried by evaporated water, and the sensible heat flux from the ocean to the atmosphere. These terms are calculated using empirical formulas based on 6-hourly NCEP fields (e.g., air temperature, wind speed, and relative humidity) and model-calculated sea surface temperature. The sea surface salinity in the model is restored to 5-day averaged salinity extracted from global ocean circulation reanalysis fields (with a horizontal resolution 1/4˚×1/4˚) produced by the British

Atmospheric Data Centre (BADC) with a restoring timescale of 20 days. Although the freshwater input from rivers in the study region are not explicitly specified in the ocean circulation model, their effects are included partially by the surface salinity restoration to the BADC data.

At lateral solid (or closed) boundaries, the normal flow, tangential stress, and normal fluxes of potential temperature and salinity are set to zero (free-slip and insulating boundary conditions). Along the model open boundaries, the normal flow, temperature and salinity fields are adjusted using a method similar to the adaptive open boundary conditions suggested by Marchesiello et al. (2001). We first use an explicit Orlanski radiation condition to determine whether the open boundary is passive (outward propagation) or active (inward propagation). If the open boundary is passive, the model prognostic variables are radiated outward to allow any perturbation generated inside the model domain to propagate outward as freely as possible. If the open boundary is active, the model prognostic variables at the open boundary are restored to the BADC fields (including 5-day mean currents, temperature and salinity) at each z level with a timescale of 5 days. Finally, the barotropic components of the normal currents at the model open boundaries (Ψ_{NOB}) are specified based on the combination of depth-integrated normal flows calculated from 5-day BADC reanalysis fields (Ψ_{BADC}) and high-frequency (daily) transport correction term diagnosed from the model results. The correction term is calculated based on the differences between the observed transports (cable data, Ψ_{cable}) and model-produced transports of the Florida Current (Ψ_{FC}) between Florida and the Bahamas using the following approach:

$$\psi_{NOB} = \psi_{BADC} + K(\psi_{cable} - \psi_{FC}) \tag{4.1}$$

where K is the transfer function (Zhai and Sheng, 2008) that interpolates differences between observed and model-produced transport of the Florida Current between Florida and the Bahamas onto model grids along the north open boundary. In this study, the transfer function *K* is computed from previous non-data-assimilative model results based on a multiple linear simultaneous regression between the model-produced transport between Florida and the Bahamas (Ψ_{FC}) at 26.8 ˚N (the same site as the cable data) and

the depth-integrated transport through the north open boundary (Ψ_{NOB}, specified based on the BADC data).

The physically-based data assimilation scheme suggested by Cooper and Haines (1996) is used in this study, which is characterized by a homogeneous vertical shift of isopycnals with no change in the bottom pressure. In this study, the 7-day Merged Maps of Sea Level Anomalies (MSLA's) with a horizontal resolution of 1/3˚ derived from satellite altimeter data (Le Traon et al., 1998) are horizontally interpolated into model interior grid points based on this data assimilation scheme. Mean sea level distribution is achieved from a 6-year model integration before applying the altimeter data assimilation. The altimeter data is assimilated into the model every 7 days without temporal interpolation.

The regional ocean circulation model is initialized using the BADC reanalyzed potential temperature and salinity on 1 January 1999 and integrated for three years from January 1999 to December 2001. Based on the model calculated kinetic energy per unit volume (not shown), the regional ocean circulation model reaches a statistical equilibrium state after 300 days of spin-up. Hence, model results between 13 July 2000 and 31 May 2001 are used for analysis in this study. During this period observational transport estimates for the Yucatan Current (from the CANEK data) and the Florida Current (from the cable data) are both available.

4.3 Model Results and Validation

We first assess the model performance by comparing the time-mean volume transport calculated from model results with the observational estimates of the transport discussed in the literature during the study period (from 13 July 2000 to 31 May 2001). In the model, the time-mean transport between Florida and the Bahamas (Ψ_{FC}) is ~28.6 Sv, which is slightly less than the observed transport of ~30.7 Sv estimated from the cable data (Baringer and Larsen, 2001), of which the difference is due mainly to smaller volume transport specified at the north open boundary condition in the model. The time-mean transport through the Yucatan Channel (Ψ_{YC}) produced by the model is ~27.5 Sv, which is larger than the mean transport of 23.2 Sv estimated from the CANEK

observations (e.g., Sheinbaum et al., 2002), but comparable to the transport estimate made by Johns et al. (2002). Our model-produced mean transport through the Yucatan Channel is also consistent with the high resolution model results of Cherubin et al. (2005). The model-calculated time-mean transport through the Old Bahama and Northwest Providence Channels combined is ~1.1 Sv, which is slightly less than the estimates made from observations during different periods (e.g., Atkinson et al., 1995; Leaman et al., 1995; Hamilton et al., 2005). Figure 4.2 shows the time-mean surface currents (2.5 m) and volume transport stream function from model results for the period between 13 July 2000 and 31 May 2001. The mean circulation and transport through the major channels in the IAS produced by the model are comparable with previous numerical results (e.g., Smith et al., 2000) and observations in the region (Johns et al., 2002).

The time-mean potential temperature distribution at the Yucatan Channel produced by the model compares well with the observations during the CANEK program (Figures 4.3a and b), with both observed and simulated isotherms being tilted toward the surface in the western upper layer of the channel. This is required to geostrophically balance the intense northward flow. The time-mean observed northward flow at the Yucatan Channel during the CANEK program was characterized by an intense northward flow into the GOM in the western upper part of the Yucatan Channel and relatively weaker and southward flow on the eastern upper and bottom layers (Figure 4.3c). A similar profile of the time-mean northward flow at the Yucatan Channel (~22 °N) is produced by the model (Figure 4.3d).

Figure 4.4 shows the model-calculated and observed daily transport anomalies (time-mean removed) of the Florida and Yucatan Currents during the study period. The regional ocean circulation model has certain skills in hindcasting the low-frequency variability in the observed transports during this period. Correlation between model-produced transport variations through the Straits of Florida between Florida and the Bahamas and observational cable data is ~0.70. Correlation between model-produced transport variations through the Yucatan Channel and observations is only ~0.34, which is relatively low. It should be noted that the regional ocean circulation model has a deficiency in reproducing high-frequency transport variations through the Yucatan Channel estimated by the CANEK program (Figure 4.4), which could be partially due to

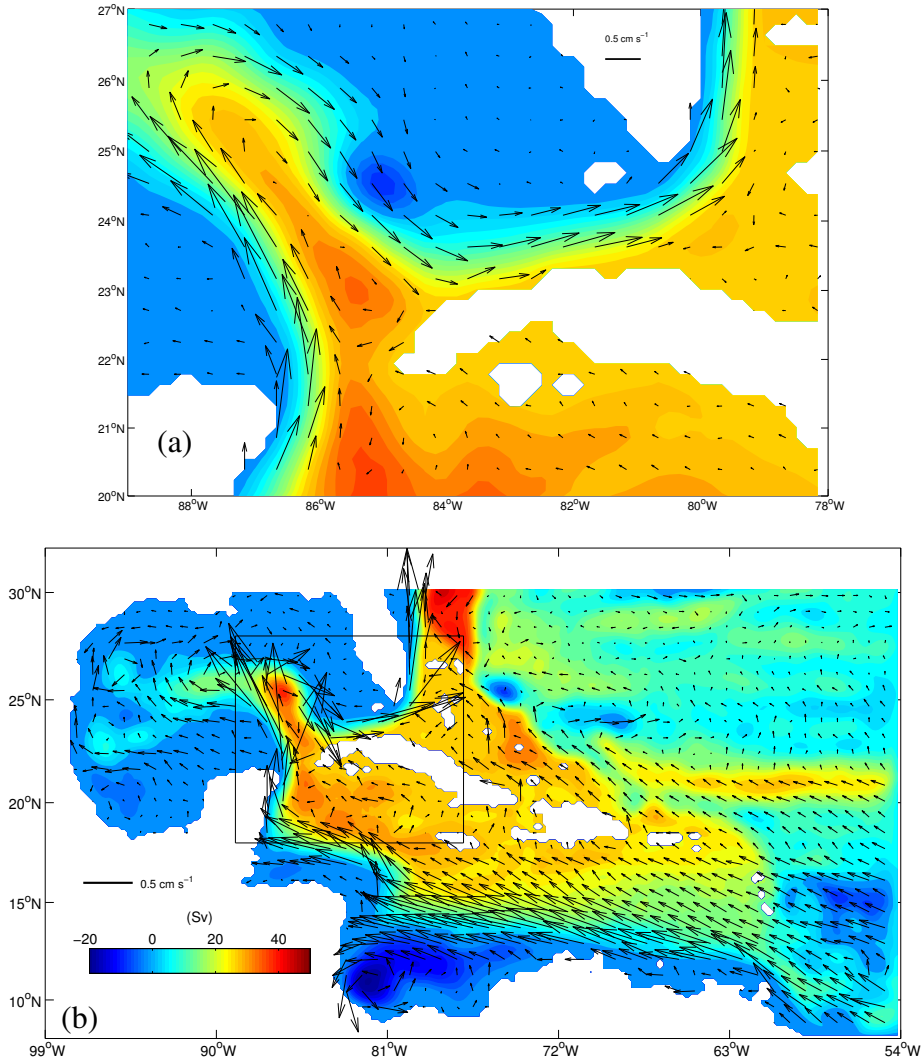

Figure 4.2. Time-mean surface currents (2.5 m, black arrows) and volume transport stream function (image) computed from model results during the period between 13 July 2000 and 31 May 2001 over (b) the IAS and (a) a sub-region covering the Yucatan Channel and adjacent areas marked by solid lines in (b). Velocity vectors are plotted at every 3rd and 6th grid point in (a) and (b), respectively.

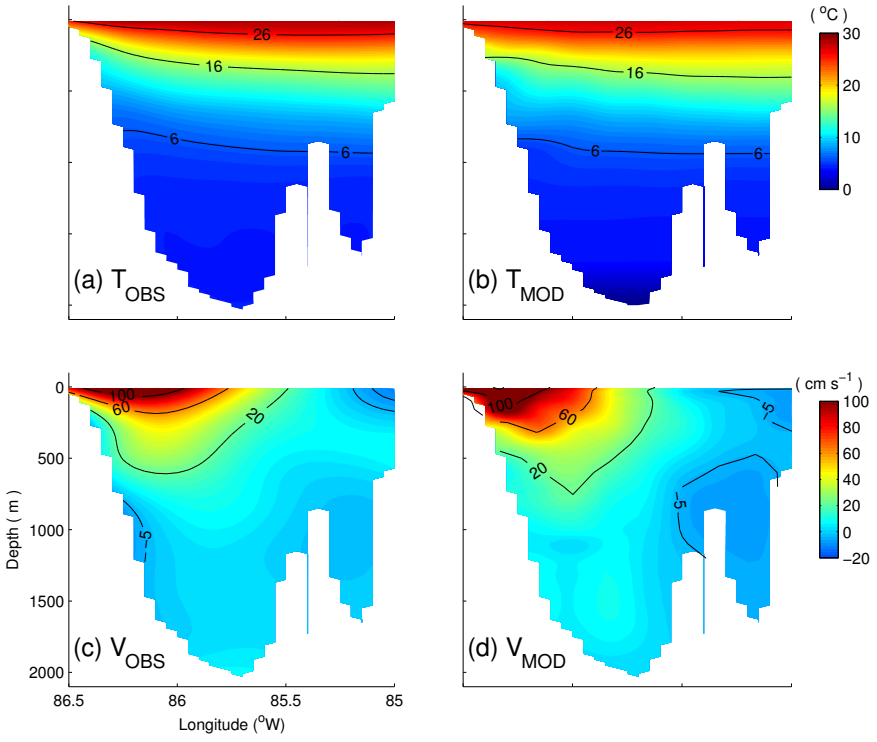

Figure 4.3. Time-mean potential temperature (top panels) and northward velocity (lower panels) between CANEK observations (left) and model results (right) at the Yucatan Channel during the period between 13 July 2000 and 31 May 2001. Model results are interpolated and extrapolated to the observation points.

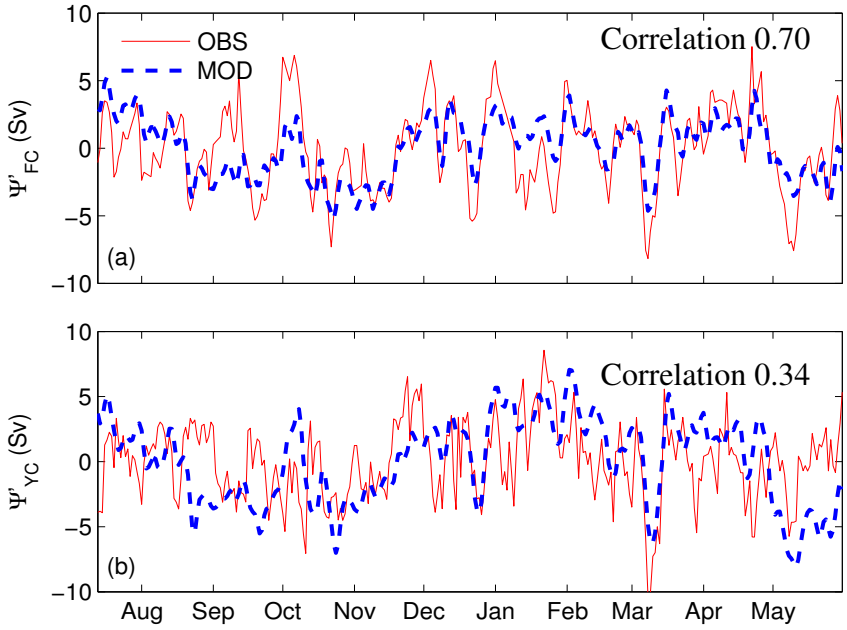

Figure 4.4. Model calculated (blue dashed lines), and observed (red solid lines) daily mean transport anomalies (time-mean removed) of the (a) Florida Current through the Florida-Bahamas section (27˚N) and (b) Yucatan Current through the Yucatan Channel (22˚N) during the period between 13 July 2000 and 31 May 2001. Positive values mean northward.

the coarse horizontal resolution of the model to resolve small-scale circulation features in the region and the resolution of the model forcing such as the wind fields.

The data-assimilative ocean circulation model also has reasonable skills in reproducing the Loop Current ring shedding, Caribbean eddies, and other mesoscale eddies in the GOM as expected. During the study period, there is one shedding event observed in early 2001. In comparison with the satellite remote sensing observations (Figures 4.5g and h), the ocean circulation model reproduces reasonable well the ring shedding in the GOM. The ring separation takes about a month in the model. From model results we found that, on 21 March 2001, the Loop Current intrudes strongly into the eastern GOM (Figure 4.5a), with an anticyclonic eddy centered at about (90.0°W, 26.0°N) tending to separate from the Loop Current. There is a pool of anomalously warm water off the northwest coast of Cuba, in association with a negative sea surface height anomaly to the farther northwest (Figure 4.5c). This anticyclonic eddy has detached completely from the Loop Current by 25 April 2001 (Figure 4.5b). After retreating, the Loop Current starts the next intrusion process. The negative and positive centers in sea surface height anomalies move away from Cuba continuously in a northwestward direction (Figure 4.5d). The ocean circulation model also reproduces other mesoscale eddies observed in the IAS, such as those on the continental shelf slope of the western GOM and the Mexican Caribbean Sea. Overall, the ocean circulation model shows a similar level of performance to that of other regional ocean models used previously (Oey et al., 2003).

An additional model experiment is conducted, in which satellite altimeter data assimilation and the correction term (Equation 1) are not used. The model experiment without data assimilation uses the same surface and boundary forcing as the model run with data assimilation. A comparison of model results with (Figures 4.5c and d) and without data assimilation (Figures 4.5e and f) demonstrates that data assimilation improves the model's accuracy in simulating mesoscale eddies in the IAS. For example, more realistic sea surface height anomalies in the western GOM are found in the data-assimilative model results on both 21 March 2001 and 25 April 2001 (Figures 4.5c-h). Smaller positive sea surface height anomaly is found at the south of the Yucatan Channel (near Cuba) in Figure 4.5d for model results with data assimilation, which is

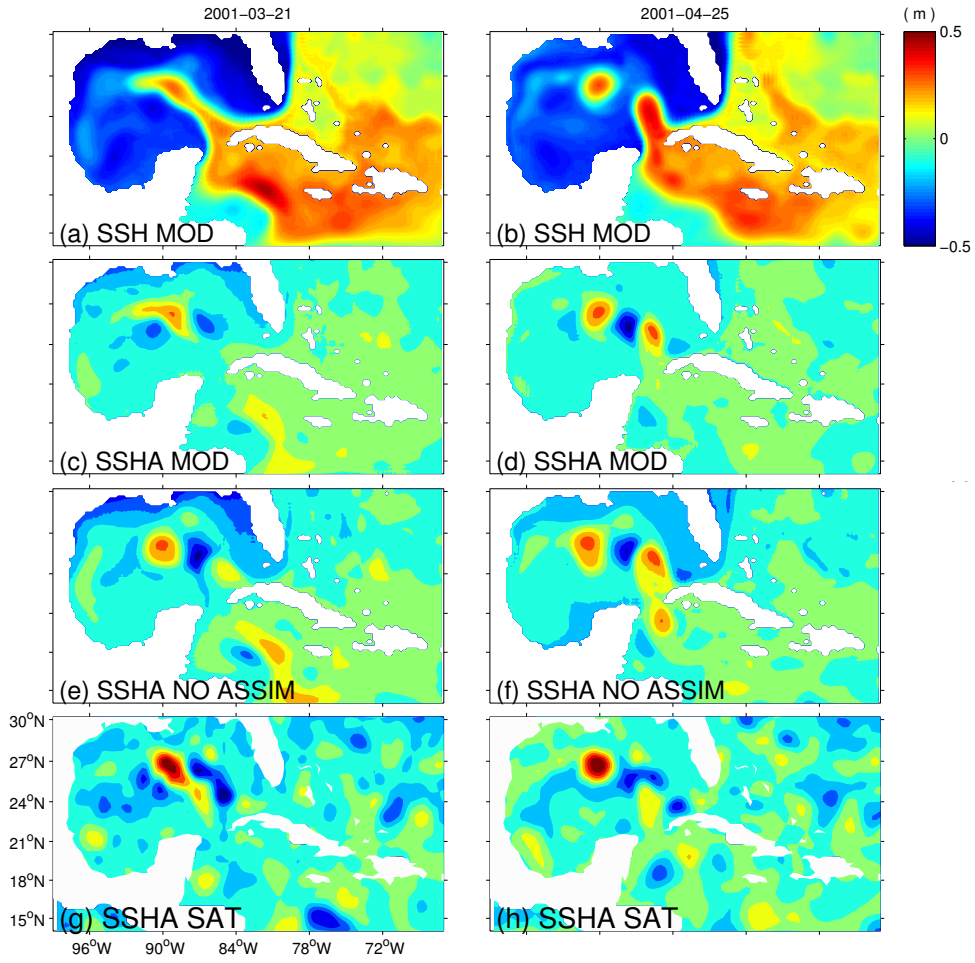

Figure 4.5. Snapshots of model-calculated Sea Surface Height (SSH) fields on (a) March 21, 2001 and (b) April 25, 2001 during a Loop Current ring shedding event. Model-calculated SSH anomalies with (c and d) and without (e and f) data assimilation, and associated satellite altimeter observations (g and h) are compared.

more in line with satellite remote sensing observations (Figure 4.5h).

Previous observational and numerical studies (e.g., Bunge et al., 2002 and Cherubin et al., 2005) used the 6˚C isotherm as the interface separating the upper and lower layers for the Yucatan Channel. The lowest temperature observed in the Straits of Florida is ~6˚C (Bunge et al., 2002), and the flow below the 6˚C isotherm at the Yucatan Channel can then be regarded as the deep circulation. The typical depth of the 6˚C isotherm estimated from the observed and model-produced temperature fields at the Yucatan Channel is about 1000 m (Figures 4.3a and b). For convenience in this study we define the deep flow through the Yucatan Channel as the currents below 1000 m.

We compute temperature transports, using temperature in degrees Celsius, in the upper (above 1000 m) and lower (below 1000 m) layers through the Yucatan Channel during the study period using model results and the CANEK data. A comparison of observed and model-calculated temperature transports is shown in Figure 4.6. The model-produced temperature transport variations through the upper and lower layer at the Yucatan Channel are comparable to the estimates from CANEK observations at low frequency. However, the correlation coefficient between model-calculated and observed temperature transport variations is only 0.29 and 0.26 at the upper and lower layers respectively. Figure 4.6 also demonstrates that the ocean circulation model has less hindcast skills in reproducing the high-frequency variability in the observed northward temperature transport, which is mainly due to the discrepancy between modeled and observed volume transports through the Yucatan Channel on short timescales (Figure 4.4b).

4.4 Compensation Effect Through Channels North of Cuba

The concept of the compensation effect in the IAS was recently suggested by Lin et al. (2009) (see also Chapter 2). It is referred to as fluctuations in transport through the Yucatan Channel compensated, at least partially, by flow north of Cuba. Figure 4.7 demonstrates that the correlation coefficient at zero lag between the model-calculated transport time series for the Florida Current between Florida and the Bahamas (Ψ_{FC}) and for the Yucatan Channel (Ψ_{YC}) is ~0.85, which is significantly different from zero at the

99% level. As noted in the introduction, the relationship between the two transport time series based on the cable data and the CANEK program is very much weaker (indeed, the correlation at zero lag between the measured transport estimates is only ~0.15). It is possible that the model overestimates the link between the variations in transport of the Florida and Yucatan Currents. On the other hand, the low correlation between the CANEK- and cable-estimated daily transport estimates could also be due to the accuracy of the observational data. For example, the mean transport through the Yucatan Channel from the CANEK data set is considerably less than the mean transport for the Florida Current between Florida and the Bahamas verified over many years against mooring observations from Baringer and Larsen (2001). The difference of more than 8 Sv is roughly twice of the transport estimated for the passages north of Cuba by Atkinson et al. (1995) and Leaman et al. (1995) (see also Johns et al, 2002). Only further detailed monitoring efforts, especially at the Yucatan Channel at which has been much less monitored than the Florida Current between Florida and the Bahamas, will be able to resolve this issue.

On the other hand, correlation analysis shows a negative correlation significantly different from zero (~ -0.75) between Ψ_{YC} and the model-calculated transport time series for the OB Channel (Ψ_{OB}). There is also a significant negative correlation coefficient (~ -0.58) between Ψ_{YC} and the model-calculated transport time series for the NWP Channel (Ψ_{NWP}), which is relatively weak compared with the compensation effect through the OB Channel. The (negative) correlation between Ψ_{YC} and the model-calculated transport time series for the NWP Channel (Ψ_{NWP}) and between Ψ_{FC} and Ψ_{NWP} is even weaker. It follows that in the model some form of "compensation effect" is operating in the model through the passageways north of Cuba (i.e. the OB and NWP Channels), and it is the transport variations through the OB Channel that mostly contribute to the compensation effect, with relatively less role for the NWP Channel.

A comparison of the model-calculated transport anomalies (i.e. differences from the time mean) for Ψ'_{YC}, $-\Psi'_{ON}$, and $-\Psi'_{WW}$ is shown in Figure 4.8, where Ψ'_{YC} presents the northward transport anomalies through the Yucatan Channel, Ψ'_{ON} presents the northwestward transport anomalies through the OB and NWP Channels, and Ψ'_{WW} presents the northeastward transport anomalies through the Windward Passage. There is a

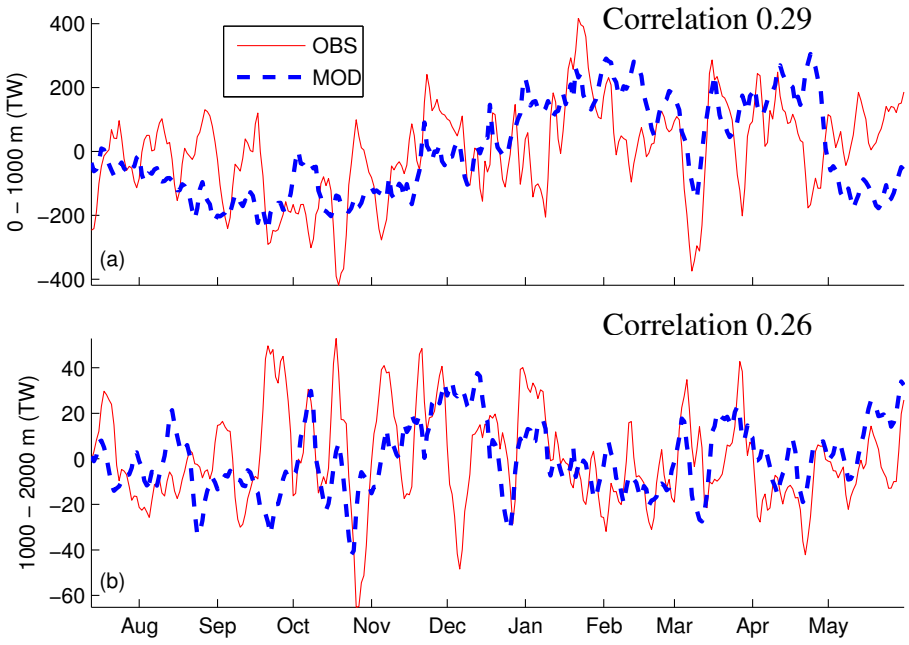

Figure 4.6. Model calculated (blue dashed lines), and observed (red solid lines) northward temperature flux anomalies (time-mean removed, in units of TW) through the Yucatan Channel in (a) the upper layer (0 – 1000 m) and (b) the lower layer (1000 m – 2000 m) during the period between 13 July 2000 and 31 May 2001.

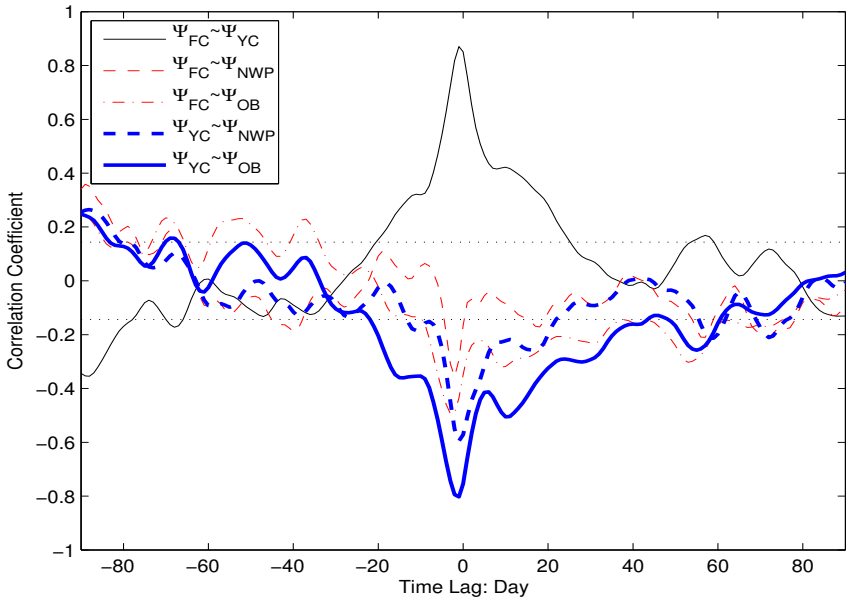

Figure 4.7. Correlation coefficients between transport anomalies of the Florida Current between Florida and the Bahamas (Ψ'_{FC}), the Yucatan Current (Ψ'_{YC}), the flow through the Northwest Providence Channel (Ψ'_{NWP}), and the flow through the Old Bahama Channel (Ψ'_{OB}) calculated from model results during the period between 13 July 2000 and 31 May 2001. Correlations outside the dotted lines are significantly different from zero at the 99% level. Positive values in Ψ'_{FC} and Ψ'_{YC} mean northward, and positive values in Ψ'_{OB} and Ψ'_{NWP} mean northwestward.

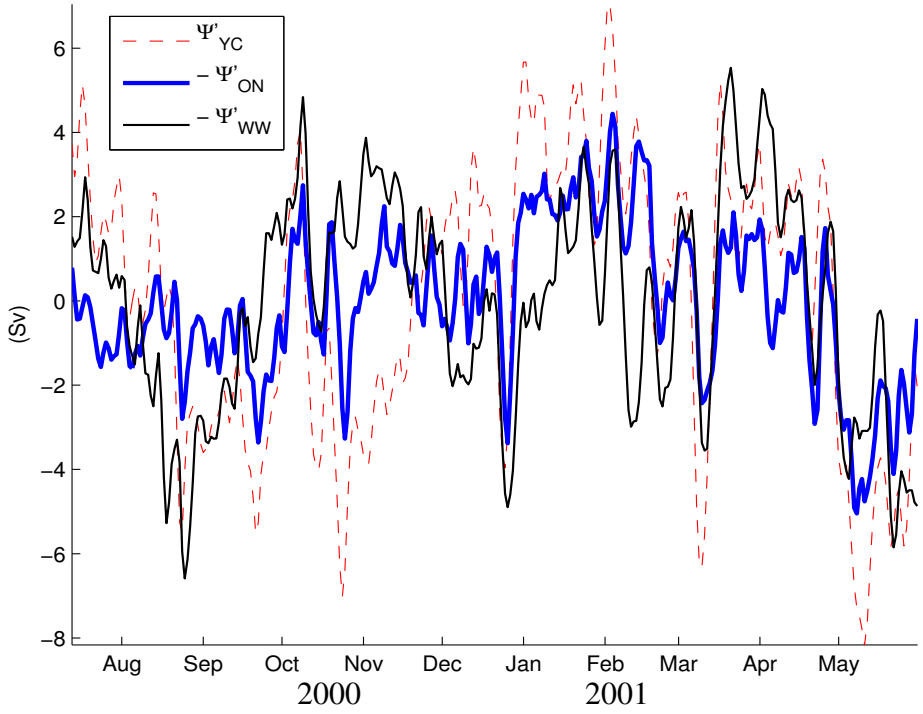

Figure 4.8. Comparison between model-calculated transport anomalies (time mean removed) through the Yucatan Channel (Ψ'_{YC}, red dashed line), the Old Bahama and Northwest Providence Channels ($-\Psi'_{ON}$, blue solid line) and the Windward Passage ($-\Psi'_{WW}$, black solid line) during the study period between 13 July 2000 and 31 May 2001. Ψ'_{YC} presents the northward transport anomalies through the Yucatan Channel. Ψ'_{ON} presents the northwestward transport anomalies through the Old Bahama and Northwest Providence Channels. Ψ'_{WW} presents the northeastward transport anomalies through the Windward Passage.

close relationship between these three time series, except for some events in November 2000 and January 2001 which require further studies. Correlation between Ψ'_{YC} and $-\Psi'_{ON}$ is ~0.76, between Ψ'_{YC} and $-\Psi'_{WW}$ is ~0.45, and between $-\Psi'_{ON}$ and $-\Psi'_{WW}$ is ~0.55 (Correlations greater than 0.14 are significantly different from zero at the 99% level). In particular, when Ψ'_{YC} increases, there is a corresponding increase in the southeastward flow through the OB and NWP Channels and also increased southwestward flow through the Windward Passage, implying an anomalous clockwise circulation around Cuba, with the opposite situation applying when Ψ'_{YC} is decreased.

Model-calculated northward velocity anomalies (time-mean removed) through the Yucatan Channel at different depths (cross-channel average) during the study period (from 13 July 2000 to 31 May 2001) are shown in Figure 4.9. There are several events during this period at the upper layer of the channel (0 – 1000 m), notably the large southward flow in November 2000 and large northward flows in the first half of 2001. The deep flow through the Yucatan Channel (1000 – 2000 m) is correlated with the Loop Current intrusion (e.g., Bunge et al., 2002 and Cherubin et al., 2005). Significant vertical structure variations of the flow at the Yucatan Channel are found in strong correlation with the Loop Current ring shedding and intrusion during December 2000 and May 2001 (Figure 4.9).

In their figure 10 (reproduced in this thesis as Figure 2.10), Lin et al. (2009) demonstrated that at high frequencies (timescale less than 30 days) westward (along the OB Channel) wind stress is important for the transport variations through the OB Channel. While for timescale longer than 30 days, the Loop Current evolution plays a significant role on the compensation transport anomalies through the OB Channel. Considering the link between the vertical structure of the flow through the Yucatan Channel, the Loop Current evolution, and the compensation effect (through the OB and NWP Channels), we now investigate the compensation effect for the upper and lower layers at the Yucatan Channel separately. Figure 4.10 shows the correlation between model-calculated northwestward transport anomalies through the OB and NWP Channels (Ψ'_{ON}) and transport anomalies (1) through the whole Yucatan Channel (Ψ'_{YC}, black dashed lines), (2) through the upper layer ($\Psi'_{YC\ 0\text{ - }1000\ m}$, red lines), (3) through the lower layer at the Yucatan Channel ($\Psi'_{YC\ 1000\text{ - }2000\ m}$, blue lines) separately.

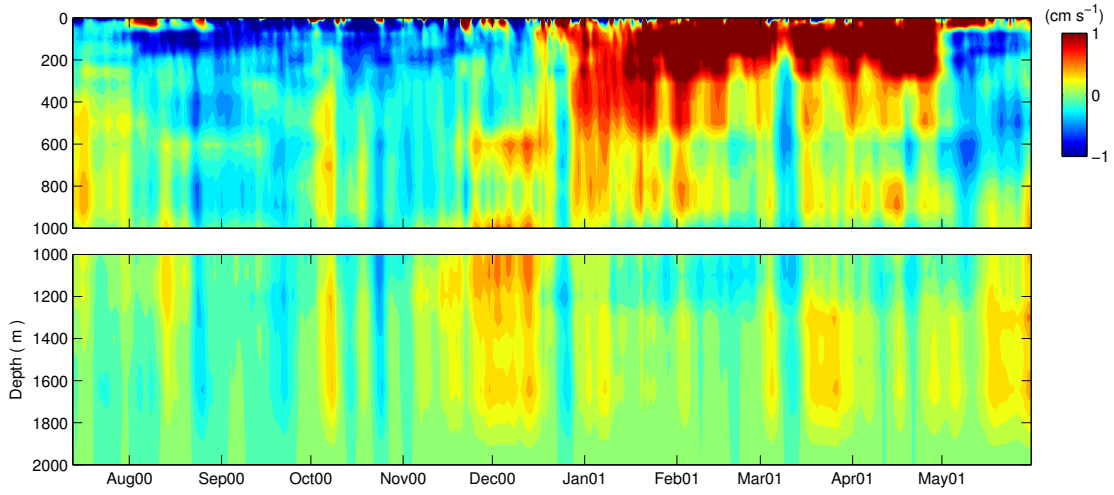

Figure 4.9. Model-produced northward velocity anomalies (time-mean removed) through the Yucatan Channel at different depths (cross-channel average) during the study period between 13 July 2000 and 31 May 2001.

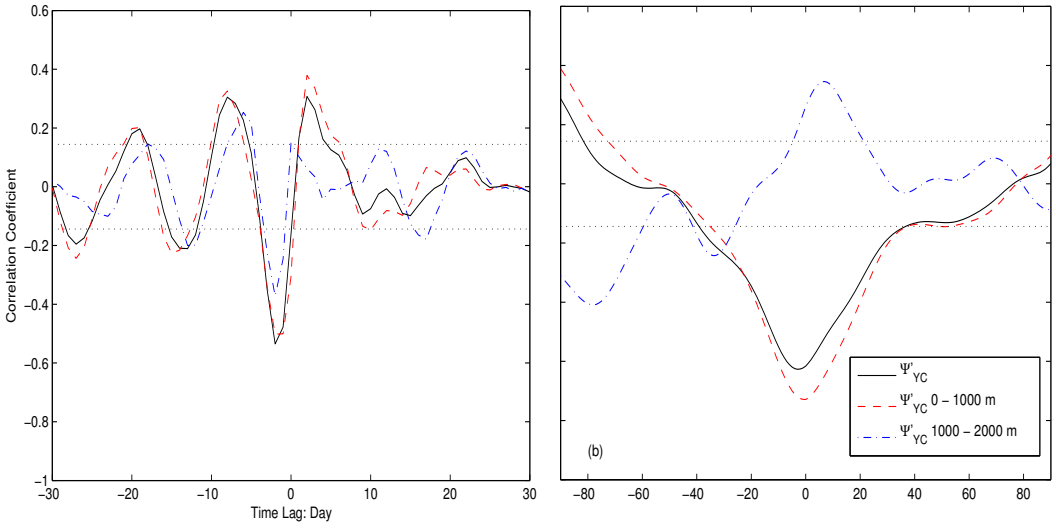

Figure 4.10. Correlation coefficients between the transport through channels north of Cuba and (1) the transport through the Yucatan Channel (black solid lines), (2) the transport through the upper layer Yucatan Channel (0 - 1000 m, red dashed lines), (3) the transport through the lower layer Yucatan Channel (1000 - 2000 m, blue dash-dotted lines), using (a) 20-day high-pass filtered model results and (b) 20-day low-pass filtered model results during the study period between 13 July 2000 and 31 May 2001. Correlations outside the dotted lines are significantly different from zero at the 99% level.

Using high-pass filtered model results (with a cutoff timescale of 20 days), the minimum correlation coefficient between Ψ'_{ON} and Ψ'_{YC} is about -0.53 at almost zero lag and is significantly different from zero at the 99% level (Figure 4.10a). Similarly, the minimum correlation coefficient between Ψ'_{ON} and $\Psi'_{YC\ 0\ -\ 1000\ m}$, as well as between Ψ'_{ON} and $\Psi'_{YC\ 1000\ -\ 2000\ m}$, is also significant (~ -0.50 and ~ -0.37) at almost zero lag (Figure 4.10a). Overall, at high frequency (timescale less than 20 days), a barotropic response is found for the compensation effect between the flow through the Yucatan Channel and the OB and NWP Channels, which is mainly driven by the wind forcing.

Using model output that has been low-pass filtered with a cutoff timescale of 20 days, on the other hand, the minimum correlation coefficient between Ψ'_{ON} and Ψ'_{YC} and between Ψ'_{ON} and $\Psi'_{YC\ 0\ -\ 1000\ m}$, is still significant (~ -0.62 and ~ -0.73) at almost zero lag (Figure 4.10b). But the correlation coefficient is different for the flow through the OB and NWP Channels and the deep flow through the Yucatan Channel. The positive correlation coefficient (~0.35, with a lag of 7 days, Ψ'_{ON} leading) is relatively small but still significantly different from zero at the 99% level, indicating that different dynamics are operating. Transport variations through the OB and NWP Channels lead transport variations of the deep flow at the Yucatan Channel, which might be an indication of a timescale for internal adjustment processes in the GOM (Bunge et al., 2002). At timescale longer than 20 days, baroclinic flow through the Yucatan Channel is found linked with the compensation effect, as we discussed before, which is mainly a result of the topographic bottom drag effect found by Lin et al. (2009) associated with the Loop Current intrusion and its ring shedding.

4.5 Summary and Conclusion

A three-dimensional data-assimilative regional ocean circulation model was used in simulating circulation and hydrographic distributions in the Intra-Americas Sea. The model was forced by 6-hourly wind fields from National Centers for Environmental Prediction (NCEP), and integrated from January 1999 to December 2001. To improve the model hindcast skills, the sea level anomalies derived from satellite altimetry observations were assimilated into the model using the data assimilation scheme

suggested by Cooper and Haines (1996). A comparison of model results with the observations during the study period demonstrates that the ocean circulation model of the IAS has reasonable skills in reconstructing the observed circulation, hydrographic distributions and associated variability (especially on timescales of greater than 20 days).

Model results from 13 July 2000 to 31 May 2001 were used in examining the main physical processes for the compensation effect between the Yucatan Channel and the Old Bahama and Northwest Providence Channels. We demonstrated that volume transports through the Yucatan Channel and between Florida and the Bahamas (at the site of the submarine cable) are not always the same due to the compensation flow in the IAS, as one of important circulation features discussed recently by Lin et al. (2009) (see also Chapter 2). In this chapter, we extended our previous work by examining the vertical structures of the flow through the Yucatan Channel during the ring shedding and intrusion (e.g., between December 2000 and May 2001) and found that baroclinic flow at the Yucatan Channel (and then the circulation in the Gulf of Mexico) is mainly associated with the compensation effect at low frequencies (timescales longer than 20 days). In addition to the influence of the Loop Current intrusion, the compensation effect between the Yucatan Channel and channels to the north of Cuba also operates on timescales shorter than 20 days, but in this case flow variations through the Yucatan Channel have a barotropic response.

Chapter 5

A Numerical Study of Monthly to Seasonal Variability of Circulation in the Intra-Americas Sea: The Role of Caribbean Eddies [1]

5.1 Introduction

The Caribbean Sea is a major component of the Intra-Americas Sea (IAS, Figure 4.1), separated from the main Atlantic basins by an island-studded enclosure. The Caribbean Sea is connected to the North Atlantic Ocean via the Lesser Antilles and Windward Passages to the east and the Gulf of Mexico via the Yucatan Channel to the north. It consists of a succession of five basins: the Grenada, Venezuelan, Columbian, Cayman, and Yucatan basins. The Grenada Basin, which is bounded to the east by the Antillean arc of islands with water depths less than ~3300 m, is the shallowest and the smallest of the Caribbean basins. The Venezuelan and Columbian Basins have water depths greater than 4000 m, separated by the Beata Ridge between the island of Hispaniola and Colombia. The Cayman Basin, with depths of more than 5,000 m, lies between the

[1] Lin, Y., J. Sheng, and R. J. Greatbatch, (2010c), A numerical study of monthly to seasonal variability of circulation in the Intra-Americas Sea: the role of Caribbean eddies, to be submitted to *Continental Shelf Research*.

Nicaragua Rise with a sill depth of ~1200 m and the Cayman Ridge with a sill depth of ~1600 m. The Yucatan Basin (with depths of more than 5,000 m) lies between the Cayman Ridge and the Yucatan Channel with a sill depth of ~2000 m.

The Caribbean Sea plays a very important role as a conduit for mass, heat, salt and other tracers in the Atlantic circulation system. The upper-ocean circulation in the region is characterized by a warm and persistent throughflow known as the Caribbean Current, which flows westward about 200–300 km off the northern coast of South America and then northward along the eastern coast of Central America (Mooers and Maul, 1998). The Caribbean Current becomes known as the Yucatan Current as it flows through the Yucatan Channel and as the Loop Current as it penetrates northward into the Gulf of Mexico. The path and dynamics of the Caribbean Current are modulated by the presence of mesoscale and sub-mesoscale eddies. Mesoscale variability of the Caribbean, known as the "eddy waves", can be traced upstream to the North Brazil Current Retroflection (Johns et al., 1990). Some eddies also enter the Cayman Sea from outside the Caribbean through the Windward Passage (Andrade and Barton, 2000).

Caribbean eddies are mostly anti-cyclonic and travel westward through a narrow corridor along the Caribbean Current with an average speed of 15 cm s^{-1} (Murphy et al., 1999). The varying bathymetry in the Caribbean Sea is an important factor in the modification of Caribbean eddies that pass through the Western Caribbean Sea (Molinari et al. 1981). Previous studies have demonstrated that Caribbean eddies tend to be eroded as they pass over the Nicaraguan Rise area due to their interaction with the topography as for instance argued by Andrade and Barton (2000) based on an analysis of altimetry data, and by Carton and Chao (1999) based on numerical simulations. Caribbean eddies exit the Cayman Sea by squeezing through the Yucatan Channel. Here they significantly affect the Loop Current's intrusion and the shedding of warm-core rings. Murphy et al. (1999) found a significant correlation between the Loop Current eddy shedding and eddies near the Lesser Antilles with a time lag of 11 months. Oey et al. (2003) demonstrated that anticyclonic eddies that squeeze through the Yucatan Channel are related to eddy shedding at periods of 14-16 months. Candela et al. (2003) found that Loop Current eddy shedding is correlated to the flux of potential vorticity through the Yucatan Channel. This potential vorticity flux is apparently driven by eddies and

meanders in the Caribbean Sea. The mechanism supporting ring shedding has been recently studied using the "momentum imbalance paradox" (see Pichevin and Nof, 1997; Nof and Pichevin, 2001; Nof, 2005). However, the effect of Caribbean eddies on the circulation variability in the Caribbean Sea is not fully understood.

Various ocean circulation models were developed in recent years for the IAS for different research purposes (e.g., Candela et al. 2003; Oey et al. 2003; Sheng and Tang 2003, 2004; Ezer et al. 2003; Jouanno et al. 2008a, 2008b). Sheng and Tang (2003) studied the circulation and month-to-month variability in the Western Caribbean Sea with a numerical model covering the area between 72˚ and 90˚W and between 8˚ and 24˚N. Their model results demonstrated that nonlinear dynamics play a very important role in simulating month-to-month and mesoscale variability in the western Caribbean, particularly over the southern Colombian Basin and eastern Cayman and Yucatan Basins.

Previous studies also demonstrated that Caribbean eddies are quite regular, appearing at near 90-day intervals west of the southern Lesser Antille (Carton and Chao, 1999). Eddies can be spun up locally by the wind stress curl with a timescale about 100 days to the south of Hispaniola (Oey et al., 2003). Jouanno et al. (2008b) found the main frequency peaks for the mesoscale variability present a westward shift, from roughly 50 days near the Lesser Antilles to 100 days in the Cayman Basin, which is associated with growth and merging of eddies.

Lin et al. (2009) (see also Chapter 2) have discussed the connectivity between transport variations through the Yucatan Channel and the Windward Passage through the channels north of Cuba (known as the "compensation effect") with time-scales longer than a month. They demonstrated that at high frequencies (with timescales less than 30 days) the westward wind stress plays an important role on the transport variations through the Yucatan Channel. At lower frequencies (time scales longer than 120 days) it was demonstrated that the intrusion of the Loop Current into the Gulf also influences transport through the Yucatan Channel (Lin et al. 2009; Lin et al. 2010a; see also Chapters 2 and 3). Better understanding is required for the main physical processes responsible for the circulation variability and connectivity at timescales between 30 to 120 days in the Caribbean Sea. Based on the guidance that generation and propagation of the Caribbean eddies fall in with the frequency band at timescales of 30-120 days, we

investigate the role played by Caribbean eddies on the monthly to seasonal circulation variability in the Caribbean Sea in this chapter.

The remainder of this chapter is arranged as follows. Section 5.2 describes the regional ocean circulation model used in our study. Section 5.3 discusses model results, with a special emphasis on the influence of Caribbean eddies on the monthly to seasonal circulation variability in the Caribbean Sea. The final section is a summary and conclusion.

5.2. Model Setup and External Forcing

The regional ocean circulation model used in this study is the primitive-equation ocean circulation model known as CANDIE (the CANadian version of DIEcast, Sheng et al., 1998). CANDIE has been successfully applied to address various modeling problems including the seasonal circulation in the northwestern Atlantic Ocean (Sheng et al., 2001) and the general circulation over the western Caribbean Sea (Sheng and Tang, 2003 and 2004; Tang et al., 2006; Lin et al., 2009). The model domain covers the IAS between 99.0 and 54.0˚W and between 8.0 and 30.3˚N (Figure 4.1). The 5-minute world topography and bathymetry dataset known as ETOPO-5 is used in the model. The model horizontal resolution is ~1/6˚ in both latitude and longitude. 32 z-levels in the vertical are used in the model, with a vertical resolution of 5 m for the top z-level, gradually expanding resolutions from 10 - 100 m for the following 12 z-levels, 100 m for the following 11 z-levels, and coarser vertical resolutions (up to 500 m) for the last 8 z-levels.

The regional ocean circulation model of the IAS is forced by 6-hourly reanalysis data produced by the National Centers for Environmental Prediction (NCEP) data, including wind speed, the flux of sunlight into the ocean, air temperature, and relative humidity. The net heat flux at the sea surface is calculated using the bulk formulae taken from Gill (1982) as following:

$$Q_{net} = Q_I + Q_B + Q_L + Q_S \tag{5.1}$$

where Q_I is the flux of sunlight into the ocean, Q_B is the net upward flux of long-wave radiation from the ocean, Q_L is the latent heat flux carried by evaporated water, and Q_S is

the sensible heat flux. These terms are calculated from the NCEP fields and model-calculated sea surface temperature. The sea surface salinity in the model is restored to 5-day averaged salinity extracted from global ocean circulation reanalysis fields (with a horizontal resolution 1/4˚×1/4˚) produced by the British Atmospheric Data Centre (BADC) with a restoring timescale of 20 days.

The lateral boundary conditions used in this study are the same as Lin et al. (2010b) (see also Chapter 4). We also specify the barotropic components of the normal currents at the model northern open boundaries based on Eq. (4.1) in the control run. Furthermore, we use the data assimilation scheme suggested by Cooper and Haines (1996) to assimilate satellite altimeter data into the model. The reader is referred to Lin et al. (2010b) and Chapter 4 for a slightly more detailed description of this method.

In addition to the model used in Lin et al. (2010b) and in Chapter 4, the smoothed semi-prognostic method (Sheng et al., 2001; Eden et al., 2004; Greatbatch et al., 2004) is used to reduce the model drift in the control run. This method adiabatically adjusts the momentum equations in the model to correct for the model errors associated with the physical processes that are not correctly represented by the model equations. The adjustment is accomplished by adding a correction term in the hydrostatic equation:

$$\frac{\partial p}{\partial z} = -\rho_m g + (1-\alpha)\overline{(\rho_m - \rho_r)}g \tag{5.2}$$

where the second term on the right hand side of Eq. (5.2) appears as a correction term, α is a linear combination coefficient with a value between 0 and 1 (we set α to 0.5 in this study), the overbar represents spatial filtering (~3^o in both latitude and longitude for this study), and g is the acceleration due to gravity. ρ_m is the model-computed density. The input density, ρ_r, comes from the 5-day BADC fields. The procedure corresponds to adding a forcing term to the momentum equation through the computation of the horizontal pressure gradient terms. The semi-prognostic method is hence adiabatic, leaving the temperature and salinity equations unconstrained and fully prognostic. The reader is referred to Sheng et al. (2001), Eden et al. (2004), and Greatbatch et al. (2004) for details of this method.

The regional ocean circulation model of the IAS is initialized using the BADC reanalyzed potential temperature and salinity on January 1, 1999 and integrated for four

years from January 1, 1999 to December 31, 2002. Two numerical experiments are conducted in this study (Table 5.1):

(1) The control run (Exp-CR). The model is driven by wind stress and surface heat flux converted from the 6-hourly NCEP fields and boundary forcing based on 5-day BADC reanalysis data as discussed above. The data assimilation scheme of Cooper and Haines, the correction term for barotropic transport along the northern open boundary described in Eq. (4.1), and the smoothed semi-prognostic method are used in the run. The model is initialized using BADC reanalysis data for potential temperature and salinity.

(2) Time-mean forcing run (Exp-MF): The model run is purely prognostic and data assimilation and the correction term based on Eq. (4.1) are not used in this experiment. The model is forced by multiyear (1999-2002) mean (steady) wind stress based on NCEP data. Model temperature, salinity, and velocities at lateral open boundaries, and model temperature and salinity at surface, are restored to multiyear (1999-2002) mean fields calculated from BADC reanalysis data.

The model results between July 13, 2000 and December 31, 2002 are used for analysis in this study, during which the cable voltage inferred transports at 27˚N between the Florida and Bahamas (Ψ_{cable}, Baringer and Larsen, 2001) and daily mean transport estimates from the 2-year observation array in the Yucatan Channel during the CANEK program (e.g. Bunge et al., 2002; Sheinbaum et al., 2002) are available for assessing model skills.

5.3. Model Results

5.3.1. General Circulation

The time-mean volume transport stream function and time-mean surface currents at 2.5 m over the IAS calculated from model results in the control run (Exp-CR) for the period between 13 July 2000 and 31 May 2001 are very similar to Figure 4.2 in Chapter 4. The mean circulation and transport through the major channels in the IAS produced by the model are comparable with observations in the region (Johns et al., 2002) and previous numerical results (e.g. Smith et al., 2000). In the model, the time-mean transport between

Table 5.1. List of methods and model external forcing used in numerical experiments.

Name of Run	Data-assimilation scheme	Semi-prognostic method	Wind Stress	Boundary Flows	Boundary T and S
Exp-CR	Yes	Yes	NCEP 6-hourly	BADC 5-day & Eq. (4.1)	BADC 5-day
Exp-MF	No	No	Steady	Steady	Steady

Florida and the Bahamas (Ψ_{FC}) is ~27.8 Sv, which is slightly less than the cable voltage inferred transports of the Florida Current (~30.7 Sv, Baringer and Larsen, 2001). The difference is due mainly to smaller volume transports specified at the north open boundary in the model. The model calculated time-mean transport through the Old Bahama and Northwest Providence Channels combined is ~1.1 Sv. This is less than the estimate of ~3.1 Sv made from observations during different periods (e.g. Atkinson et al., 1995; Leaman et al., 1995). The time-mean transport through the Yucatan Channel (Ψ_{YC}) produced by the model is ~26.7 Sv, which is comparable to the transport estimate made by Johns et al. (2002) but larger than the mean transport of 23.2 Sv estimated from the CANEK observations during the period between 13 July 2000 and 31 May 2001 (e.g. Sheinbaum et al., 2002). Concerning the 30 Sv accepted as the nominal transport of the Florida Current and the observed time-mean transport through the Old Bahama and Northwest Providence Channels, it should be noted that the time-mean transport of 23.2 Sv through the Yucatan Channel estimated from the CANEK program is less than the transport normally attributed to the Yucatan Channel.

In the following discussion, we focus on the variability and dynamics in the Caribbean Sea. Figure 5.1a shows the time-mean currents at 30 m in the Caribbean Sea calculated from model results in the control run between July 13, 2000 and December 31, 2001. The main Caribbean Current produced by the model crosses the Caribbean Sea from the coast of Venezuela to the western Yucatan Basin. The time-mean upper ocean currents are westward and relatively broad in the central and eastern Colombia Basin.

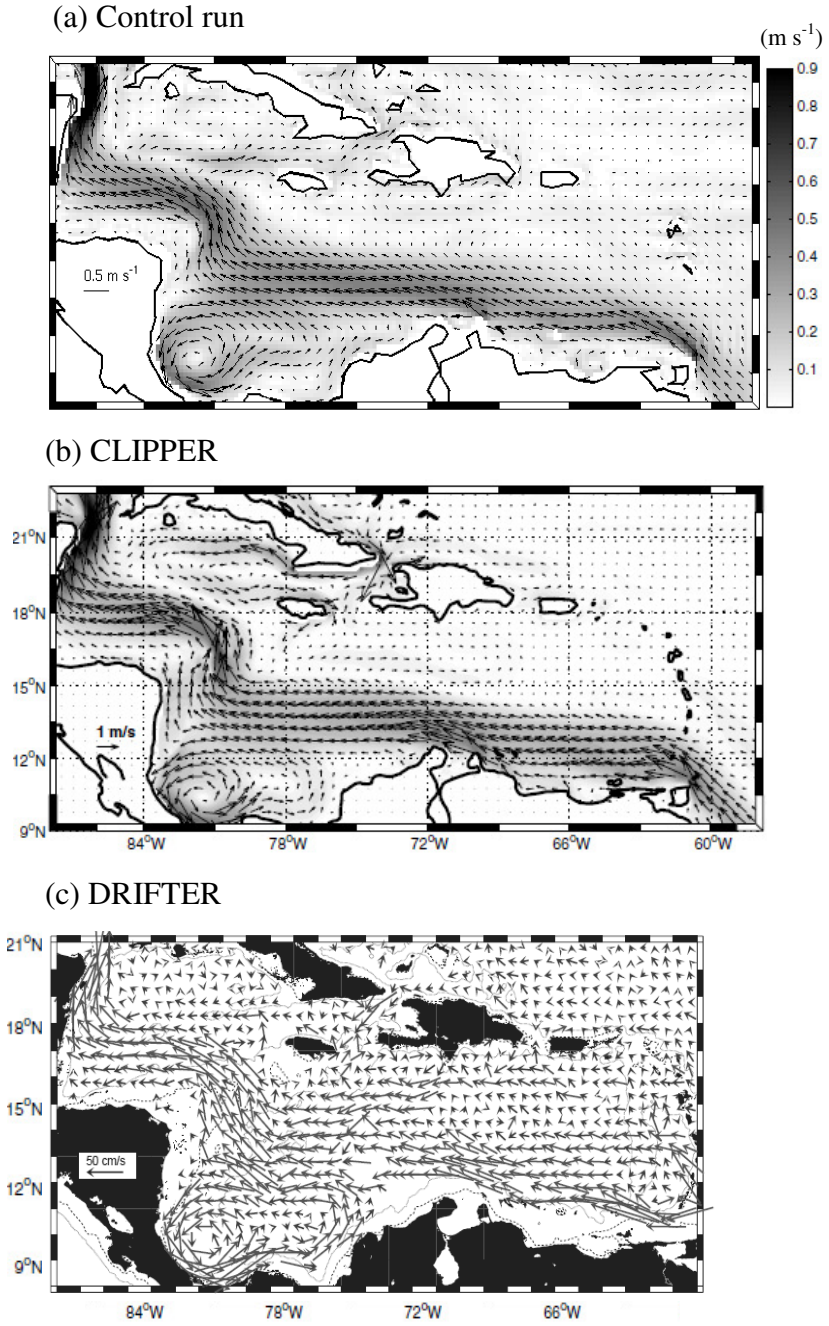

Figure 5.1. (a) Time-mean currents calculated from model results at 30 m depth in the control run during the period between July 13, 2000, and May 31, 2001; (b) from model results at 30 m depth produced by OPA (acronym for "Ocean PArallelise") model in CLIPPER-ATL6 (1/6˚) adapted from Jouanno et al. (2008b); and (c) inferred from drifter trajectories produced by Richardson (2005). Only selected velocity vectors plotted for better clarity. Gray scale in (a) and (b) indicates magnitude of velocity.

The westward currents bifurcate before reaching the Nicaragua Rise. The small branch veers southwestward to form the Panama–Colombia Gyre in the southwestern Caribbean Sea. The main branch turns northwestward off the coast of Honduras, forming a very strong coastal jet running northward along the east coast of Belize and Mexico. For comparison, Figure 5.1b shows the time-mean currents at 30 m in the Caribbean Sea in a 1/6˚-resolution numerical simulation of the Atlantic Ocean circulation using OPA (acronym for "Ocean PArallelise") model for 15-years (1979 to 1993) (CLIPPER-ATL6, Treguier et al., 2005; Jouanno et al., 2008b). Figure 5.1c shows the time-mean surface currents inferred from 8-year drifter data by Richardson (2005). Our model results shown in Figure 5.1a agree very well with the CLIPPER-ATL6 numerical experiment and drifter observations. In the drifter data, the Caribbean Current is characterized by two jets centered near 13°N and 15°N in the Eastern Caribbean Sea (Morrison and Nowlin, 1982), which can be seen in our model results (Figure 5.1a). It should be noted that the time-mean currents at 30 m through the Windward Passage produced by our model differ from the strongly southwestward flow produced the OPA model in CLIPPER-ATL6 and drifter-inferred currents, due mainly to the flow structure specified at the north open boundary in our model.

Figure 5.2 shows snapshots of near-surface currents (at 2.5 m) and sea surface height fields in early 2001 produced by the model in the control run. The Caribbean Current and associated mesoscale eddies in the Caribbean Sea are simulated well by the model. For example, there is an small-size anti-cyclonic eddy in the upper ocean of the eastern Colombian Basin (centered at 15.5°N, 72.3°W, see Figure 5.2a) on January 10, 2001. This eddy propagates westward with the Caribbean Current and increases in strength and size from January 10 to January 31 (Figures 5.2a and b). It reaches the Nicaraguan Rise on February 21 (centered at 15.3°N, 77.8°W in Figure 5.2c). At the same time, the main path of the Caribbean Current in the western Colombian Basin shifts southward onto the region of the Columbia-Panama Gyre, with enhanced strength of the Current due to the current-eddy interaction (Figure 5.2c). This anti-cyclonic eddy passes over the Nicaraguan Rise on March 21 with the near-surface Caribbean Current flowing more westward in the Colombia Basin region (Figure 5.2d). The eddy reaches the Yucatan Basin on April 18 and squeezes through the Yucatan Channel on May 16

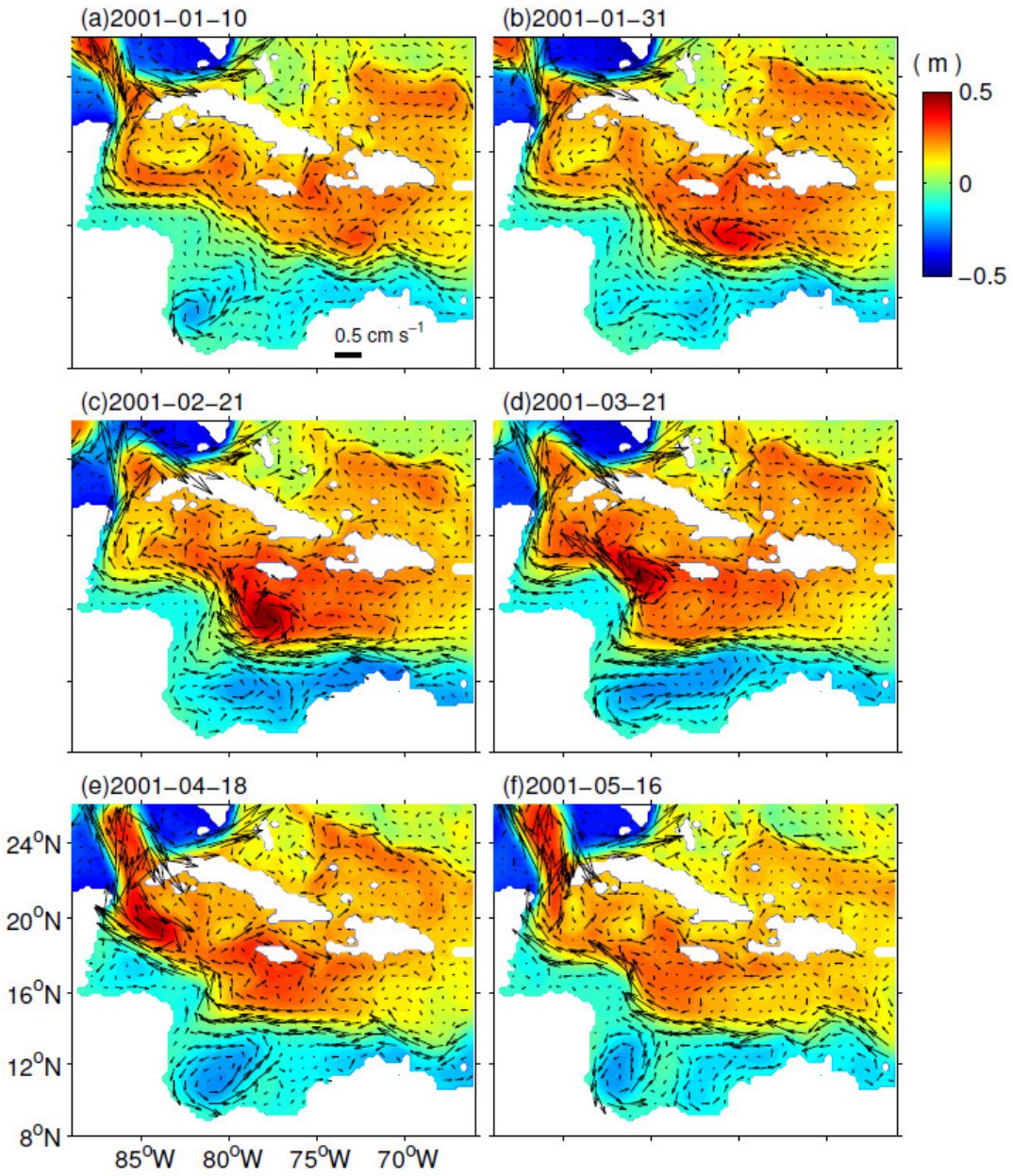

Figure 5.2. Snapshots of near-surface currents (2.5 m, black arrows) and sea surface height fields (image) produced by the model in the control run (Exp-CR). Velocity vectors are plotted at every 3rd grid point.

(Figures 5.2e and f). There is a Loop Current shedding event produced by the model in February 2001 (Figures 5.2b-f), as observed in satellite altimeter fields.

Figure 5.3 presents vertical distributions of observed and simulated time-mean zonal velocity and potential temperature (<300 m) along a meridional transect at 66.0˚W in the eastern Venezuelan Basin, which were calculated respectively from in-situ observations during August-September 1997 (Hernandez-Guerra and Joyce, 2000) and composites made from model results in the control run (Exp-CR) for August-September during 2000-2002. The general structure of the simulated time-mean potential temperature (Figure 5.3b) is characterized by relatively horizontally uniform isotherms over the northern part of the transect and tilting isotherms over southern part of the transect with colder water over the south coast, which is consistent with in situ observations. For instance, in both observations and model results, the depths of the 25˚C isotherm are less than 50 m at 12˚N and as deep as 120 m at 15˚N (Figure 5.3a). The observed and simulated time-mean zonal currents shown in Figures 5.3c and d are characterized by an intense and shallow westward flow centered at 66.0˚W and an eastward flow in the narrow coastal region between 11˚N and 12˚N. Model results are relatively smooth in both the potential temperature and velocity distribution compared to the observed profile because, at least partly, of time averaging.

We next compare model results in the control run with the observations made at the Yucatan Channel during the CANEK program (e.g. Sheinbaum et al., 2002) between July 13, 2000 and May 31, 2001. The vertical structure of the time-mean flow and temperature distribution produced by the model in the control run at the Yucatan Channel are very similar to Figure 4.3 in Chapter 4. Figure 5.4a compares vertical profiles of observed and simulated time-mean northward velocities (cross-channel averaged) through the Yucatan Channel calculated respectively from in-situ observations made during the CANEK program and model results in the control run. The time-mean cross-channel averaged northward velocity decreases from ~10 cm s^{-1} at surface to near zero below 1000 m in both model and observational results. The standard deviations of the simulated daily-mean cross-channel averaged northward velocities agree well with the observations during the CANEK program (Figure 5.4b), with large temporal variations at depths shallower than 200 m.

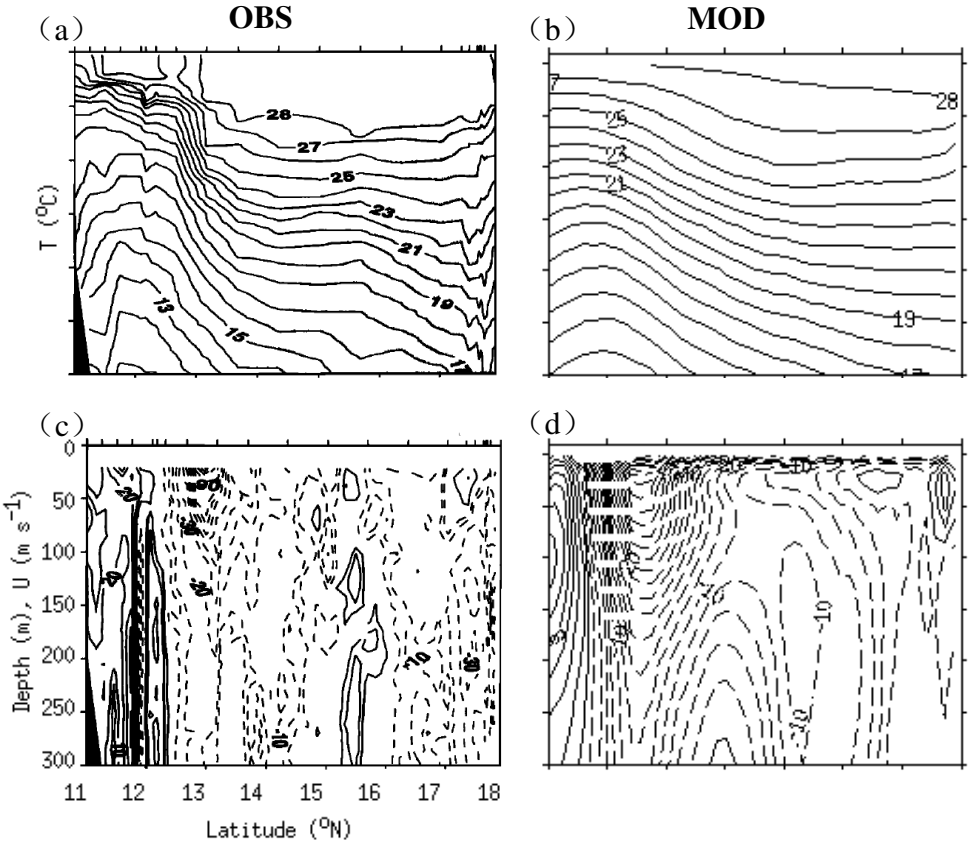

Figure 5.3. Vertical distributions of observed (a and c) and simulated (b and d) time-mean potential temperature (upper panels) and eastward velocity (lower panels) in the upper ocean (< 300 m) along a meriodional cross section at 66.0˚W in the eastern Colombian Basin. The observed fields in (a) and (c) are calculated from in-situ observations made during August-September 1997 (adopted from Hernandez-Guerra and Joyce, 2000). The simulated fields in (b) and (d) are composites made from model results in the control run (Exp-CR) for August-September during 2000-2002.

To investigate how the vertical structure of the flow at the Yucatan Channel changes in association with the variability of section integrated transports, we calculate the correlation between the transport and cross-channel averaged northward velocities at the Yucatan Channel. Correlation coefficients at different depths calculated from model results in the control run and from observations (the CANEK program) during the period between July 13, 2000 and May 31, 2001 are shown in Figure 5.4c. In both simulated and observational results in the Yucatan Channel, significant correlation is found above the depth of 1000 m, which is the typical depth of the isotherm of 6˚C in the Yucatan Channel and at which the lowest water temperature observed over the shallow Straits of Florida (Bunge et al., 2002). It should be noted that the model in the control run overestimates the correlation coefficient between the vertically integrated transport and most vertical components (northward velocities), which is due mainly to the model deficiency in simulating small-scale and highly variable circulation features observed in the real ocean.

Figure 5.5 shows the simulated daily transport anomalies (time-mean removed) of the Florida and Yucatan Currents in the control run during the period between July 13, 2000 and May 31, 2001. Results directly calculated from BADC fields and observational estimates are also shown in the figure for comparison. The model results in the control run reproduces well the Florida Current transport anomalies as expected due to the use of the correction term described in Eq. (4.1). The model also has reasonable skills in simulating the variability in the observed transport anomalies through the Yucatan Channel during the same period (Figure 5.5b). It should be noted that our model has a certain deficiency in reproducing high-frequency (timescales less than a month) Yucatan Channel transport anomalies estimated by the CANEK program, which could be partially due to the coarse horizontal resolution of the model to resolve small-scale circulation features in the region and the resolution of the model forcing such as the wind fields.

5.3.2 Variability of Temperature and Salinity

Figures 5.6 and 5.7 present standard deviations of simulated potential temperature and salinity fields at depths of 10, 200, 500, and 1000 m based on model results in the control

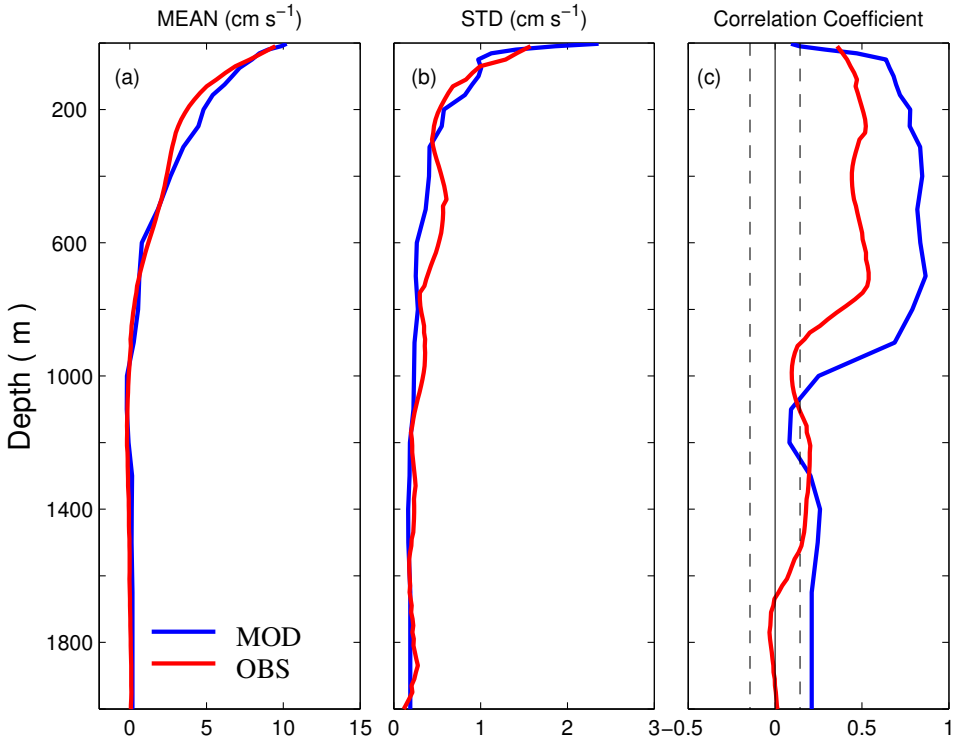

Figure 5.4. Vertical profiles of (a) the time-mean and (b) standard deviation of northward velocities (cross-channel averaged) at the Yucatan Channel calculated from in-situ observations (red line) and model results in the control run (blue line) during the period between July 13, 2000 and May 31 2001. (c) Vertical profiles of correlation coefficients between northward velocities (cross-channel averaged) and the section integrated transport at the Yucatan Channel, calculated from in-situ observations (red line) and model results in the control run (Exp-CR, blue line) during the same period. Correlations outside the dashed vertical lines in (c) are significantly different from zero at the 99% level.

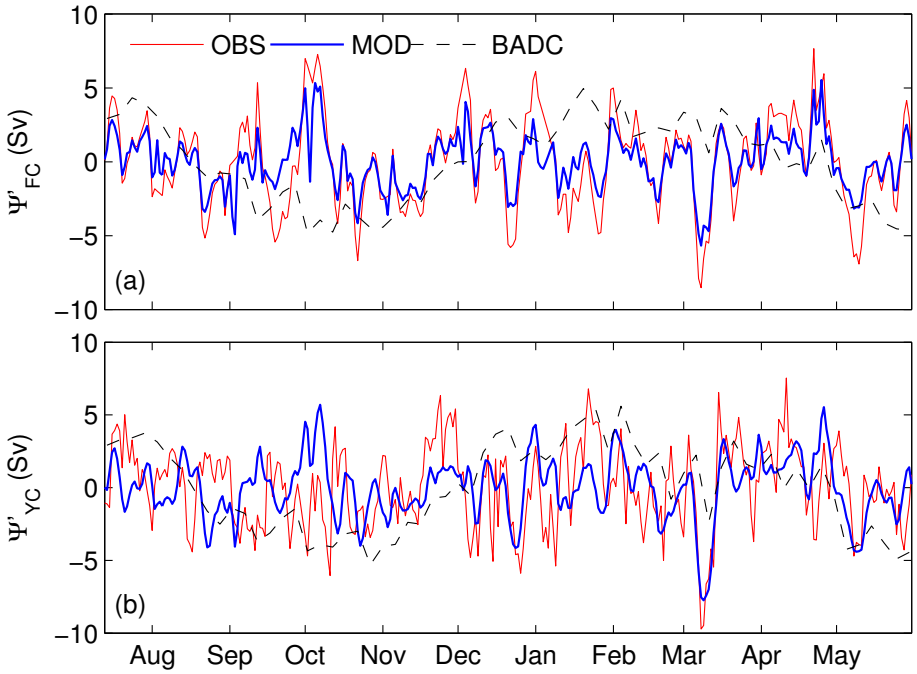

Figure 5.5. Time series of daily mean transport anomalies (the long-term time-mean removed) of the (a) Florida Current between Florida and the Bahamas and (b) Yucatan Current, calculated from model results in the control run (Exp-CR, blue solid lines); BADC reanalysis data (black dashed lines), and observational estimates from cable and CANEK data (red solid lines) separately, during the period between July 13, 2000 and May 31, 2001. Positive values mean northward.

run (Exp-CR) during the period between July 13, 2000 and December 31, 2002. Standard deviations are calculated from daily mean temperature and salinity fields produced by the model. For comparison, the climatological standard deviations of the World Ocean Atlas Data 2005 (WOA05) at same depths provided by the National Oceanographic Data Center (NODC) are also shown in the figures. The general distribution of temporal variability in simulated potential temperature fields at 10 m produced by the model is comparable to the climatological data (Figures 5.6a and b), including main features such as larger seasonal variations at higher latitudes and the Guajira upwelling system in the south Caribbean Sea (Andrade and Barton, 2005). As shown in Figures 5.7a and b, the model results reproduced the observed temporal variability of the freshwater plume in the east Caribbean Sea originating from the Amazon River (Cherubin and Richardson, 2007). It should be noted that the salinity variations associated with freshwater discharge from rivers inside the model domain are underestimated, such as the Orinoco and Mississippi Rivers, due mainly to the fact that the direct effect of river runoff is not included in this modelling study.

Figures 5.6c-f and 5.7c-f show that observed and simulated potential temperature and salinity fields have significant temporal variability at 200 and 500 m in the Caribbean Sea and southern Gulf Mexico, particularly the temperature fields at 200 m over the Nicaraguan Rise and temperature and salinity fields at 500 m at Yucatan Basin. The temporal variability in the observed and simulated potential temperature and salinity decreases with the depth and is very small below 1000 m (Figures 5.6g-h and 5.7g-h). It should be noted that the temporal variability of simulated potential temperature and salinity fields at 200 and 500 m in the Caribbean Sea during the period between July 13, 2000 and December 31, 2002 are relatively smaller than observed variability, due probably to the model resolution and model deficiency in simulating small-scale structures.

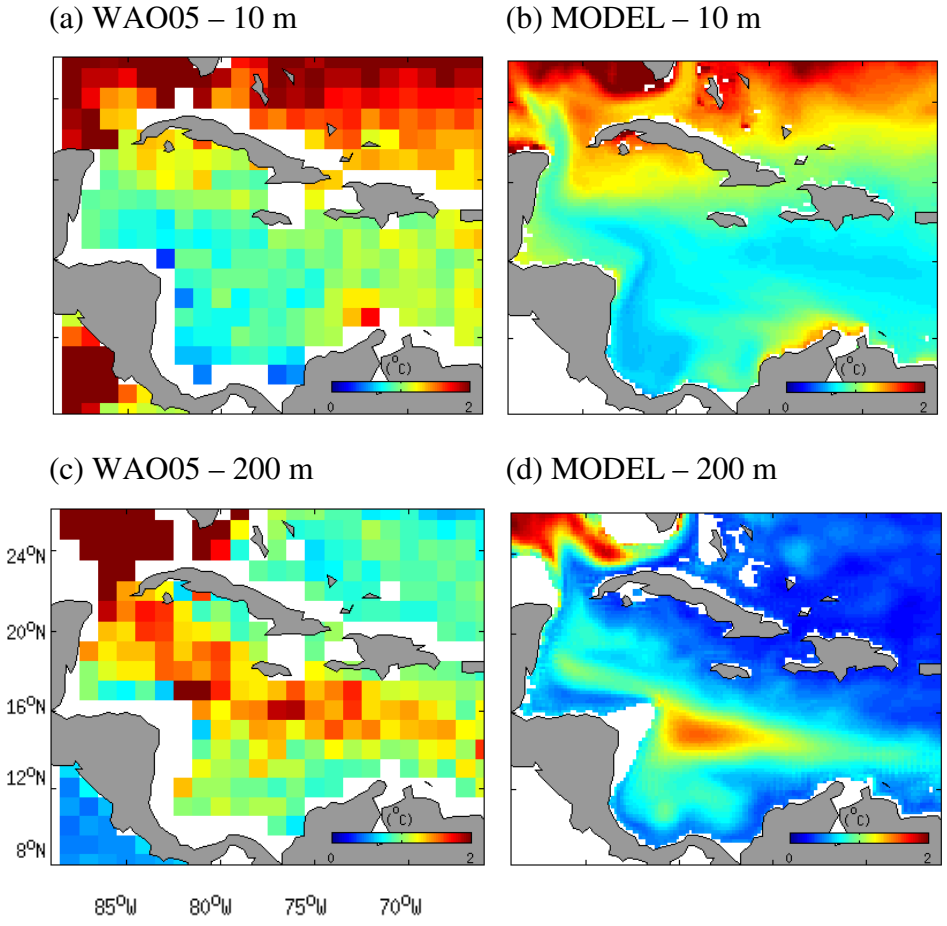

Figure 5.6. Standard deviations of simulated potential temperature in the control run (Exp-CR, right panels) at depths of (b) 10 m, (d) 200 m, (f) 500 m, and (h) 1000 m during the period between July 13, 2000 and December 31, 2002. Climatological data (left panels) at (a) 10 m, (c) 200 m, (e) 500 m, and (f) 1000 m from the World Ocean Atlas Data 2005 (WOA05) are also shown for comparison.

(e) WAO05 – 500 m

(f) MODEL – 500 m

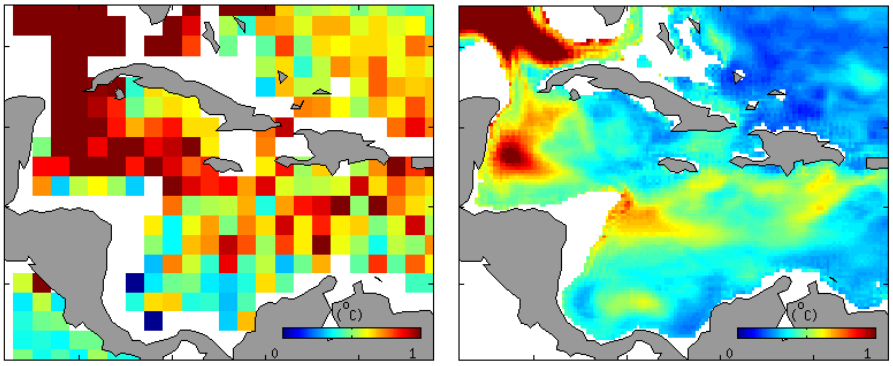

(g) WAO05 – 1000 m

(h) MODEL – 1000 m

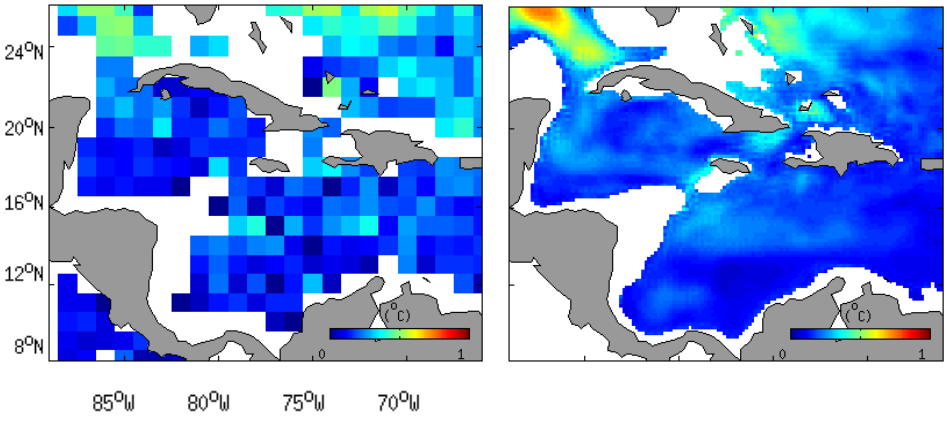

Figure 5.6. (continued)

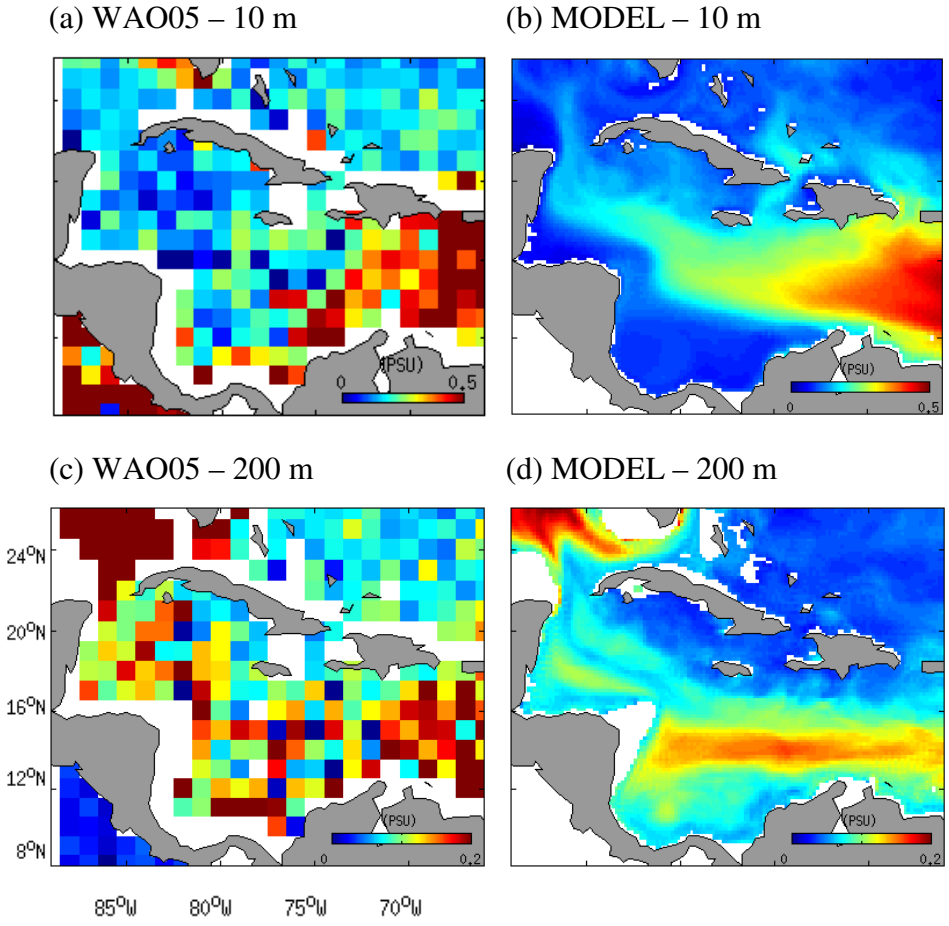

Figure 5.7. Standard deviations of simulated salinity in the control run (Exp-CR, right panels) at depths of (b) 10 m, (d) 200 m, (f) 500 m, and (h) 1000 m during the period between July 13, 2000 and December 31, 2002. Climatological data (left panels) at (a) 10 m, (c) 200 m, (e) 500 m, and (f) 1000 m from the World Ocean Atlas Data 2005 (WOA05) are shown for comparison.

(e) WAO05 – 500 m

(f) MODEL – 500 m

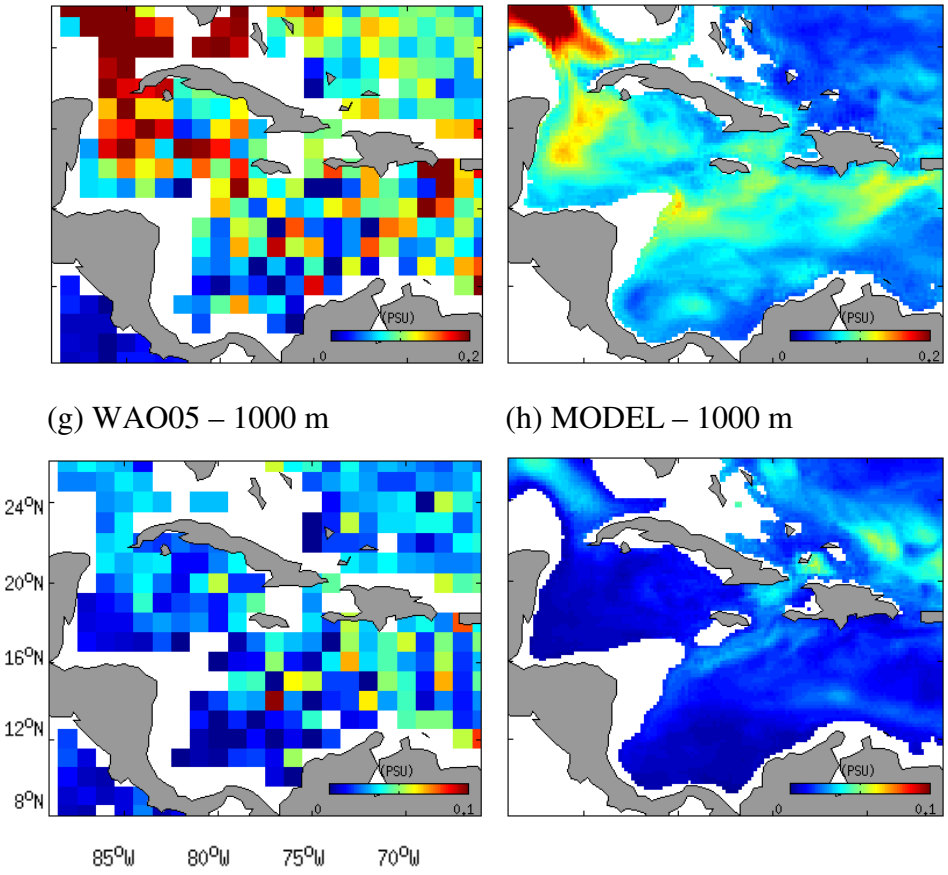

Figure 5.7. (continued)

5.3.3 Role of Eddies on the Circulation Variability in the Caribbean Sea

In this section we investigate the role of the eddies on circulation variability in the Caribbean Sea using model results in the control run (Exp-CR). The simulated potential temperature fields at 200 m are used for the analysis here since relatively large standard deviations were found in the model results at this depth than other depths in the Caribbean Sea (Figure 5.6) associated with the generation and propagation of mesoscale eddies. As mentioned in the introduction, the generation and propagation of Caribbean eddies have mainly timescales within 30-120 days. By applying a band-pass filter with timescales of 30-120 days to model results in the control run, we obtain a significant correlation between the band-pass filtered potential temperature fields at 200 m and the band-pass filtered transport between Nicaragua and Jamaica (Ψ_{NJ}) during the period between July 13, 2000 and December 31, 2002, with positive correlation coefficients (~0.47, significant at the 99% level) over the east side and negative coefficients (~0.40, significant at the 99% level) over the west side of Nicaraguan Rise (Figure 5.8b). The standard deviation distribution of band-pass filtered (30-120 days) simulated potential temperature fields at 200 m (Figure 5.8a) presents significant temporal variations in the locations of significant correlation shown in Figure 5.8b. Also in Figure 5.8a, there is a narrow corridor of large temperature perturbations found in the Western Caribbean Sea, which is mainly associated with eddies drifting with the Caribbean Current.

A Hovmoeller diagram shown in Figure 5.9 demonstrates the evolution of potential temperature fields at 200 m (band-pass filtered with timescales of 30-120 days) along the central axis of the narrow corridor marked by the dashed line in Figure 5.8b. Quasi-periodical perturbations are found associated with northwestward propagation of Caribbean eddies. The northwestward speed of the eddy propagation along the transect is about 15 cm s^{-1}, which is consistent with the speed found by Murphy et al. (1999) for the eddies drifting with the Caribbean Current cross the Caribbean Sea.

Figure 5.10a shows the vertical distribution of standard deviations of band-pass filtered (with the timescales of 30-120 days) simulated potential temperature fields along

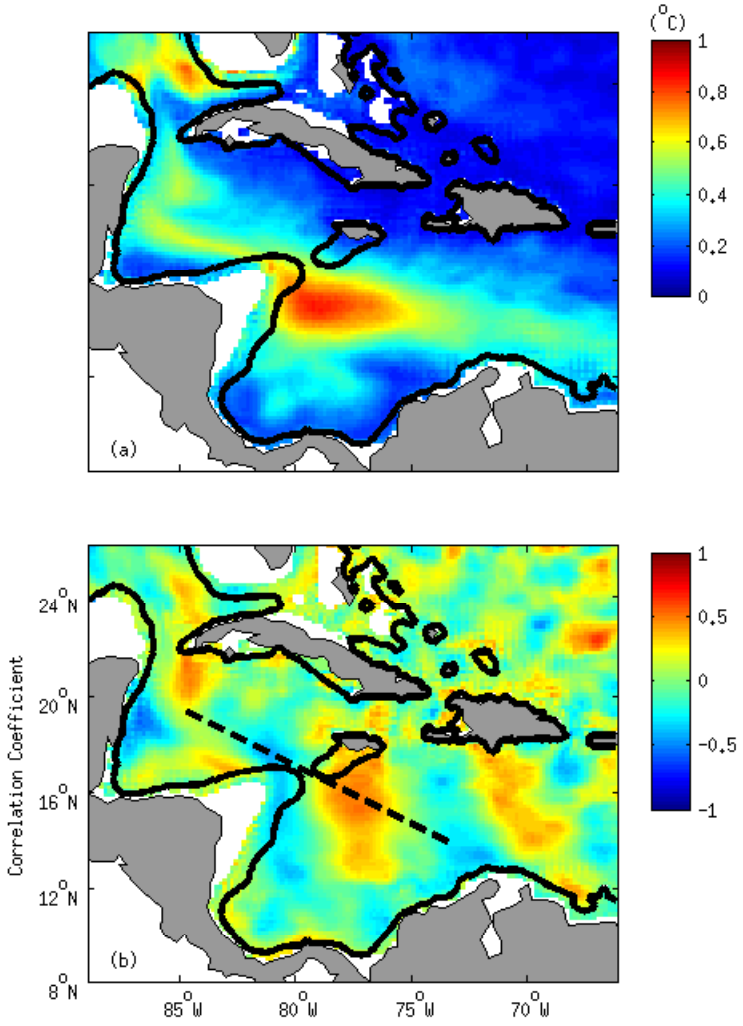

Figure 5.8. (a) Standard deviations of band-pass filtered (30-120 days) temperature fields at 200 m from model results in the control run (Exp-CR) during the period between July 13, 2000 and December 31, 2002. (b) Correlation coefficients between the temperature fields at 200 m and the transport between Nicaraguan and Jamaica calculated from band-pass filtered (30-120 days) model results in the control run (Exp-CR) during the same period. A thick solid line is the depth contour of 1000 m. A dashed line marks approximately the central axis of the corridor of large temporal temperature perturbations shown in (a).

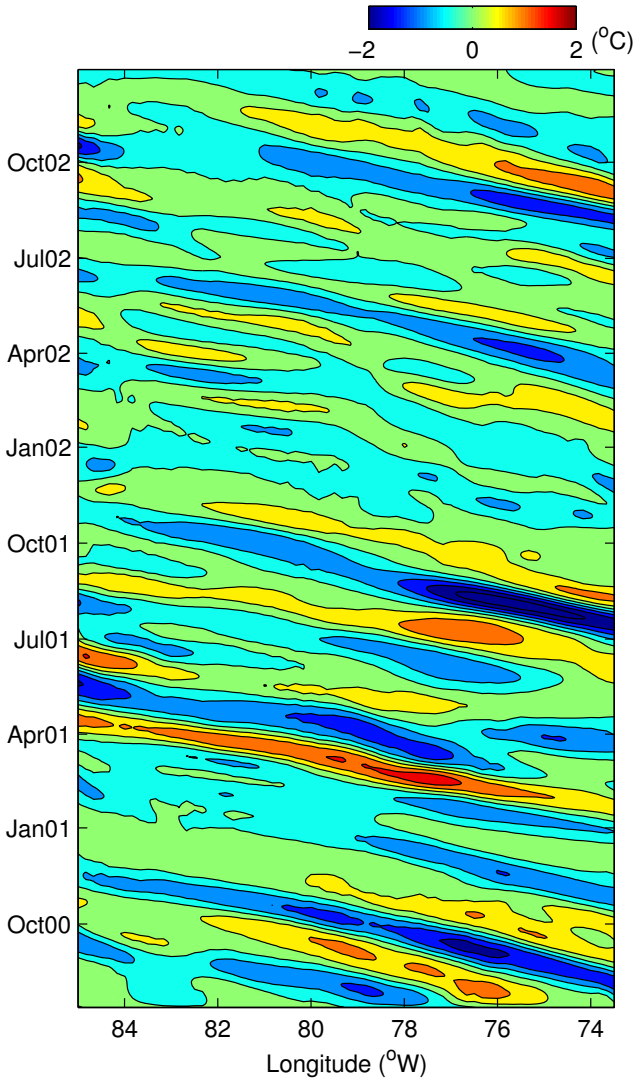

Figure 5.9. Hovmoeller diagram calculated with the band-pass filtered (30-120 days) potential temperature fields at 200 m along the transect marked by a dashed line in Figure 5.8b from model results in the control run (Exp-CR) during the period between July 13, 2000 and December 31, 2002.

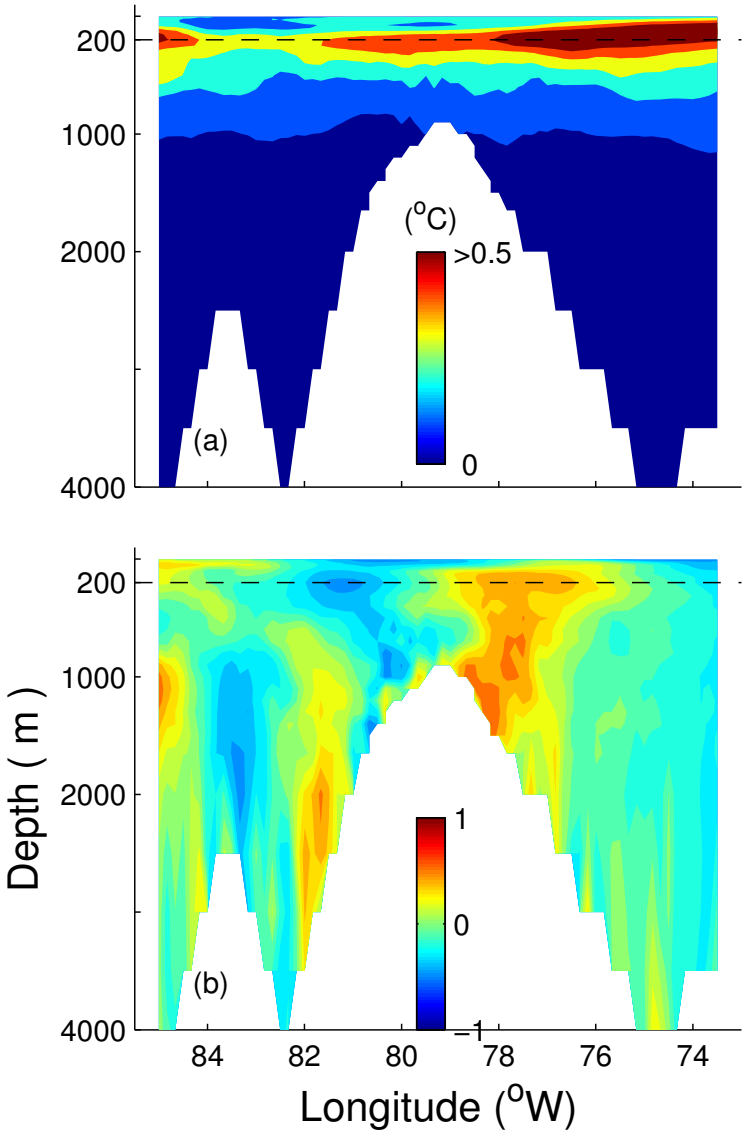

Figure 5.10. (a) Standard deviation of band-pass filtered (30-120 days) temperature fields along the transect marked in Figure 5.8b calculated from model results in the control run (Exp-CR) during the period between July 13, 2000 and December 31, 2002. (b) Correlation coefficients between temperature fields at the same transect and the transport between the Nicaragua and Jamaica, based on band-pass filtered (30-120 days) model results during the study period in the control run. The horizontal dashed lines mark the depth of 200 meters.

the transect marked in Figure 5.8b during the study period. Large temporal perturbations are mainly found in the upper waters of less than 1000 m, with largest perturbations centered at the depth of 200 m. Figure 5.10b presents the correlation coefficients between the band-pass filtered vertical potential temperature distributions along the same transect and the transport between Nicaragua and Jamaica ($<\Psi_{NJ}>$, where angle brackets represent the band-pass filtering) during the same period. A large correlation between the potential temperature fields (band-pass filtered with timescales of 30-120 days) and throughflow transports ($<\Psi_{NJ}>$) is found in the model at both sides of the Nicaraguan Rise at depths less than 1000 m. There is a significant positive correlation over the east slope and a significant negative correlation over the west slope of the Nicaraguan Rise (significant at the 99% level).

The significant correlation between $<\Psi_{NJ}>$ and the monthly to seasonal temperature (density) variations in the model can be interpreted as the result of the interaction between the density anomalies and the underlying variable bottom topography, known as the form drag mechanism, exactly as described by (Lin et al., 2009; see also Chapter 2) but here applied to the Nicaraguan Rise. Physically, the pressure differences across the Nicaraguan Rise can affect the throughflow transport between Nicaragua and Jamaica. Increased northwestward $<\Psi_{NJ}>$ is associated with warm-core eddies (lighter water) above the east slope and/or cold-core eddies (denser water) above the west slope. As a consequence, the bottom pressure is lower on east side of the rise and/or larger on the west side. The resulting pressure difference across the Nicaraguan Rise then drives the enhanced northwestward transport between the Nicaragua and Jamaica by the form drag effect.

5.3.4 Eddy-driven Circulation

To address the issue of whether the monthly to seasonal circulation variability in the Caribbean Sea is associated mainly with the external forcing or with the internal dynamics, we examine model results in EXP-MF, in which the regional circulation model is forced by multiyear (1999-2002) time-mean wind stress and multiyear (1999-2002)

time-mean potential temperature, salinity and velocities at lateral open boundaries (Section 5.2 and Table 1).

Figures 5.11 and 5.12 present the standard deviation distributions of potential temperature and salinity fields at depths of 10, 200, 500, and 1000 m, calculated from model results in Exp-MF corresponding to the study period July 13, 2000 to December 31, 2002. The modelled temperature and salinity variability at 10 m in Exp-MF (Figures 5.11a and 5.12a) is much smaller than in the control run (Figures 5.6b and 5.7b), due mainly to the fact that there is no seasonal variations of the surface heat and freshwater flux in Exp-MF. Since the wind forcing is time independent in Exp-MF, temporal variability of temperature associated with the Guajira upwelling system in the south Caribbean Sea shown in Figure 5.6b does not appear in the model results in Exp-MF (Figure 5.12a). There are no seasonal freshwater plume extensions in the eastern Caribbean Sea as seen in the control run. Although external forcing, such as wind and boundary flow, is time independent in Exp-MF, the model produced temperature and salinity fields in Exp-MF still exhibit large temporal variability at 200 and 500 m in the Caribbean Sea (Figures 5.11b-c and 5.12b-c), which is mainly associated with eddy activities. The eddy activities and their influence become weak below 1000 m (Figures 5.11d and 5.12d).

Figure 5.13 shows transport time series through the Yucatan Channel (Ψ_{YC}), the passage between Nicaragua and Jamaica (Ψ_{NJ}), the Windward Passage (Ψ_{WP}), and the passage between Jamaica and Hispaniola (Ψ_{JH}), calculated from model results in Exp-MF. Ψ_{YC} is positive to the north. Ψ_{WP} is positive to the northeast. Ψ_{NJ} and Ψ_{JH} are positive to the northwest. Ψ_{YC} has low-frequency variations with typical timescales of about 9 months (Figure 5.13a), which is found in association with the Loop Current intrusion. The reader is also referred to model results in Exp-Mean discussed in Lin et al. (2009) for details of the role played by the Loop Current eddy shedding on Ψ_{YC}. Fluctuations in Ψ_{NJ} and Ψ_{JH} have dominant timescales of ~80 days. To identify the role played by Caribbean eddies and eliminate the influence of the Loop Current eddy shedding, we again use a band-pass filter with timescales of 30-120 days on the model results in Exp-MF.

The band-pass filtered (with timescales of 30-120 days) transports $<\Psi_{WP}>$ and $<\Psi_{YC}>$ in Exp-MF have a correlation coefficient of -0.71 (significant at the 99% level) with zero

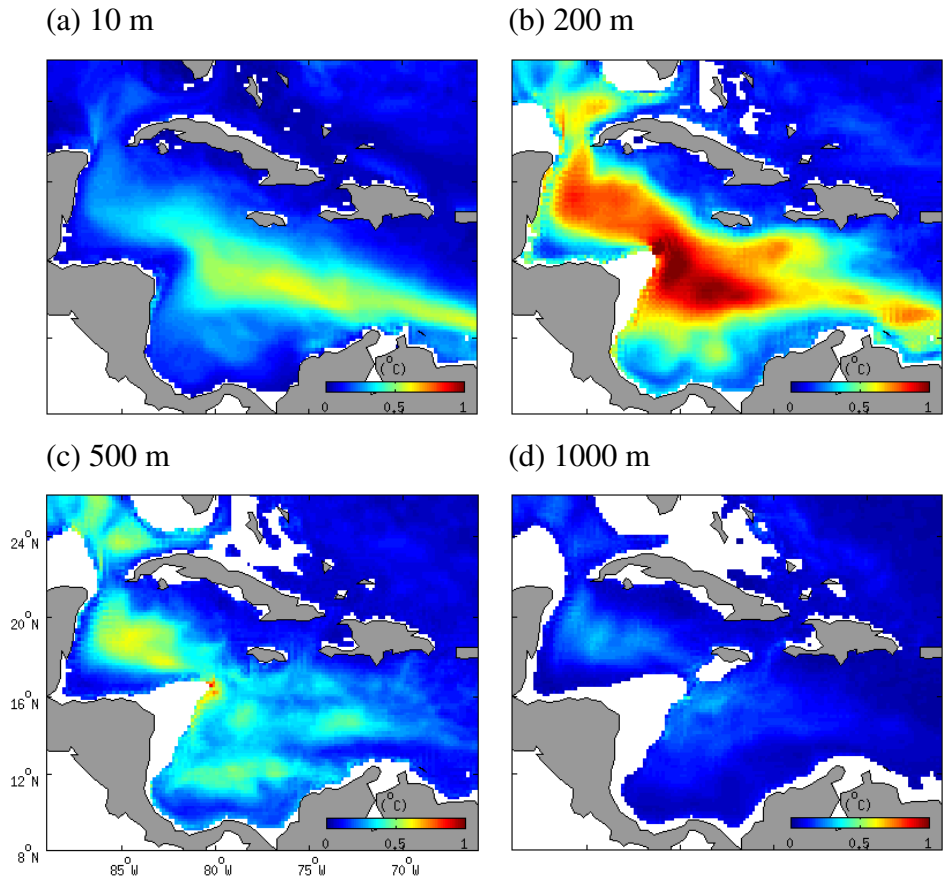

Figure 5.11. Standard deviations of modelled potential temperature fields calculated from model results in Exp-MF at depths of (a) 10 m, (b) 200 m, (c) 500 m, and (d) 1000 m corresponding to the study period July 13, 2000 to December 31, 2002.

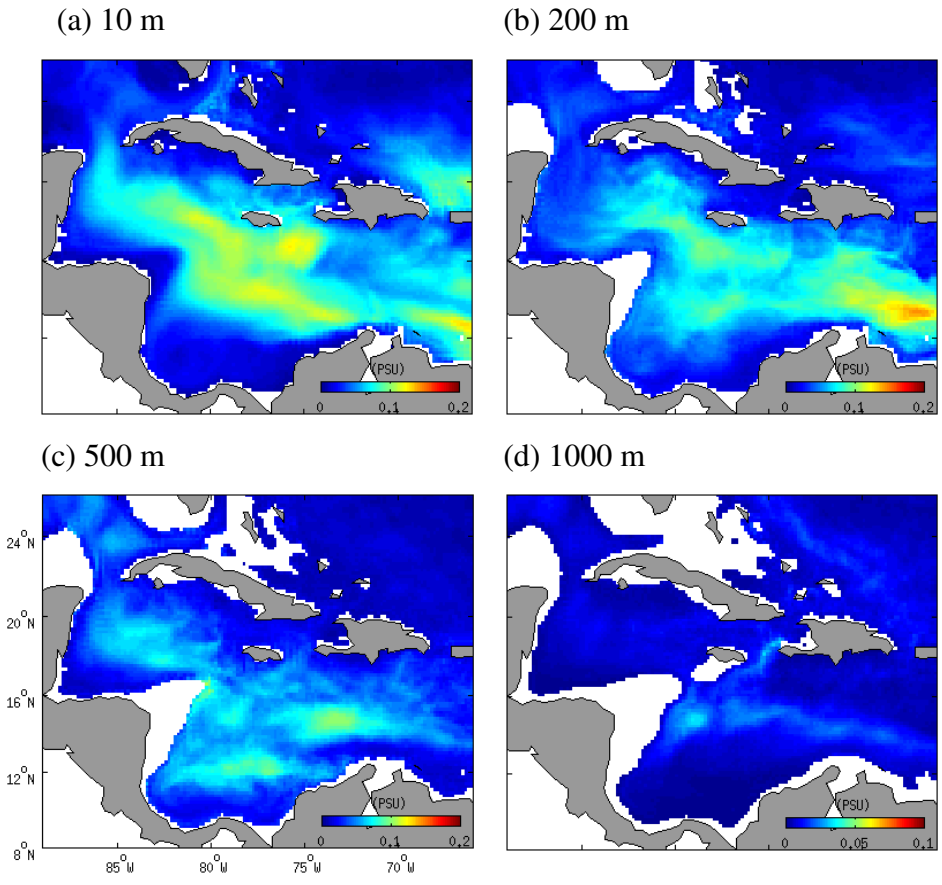

Figure 5.12. Standard deviations of modelled salinity fields calculated from model results in Exp-MF at depths of (a) 10 m, (b) 200 m, (c) 500 m, and (d) 1000 m corresponding to the study period July 13, 2000 to December 31, 2002.

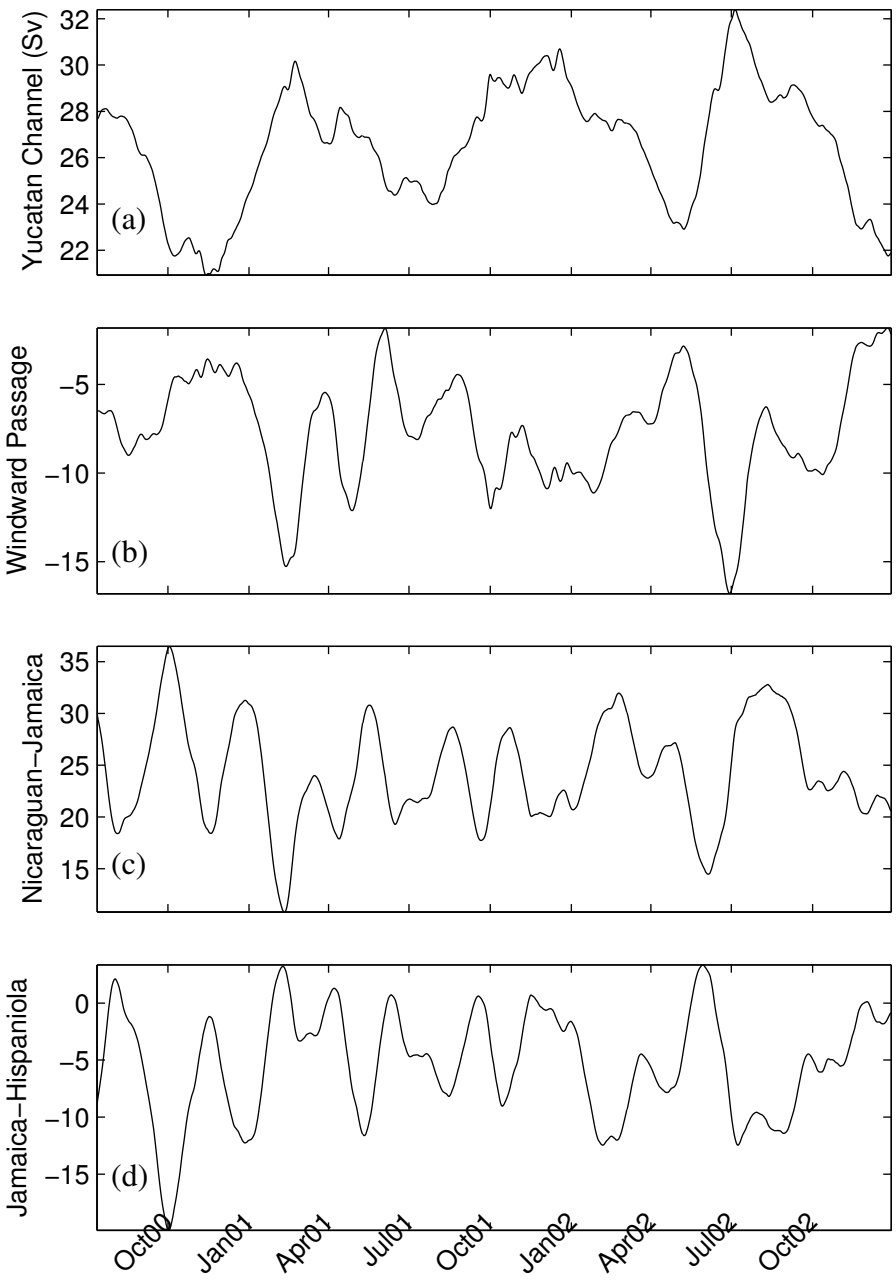

Figure 5.13. Time series of the model-calculated daily-mean transports in Exp-MF corresponding to the study period July 13, 2000 to December 31, 2002 through (a) the Yucatan Channel (Ψ_{YC}), (b) the Windward Passage (Ψ_{WP}), (c) the passage between Nicaragua and Jamaica (Ψ_{NJ}), and (d) the passage between Jamaica and Hispaniola (Ψ_{JH}). Ψ_{YC} is positive to the north. Ψ_{WP} is positive to the northeast. Ψ_{NJ} and Ψ_{JH} are positive to the northwest.

time lags, indicating that the dynamic connectivity between the Yucatan Channel and the Windward Passage known as the compensation effect (Lin et al., 2009) operates not only in connection with Loop Current intrusion into the Gulf but also in response to Caribbean eddy activities. The band-pass filtered transport $<\Psi_{NJ}>$ and $<\Psi_{JH}>$ are also out of phase, with a correlation coefficient of -0.91 with zero time lags. These fluctuations are driven by the interaction between Caribbean eddies and the Nicaraguan Rise as we discussed in section 5.3.3 and show that the compensation for the transport variations across the Nicaraguan Rise takes place around the island of Jamaica.

To further examine the role played by Caribbean eddies on the circulation variability in the Caribbean Sea, we conduct a complex empirical orthogonal function (CEOF, Horel, 1984; Merrifield and Guza, 1990) analysis on the band-pass filtered (with timescales of 30-120 days) potential temperature and velocity fields at 200 m (together) during the period between July 13, 2000 and December 31, 2002 in Exp-MF. Only the model results over the region between 8 and 26˚N and between 90 and 73˚W are used to isolate propagating structures of eddies in the Western Caribbean Sea. Figure 5.14 shows the percentage of the variance accounted by the first ten CEOF modes. The first three CEOFs account for ~40.0%, ~19.1% and ~10.3% respectively of the total monthly to seasonal temperature and velocity variance at 200 m in Exp-MF.

As revealed by Figure 5.15, amplitudes of the first CEOF mode are characterized by significant variations in the area of the Colombia Basin and Nicaraguan Rise (Figure 5.15a) due to eddy activities there. Large amplitudes also concentrated along the corridor taken by the Caribbean eddies. From the view of phase differences, the first CEOF mode represents the dominant westward propagation features of eddies in the Caribbean Sea (Figure 5.15c). The second CEOF has large amplitudes mainly concentrated in the area of the Yucatan Basin and Colombia Basin (Figure 5.15b). This mode represents a westward propagation of eddies crossing the Caribbean Sea, and a veering propagation in the region of the Columbia-Panama Gyre (Figure 5.15d).

From the amplitude and phase patterns shown in Figure 5.15, we reconstruct the evolution of propagation structure of each CEOF based on the following equation:

$$T(x, y, t) = A(x, y)Cos(\omega_0 t + \Phi(x, y)) \tag{5.3}$$

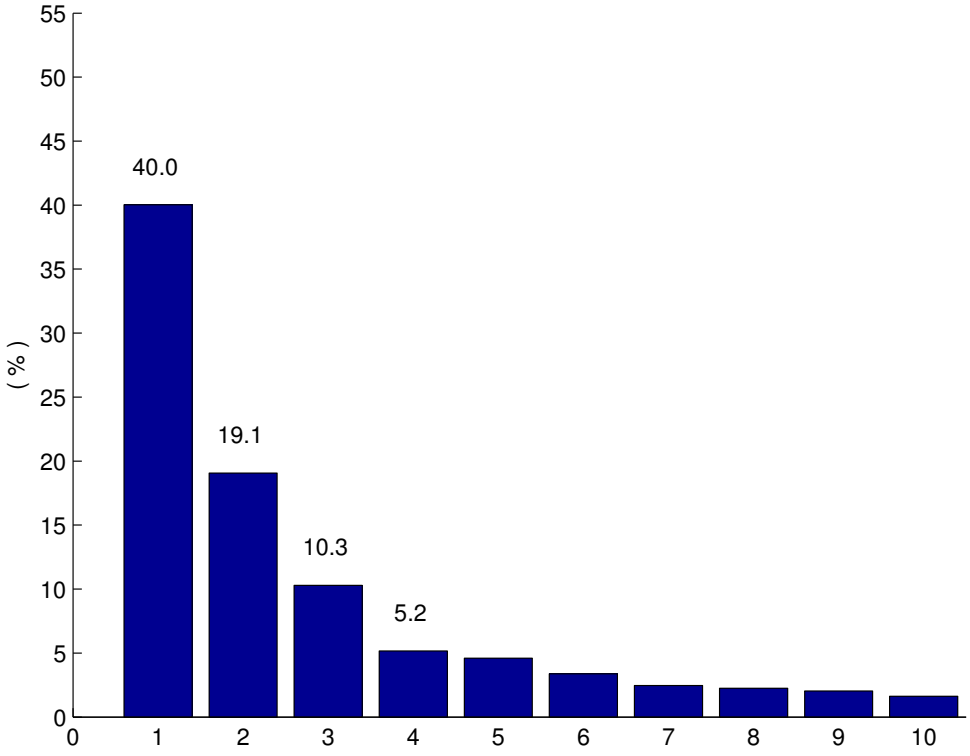

Figure 5.14. Percentages of variance accounted by the first ten CEOFs based on band-pass filtered (30-120 days) temperature fields at 200 m calculated from model results in Exp-MF during the period between July 13, 2000 and December 31, 2002.

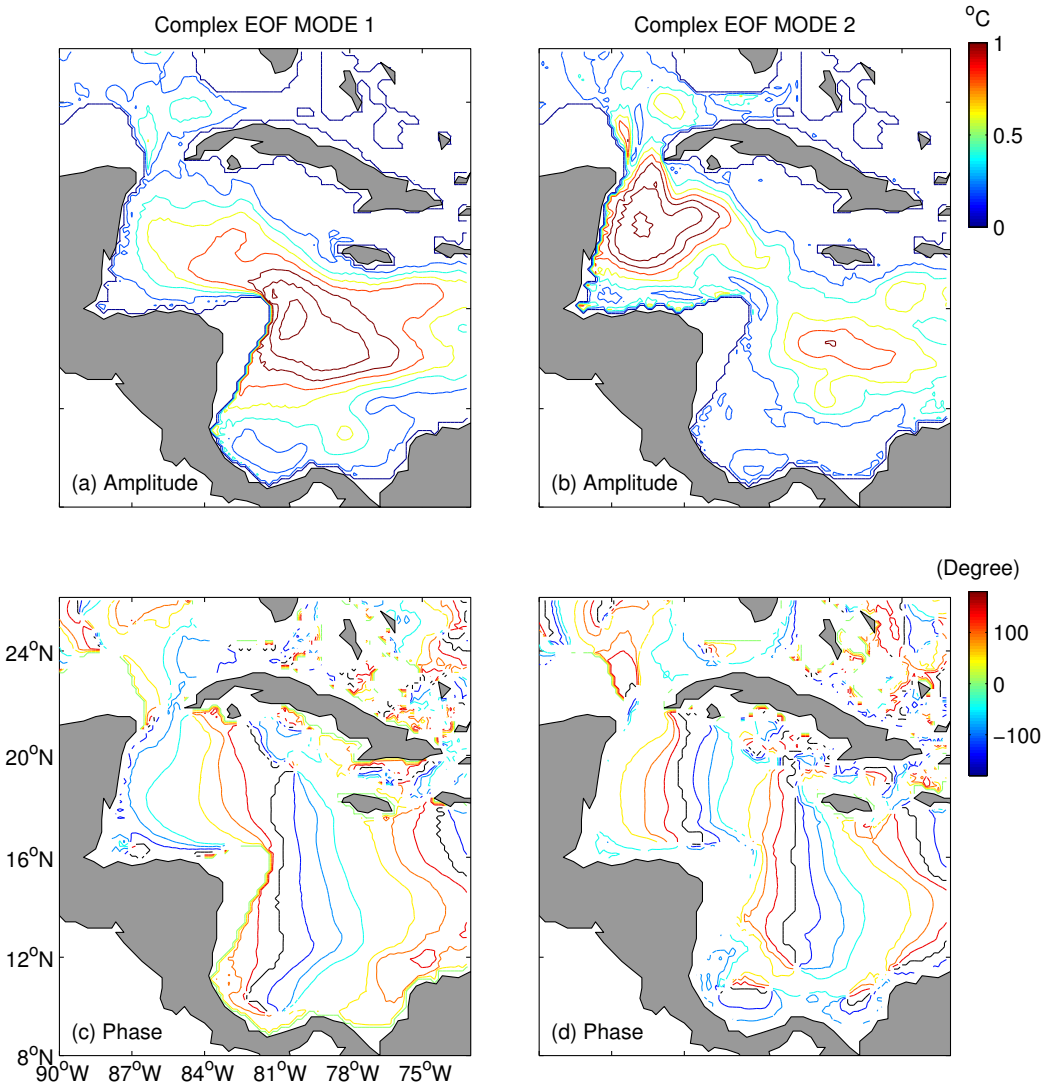

Figure 5.15. (a and b) Amplitudes and (c and d) phases of the first two CEOF modes based on band-pass filtered (30-120 days) temperature fields at 200 m from model results in Exp-MF during the period between July 13, 2000 and December 31, 2002.

where A(x,y) and Φ(x,y) are amplitudes and phases of each CEOF mode; $\omega_0=2\pi/T_0$. T_0 is the dominative period based on the spectrum of time series of the first two CEOF modes, which equals 82 days for the first CEOF mode and 69 days for the second CEOF mode. Figures 5.16 and 5.17 present snapshots for one propagation cycle of the first two CEOF modes from 0 to T_0 with a time interval of $T_0/8$ (i.e. propagation phases at every $\pi/8$ between 0 and 2π), respectively.

In the propagation cycle of the first CEOF mode (Figure 5.16), warm-core (anticyclonic) eddies and cold core anomalies propagate from the Eastern Caribbean Sea to the Yucatan Basin alternatively. For example, a warm-core (anti-cyclonic) eddy is to the south of Hispaniola (centered at 16.5°N and 75.0°W) in Figure 5.16e, propagates southwestward, and approaches the Nicaraguan Rise after $3T_0/8$ (~31 days, Figures 5.16h and a). Jamaica is then inside the anti-cyclonic flow driven by the warm-core eddy over the east slope of the Nicaraguan Rise. The warm-core eddy propagates westwards (Figures 5.16b and c) for ~41 days ($T_0/2$) interacting with the topography (Figures 5.16d and e). The warm-core eddy bifurcates (Figures 5.16f and g) with the main part continuously propagates westward to the Yucatan Basin. The southern part is trapped by the Nicaraguan Rise, veers cyclonically along the Atlantic coast of Central America (Figure 5.16h), and merges with the next eddy from the eastern Caribbean Sea in the Guajira upwelling region (Figures 5.16a and b).

The first CEOF also demonstrates the effect of Caribbean eddies squeezing through the Yucatan Channel. The warm-core eddy reaches the Yucatan Basin in Figure 5.16a and squeezes through the Yucatan Channel (Figures 5.16b-e). After the warm-core eddy squeezes through the Yucatan Channel, a southeastward flow along the north Cuba and a southwestward flow through the Windward Passage into the Caribbean Sea at 200 m is enhanced (Figures 5.16e and f), indicating the compensation effect around Cuba suggested by Lin et al. (2009).

The propagation cycle of the second CEOF mode is shown in Figure 5.17. A warm-core eddy centered at 14.4°N and 76.2°W (Figure 5.17a) propagates westward (Figures 5.17b-f), interacts with the Nicaraguan Rise between Nicaraguan and Jamaica (Figure 5.17g). The interaction is relatively weak and most of the warm-core eddy continuously propagates northwestward into the Yucatan Basin (Figures 5.17a-f). The

warm-core eddy then interacts with the east coast of Belize and Mexico and the Yucatan Channel (Figures 5.17g-h and a-b) and some warm water propagates back to the east along the coast (Figures 5.17b-d).

The CEOF results shown in Figures 5.16 and 5.17 demonstrate the role played by Caribbean eddies on the monthly to seasonal circulation variability (with timescales of 30-120 days) in the Caribbean Sea. We calculate the correlation coefficient between the reconstructed time series (the real part) for the first two CEOFs and the volume transports at the main channels and passages in the Western Caribbean Sea, including the Yucatan Channel, Windward Passage, and the section between Nicaragua and Jamaica. Transport time series are calculated from band-pass filtered (30-120 days) model results in Exp-MF.

Correlation between time series of the first CEOF mode and transports between Nicaragua and Jamaica ($<\Psi_{NJ}>$, where angle brackets represent the band-pass filtering with timescales of 30-120 days) and between Jamaica and Hispaniola ($<\Psi_{JH}>$) is shown in Figure 5.18a. There is a positive correlation coefficient (0.84) between the time series of the first CEOF and $<\Psi_{NJ}>$ with CEOF leading by ~4 days, and a negative correlation coefficient (-0.75) between the time series of the first CEOF and $<\Psi_{JH}>$ with CEOF leading by ~8 days, which is associated with the pattern between Figures 5.16h and a. Physically it means that the enhanced northwestward $<\Psi_{NJ}>$ and decreased northwestward $<\Psi_{JH}>$ are related with a warm-core eddy over the east slope of the Nicaraguan Rise, driving the anti-cyclonic flow around the island of Jamaica. The negative correlation coefficient (-0.77) between the time series of the first CEOF and $<\Psi_{NJ}>$ with time lags of about 34 days (transport leads CEOF), and the positive correlation coefficient (0.69) between the time series of the first CEOF and $<\Psi_{JH}>$ with time lags of about 29 days (transport leads CEOF), is mainly associated with the pattern between Figures 5.16d and e. The decreased northwestward $<\Psi_{NJ}>$ and enhanced northwestward $<\Psi_{JH}>$ are associated with the cold anomaly driving the cyclonic flow over the east slope of the Nicaraguan Rise.

There is a positive correlation (-0.51) between time series of the first CEOF and the band-pass filtered Yucatan Channel transport ($<\Psi_{YC}>$), with time series of the first CEOF

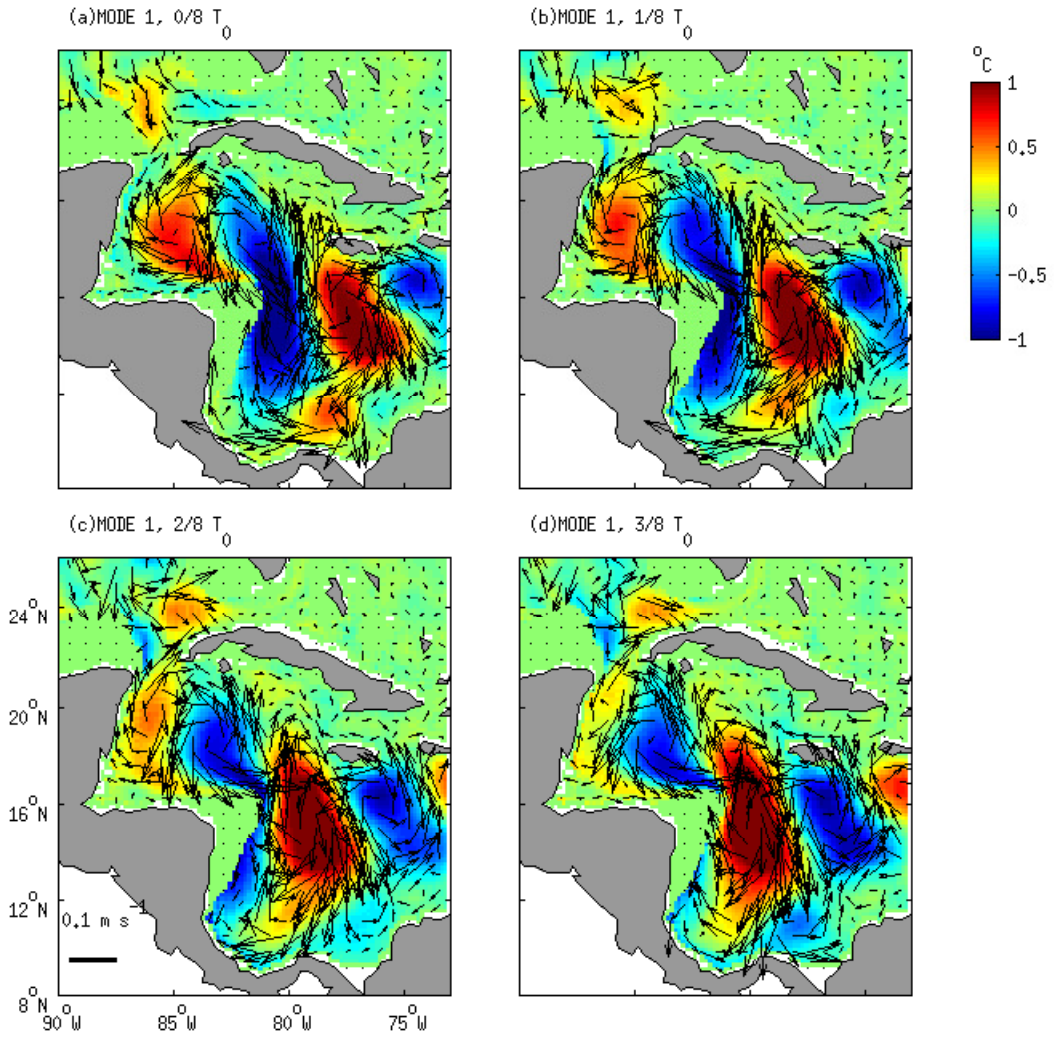

Figure 5.16. Evolution of the propagation structure of the first CEOF mode calculated from band-pass filtered (30-120 days) temperature and velocity fields at 200 m based on model results in Exp-MF during the period between July 13, 2000 and December 31, 2002. T_0 = 82 days.

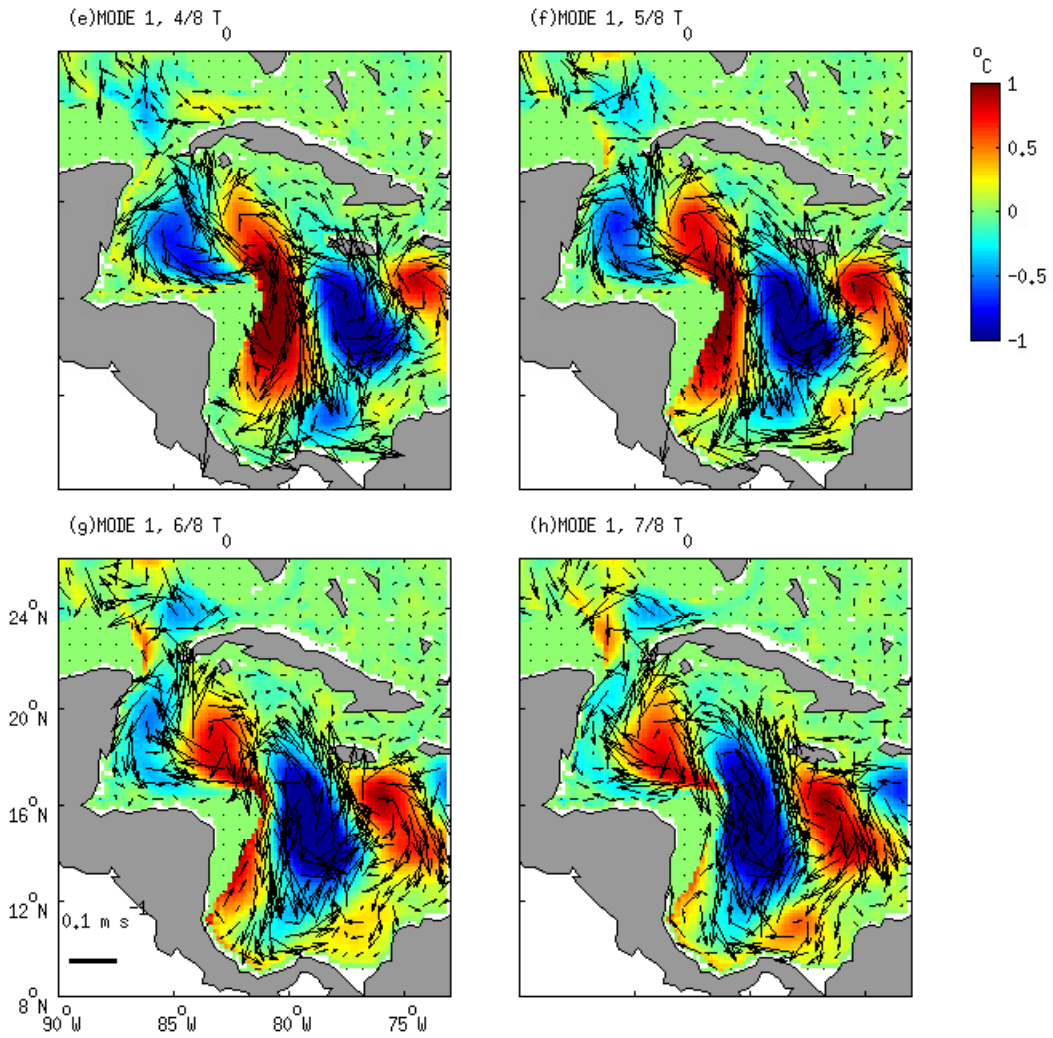

Figure 5.16. (continued)

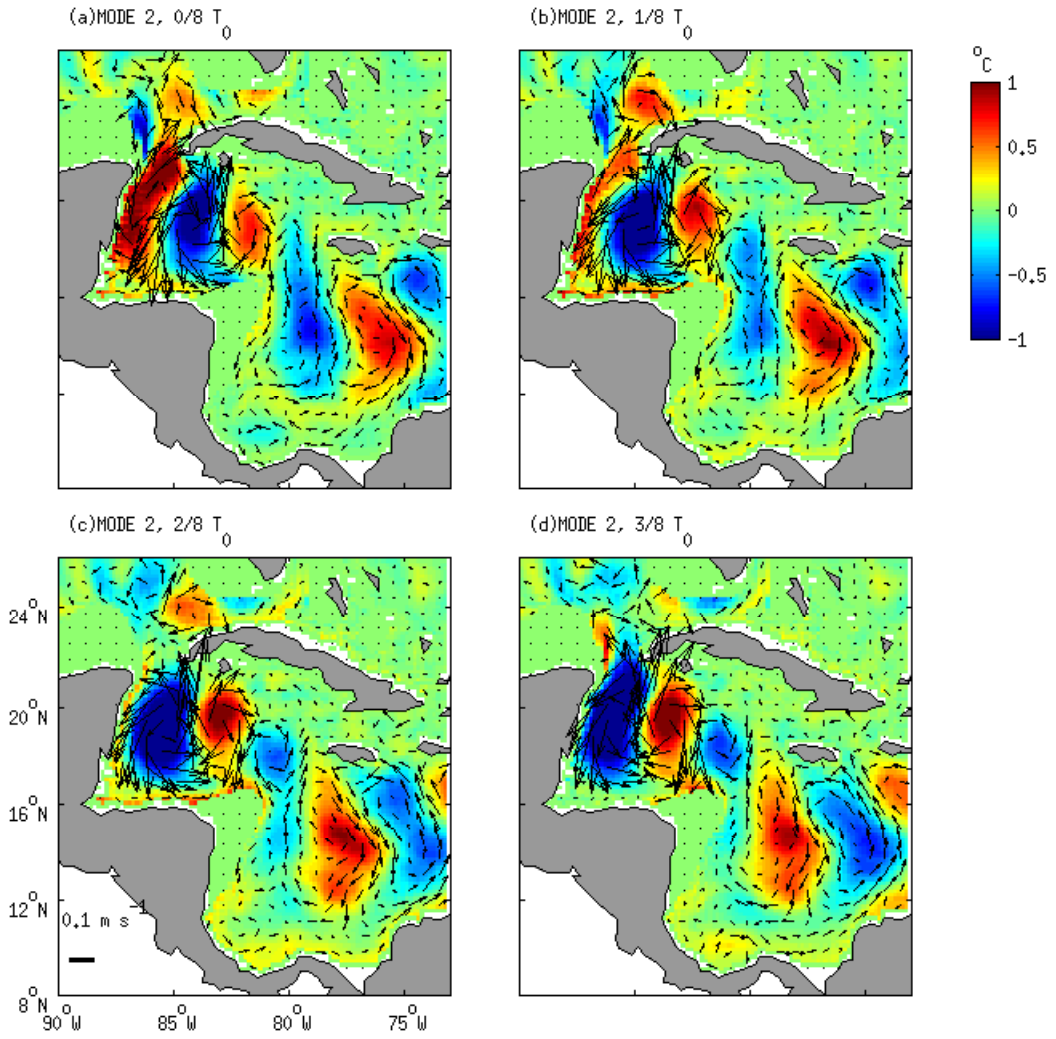

Figure 5.17. Evolution of the propagation structure of the second CEOF mode calculated from band-pass filtered (30-120 days) temperature and velocity fields at 200 m based on model results in Exp-MF during the period between July 13, 2000 and December 31, 2002. T_0 =69 days.

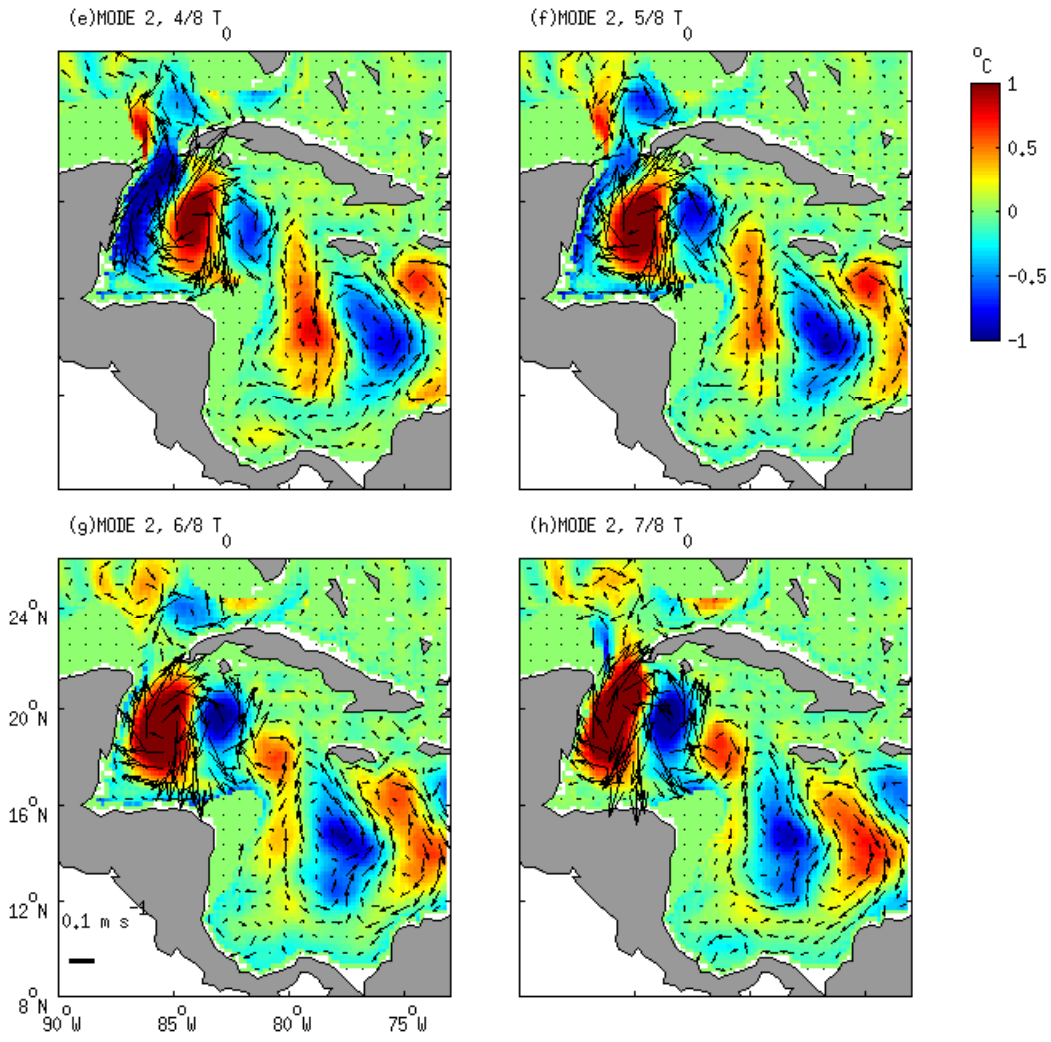

Figure 5.17. (continued)

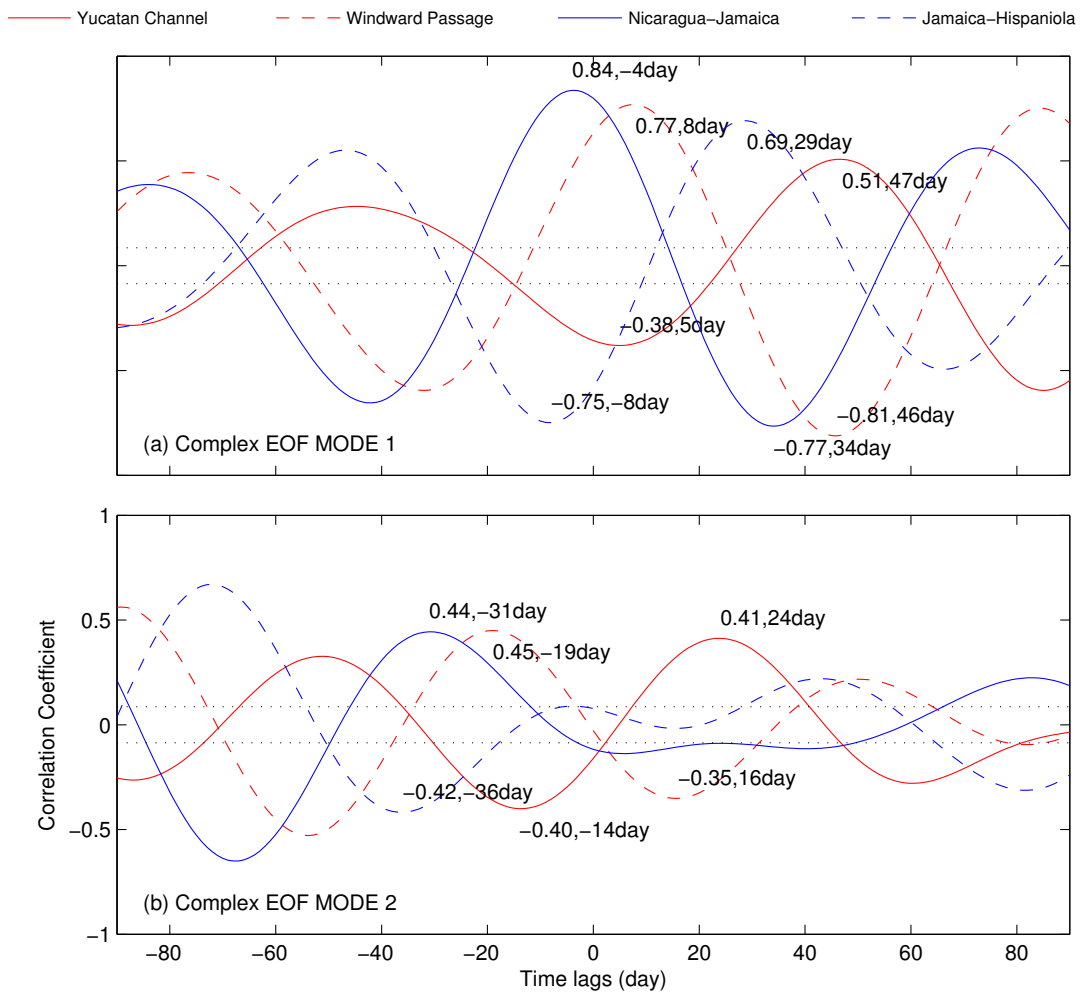

Figure 5.18. Correlation coefficients between the real part of reconstructed time series of the first two CEOF modes and model-calculated transports through the Yucatan Channel, the passage between the Nicaragua and Jamaica, and the Windward Passage, based on band-pass filtered (30-120 days) model results in Exp-MF during the period between July 13, 2000 and December 31, 2002. Correlations outside the horizontal dotted lines are significantly different from zero at the 99% level.

lagging by 47 days (Figure 5.18a). With similar time lags (CEOF lagging by 46 days), there is a negative correlation (-0.81) between time series of the first CEOF and the band-pass filtered Windward Passage transport ($<\Psi_{WP}>$). This relation between the eddy propagation and transport variations is associated with the pattern between Figures 5.16e and f, where an anticyclonic compensation flow around Cuba is enhanced. Similarly, the cyclonic flow around Cuba shown in Figures 5.16a and b is related to the negative correlation (-0.38) between the time series of the first CEOF and $<\Psi_{YC}>$ and the positive correlation (0.77) between CEOF and $<\Psi_{WP}>$.

The correlation between the time series of the second CEOF and transports, $<\Psi_{NJ}>$ and $<\Psi_{JH}>$, is relatively lower (Figure 5.18b), indicating that the interaction between eddies and the Nicaraguan Rise is weaker than for the first CEOF mode. There is a positive correlation (0.44) between the time series of the second CEOF and $<\Psi_{NJ}>$, and a negative correlation (-0.42) between the second CEOF and $<\Psi_{JH}>$, with CEOF leading by 31 and 36 days separately. The time series of the second CEOF is correlated with band-pass filtered transports through the Yucatan Channel ($<\Psi_{YC}>$) and the Windward Passage ($<\Psi_{WP}>$), with similar time lags but almost reversed values (see Figure 5.18b), indicating the compensation effect connecting the Yucatan Channel and the Windward Passage is generated when the warm and cold anomalies interact with the Yucatan Channel (patterns shown in Figures 5.17b and f).

5.4. Summary and conclusion

We examined circulation and hydrographic distributions in the Caribbean Sea, with a special emphasis on the role of Caribbean eddies on the circulation variability and connectivity in the study region using a regional ocean circulation model. The model was integrated from January 1999 to December 2002 and forced by 6-hourly wind fields from National Centers for Environmental Prediction (NCEP). Temperature, salinity, and velocity fields used for surface and lateral boundary conditions were extracted from global ocean circulation reanalysis fields produced by the British Atmospheric Data Centre (BADC). To improve model hindcast skills, the sea level anomalies derived from satellite altimetry observations were assimilated into the model using the physically-

based data assimilation scheme suggested by Cooper and Haines (1996). A correction term for barotropic transports was added to the north open boundary of the model based on the differences between model-produced and observed (inferred from cable voltages) transports of the Florida Current between Florida and the Bahamas. The semi-prognostic method suggested by Sheng et al. (2001) was also used to reduce model errors. Two numerical experiments (Table 1) were made in this study: (1) the control run (Exp-CR) and (2) steady forcing Run (Exp-MF). In each experiment, the model was integrated from January 1, 1999 to December 31, 2002. Model results during the period between 13 July 2000 and 31 December 2002 were discussed in this study, during which the observed transports of the Florida Current (Baringer and Larsen, 2001) and Yucatan Current (CANEK, e.g. Bunge et al., 2002; Sheinbaum et al., 2002) are available for model validation and calibration.

We demonstrated that the ocean circulation model of the IAS in the control run (Exp-CR) has some skill at reconstructing the observed circulation, hydrographic distributions and associated variability in the IAS during the study period. The time-mean potential temperature and velocity fields along the meridional transect at 66.0˚W over the eastern Colombian Basin produced by the model in Exp-CR agree quantitatively with the observations made during August-September 1997 (Hernandez-Guerra and Joyce, 2000). Model results in Exp-CR are also comparable quite well with the observed circulation and hydrography at the Yucatan Channel made during the CANEK program between July 13, 2000 and May 31, 2001. Variability of temperature and the salinity fields produced by the model have similar vertical structure and horizontal distributions as in the climatological data extracted from the World Ocean Atlas Data 2005 by the National Oceanographic Data Center.

Model results in the control run were used in examining the main physical processes for the monthly to seasonal circulation and associated variability (with timescales of 30-120 days). Significant variability of simulated temperature fields at 200 m was found in the model, as results from Caribbean eddy activities. A significant correlation was found between the band-pass filtered (with timescales of 30-120 days) simulated potential temperature fields at 200 m and transports between Nicaragua and Jamaica ($<\Psi_{NJ}>$, where angle brackets represent the band-pass filtering) during the study period,

with a positive correlation coefficient over the east slope and a negative correlation coefficient over the west slope of Nicaraguan Rise. High correlation between the temperature variations and the throughflow transport over the Nicaraguan Rise was also found along the vertical transect along the narrow corridor of Caribbean eddies. The dynamics can be understood as the result of the interaction between the density anomalies and the underlying variable bottom topography known as the form drag mechanism (Lin et al., 2009). Increased northwestward $<\Psi_{NJ}>$ is associated with warm-core eddies (lighter water) over the eastern slope and/or cold-core eddies (denser water) over the western slope. The resulting pressure difference across the ridge then drives enhanced northwestward transport over the Nicaraguan Rise by the form drag effect.

Model results in Exp-MF was used to quantify the role of Caribbean eddies and associated dynamics responsible for the circulation variability in the Caribbean Sea. A complex empirical orthogonal function (CEOF) analysis was conducted for potential temperature and velocity fields at 200 m produced by the model in Exp-MF. The first two CEOF modes account for 40.0% and 19.1% of the temperature and velocity variance at 200 m in the experiment. We reconstructed the propagation cycle of each CEOF mode and correlated time series of each CEOF mode and transports through the Yucatan Channel, Windward Passage, and the section between the Nicaragua and Jamaica. The first CEOF mode mainly demonstrated that the interaction of Caribbean eddies and the Nicaraguan Rise is responsible for the monthly to seasonal variability of circulation in the Western Caribbean Sea in Exp-MF. The first CEOF mode also presented the relation between Caribbean eddies squeezing through the Yucatan Channel and the compensation flow around Cuba (Lin et al., 2009) on timescales of 30-120 days.

Chapter 6

Conclusion

The Intra-Americas Sea (IAS) plays an important role as a conduit for mass, heat, salt and other tracers in the Atlantic circulation system, which comprises the Yucatan and Florida currents. The circulation system is important because it is the major feeder for the Gulf Stream. Observations and numerical simulations, including the numerical simulations presented in this thesis, illustrate the highly variable nature of the Loop Current and its ring shedding, as well as the meandering of the Caribbean Current and the propagation of mesoscale eddies in the IAS. While much is understood about the dynamics of the mean circulation in the IAS, many issues remain concerning the variability of the current and the role played by the eddies. Using a number of different model experiments and various observations, we have examined the circulation and associated variability in the IAS.

Chapter 2: For there to be no net accumulation of water in the Gulf of Mexico, the transport into the Gulf through the Yucatan Channel must be exactly balanced by the transport out through the Straits of Florida between the Florida and Cuba. However, not all the transport exiting the Gulf between Florida and Cuba has to pass between Florida and the Bahamas because of leakage through the Old Bahama and Northwest Providence Channels (Maul and Vukovich, 1993; Hamilton et al., 2005). Using a numerical model, we demonstrated that transport variations through the Yucatan Channel are partly compensated by flow variations through the channels north of Cuba, notably the Old Bahama Channel (what we have called the “compensation effect”). We note that because

of the compensation effect, transport through the Yucatan Channel and between Florida and the Bahamas (at the site of the submarine cable; Baringer and Larsen, 2001) do not vary in unison in the model. The correlation between the transport times series measured during the CANEK program (Sheinbaum et al., 2002) and the cable estimate (Baringer and Larsen, 2002) is even much lower (only 0.15).

The compensation effect is found to operate on a wide range of time scales in the model. On time scales shorter than 30 days, the compensation effect is associated with wind forcing in the model. On time scales longer than a month, the link between the vertically integrated transport through the Yucatan Channel and the intrusion of the Loop Current into the Gulf of Mexico has been discussed in detail in Chapter 2. In the model the minimum transport of the Yucatan Channel is associated with a maximum intrusion of the Loop Current into the Gulf of Mexico. Likewise, the transport through the Yucatan Channel reaches its maximum when a bulging of the Loop Current is built away from the northwest coast of Cuba. We argued that the transport variations associated with the Loop Current intrusion arise from the interaction between the density anomalies associated with the Loop Current evolution and the variable bottom topography, the mechanism being the form drag effect across the ridge connecting Florida and Cuba.

Chapter 3: On timescales longer than 120 days, an index was introduced based on the difference in sea surface height anomalies between two locations in the southeastern Gulf of Mexico; one is centered at 25.0˚N, 86.0˚W and the other at 23.5˚N, 84.0˚W off the northwest coast of Cuba. We choose these locations based on an EOF analysis of satellite altimeter data following guidance from the numerical model. The satellite altimeter derived transport index is comparable with the CANEK estimates of vertically integrated transport through the Yucatan Channel during the period between September 1999 and May 2001. Comparing the index to the long-term (1992-2009) daily mean transport of the Florida Current inferred from voltage differences across the Florida-Bahamas submarine cable at 27˚N, we showed that the cable transport estimates are affected by influences from upstream in the Gulf of Mexico and, in particular, the time-varying intrusion of the Loop Current into the Gulf of Mexico. Given the geometric connectivity between the Yucatan Channel and the Straits of Florida, it is possible that

intrusion-induced fluctuations in vertically integrated transport through the Yucatan Channel also have a signature in the cable-estimated transports of the Florida Current.

Chapter 4: We then sought to improve the model by replacing the seasonally varying transport on the northern boundary with a more realistic representation of the variability extracted from 5-day global ocean circulation reanalysis fields produced by the British Atmospheric Data Centre (BADC). Sea level anomalies derived from satellite altimetry observations were assimilated into the model using the data assimilation scheme suggested by Cooper and Haines (1996). A correction term for barotropic transports was added to the north open boundary condition based on the differences between model-produced and observed (inferred from cable voltages) transports of the Florida Current between Florida and the Bahamas. The data-assimilative ocean circulation model has some skill at reconstructing the observed circulation, hydrographic distributions and associated variability in the IAS during the study period between July 13, 2000 and December 31, 2002.

We extended our previous work by examining the vertical structures of the flow through the Yucatan Channel during ring shedding and intrusion in the model. Baroclinic flow at the Yucatan Channel is found to be mainly associated with the compensation effect at low frequencies (timescales longer than 20 days). The compensation effect between the Yucatan Channel and channels to the north of Cuba also operates at high frequencies (timescales shorter than 20 days). At high frequencies, flow variations through the Yucatan Channel have a barotropic response, which results from wind driven circulation variability based on our previous study.

Chapter 5: Better understanding is required for the main physical processes in the IAS responsible for the monthly to seasonal circulation variability and connectivity (timescales between 30 to 120 days). Circulation on this frequency band is influenced by Caribbean eddies based on previous numerical and observational studies (i.e. Carton and Chao, 1999; Oey et al., 2003; Jouanno et al., 2008b). We analyzed model produced temperature fields at 200 m where significant variance was found in association with Caribbean eddy activities. A significant correlation was found between the band-pass filtered (with the timescale of 30-120 days) potential temperature fields at 200 m and the vertically integrated transports between Nicaragua and Jamaica ($<\Psi_{NJ}>$, where angle

brackets represent the band-pass filtering) during the study period, with positive correlation coefficients (~0.47) over the east side and negative coefficients (~0.40) over the west side of the Nicaraguan Rise. Increased northwestward $<\Psi_{NJ}>$ is associated with warm-core eddies (lighter water) over the east slope and/or cold-core eddies (denser water) over the west slope. We proposed that the dynamics can also be understood as the form drag mechanism. The interaction between the density anomalies and the underlying variable bottom topography changes the pressure difference across the ridge and drives transport variations between Nicaragua and Jamaica.

To understand the role of Caribbean eddies and associated dynamics responsible for the monthly to seasonal circulation and associated variability in the Caribbean Sea, we ran the model with time-mean model forcing (EXP-MF), in which the regional circulation model is forced by multiyear (1999-2002) time-mean wind stress and multiyear (1999-2002) time-mean potential temperature, salinity and velocities at lateral open boundaries. We conducted a complex empirical orthogonal function (CEOF) analysis on the band-pass filtered (with timescales of 30-120 days) potential temperature and velocity fields at 200 m during the period between July 13, 2000 and December 31, 2002 in Exp-MF. In this numerical experiment, we identified the role played by the Caribbean eddies on the monthly to seasonal circulation and associated variability in the Caribbean Sea. The connectivity between the Yucatan Channel and the Windward Passage along the north of Cuba (with timescale of 30-120 days) was also found to operate when Caribbean eddies squeeze through the Yucatan Channel.

Appendix A

Copyright

1. An edited version of **Chapter 2** was published by American Geophysical Union (AGU). Copyright (2009) American Geophysical Union. It is reproduced here by permission of AGU:

Rights Granted to Authors

AGU's philosophy recognizes the need to ensure that authors have a say in how their works are used and the necessity to foster broad dissemination of scientific literature while protecting the viability of the publication system. The following nonexclusive rights are granted to AGU authors:

All proprietary rights other than copyright (such as patent rights)

The right to present the material orally

The right to reproduce figures, tables, and extracts properly cited

The right to make paper copies of all or part of the contribution for classroom use

The right to deny subsequent commercial use of the contribution

The right to place the contribution or its abstract on his/her personal Web site as described below…

(See http://www.agu.org/pubs/authors/usage_permissions.shtml)

2. An edited version of **Chapter 3** was accepted for publication by Springer.

Confirmation of your Copyright Transfer

Dear Author,

Please note: This e-mail is a confirmation of your copyright transfer and was sent to you only for your own records. The copyright to this article is transferred to "Springer-Verlag" (for U.S. government employees: to the extent transferable) effective if and when the article is accepted for publication…

An author may self-archive an author-created version of his/her article on his/her own website. He/she may also deposit this version on his/her institution's and funder's (funder designated) repository at the funder's request or as a result of a legal obligation, including his/her final version, provided it is not made publicly available until after 12 months of official publication…

Kind regards,

Springer Author Services

Article Details

Journal title: Ocean Dynamics

Article title: The influence of Gulf of Mexico Loop Current intrusion on the transport of the Florida Current

DOI: 10.1007/s10236-010-0308-0

Corresponding Author: Yuehua Lin

Copyright transferred to: Springer-Verlag

Transferred on: Tue May 25 21:39:20 CEST 2010

3. Chapters 4 is reproduced here by permission of the American Society of Civil Engineers (ASCE):

Reuse Author's Own Material

ASCE grants $0 license to authors who request to reuse their own content. The content may be used as follows:

Reuse in book/CD-ROM

Reuse in journal

Reuse in magazine

Reuse in coursepack

Reuse in brochure/flyer

Reuse in newspaper/newsletter

Photocopy

Post on Internet/intranet

Digital reprint

Reuse in masters/doctoral thesis

Reuse in electronic media

…

（See http://www.asce.org/Content.aspx?id=21545#thesis）

Reuse in masters/doctoral thesis

This permission allows a masters/doctoral degree candidate to republish the requested content in his/her doctoral thesis. This permission is free of charge.

（See http://www.asce.org/Content.aspx?id=21545#thesis）

Bibliography

[1] Abascal, A. J., J. Sheinbaum, J. Candela, J. Ochoa, and A. Badan (2003), Analysis of flow variability in the Yucatan Channel, *J. Geophys. Res*., 108(C12), 3381, doi: 10.1029/2003JC001922.

[2] Anderson, D. L. T., and R. A. Corry (1985), Seasonal transport variations in the Florida Straits: A model study, *J. Phys. Oceanogr.*, 15, 773–786.

[3] Andrade, C., and E. Barton (2000), Eddy development and motion in the Caribbean Sea, *J. Geophys. Res.*, 105(C11), 26191-26201.

[4] Andrade, C., and E. Barton (2005), The Guajira upwelling, *Cont. Shelf Res.*, 25, 9, 1003-1022.

[5] Atkinson, L. P., T. Berger, P. Hamilton, E. Waddell, K. Leaman, and T. N. Lee (1995), Current meter observations in the Old Bahama Channel, *J. Geophys. Res.*, 100, 8555 –8560, doi:10.1029/95JC00586.

[6] AVISO/Altimetry (1996), AVISO user handbook for merged TOPEX/POSEIDON products, AVI-NT-02-101, Edition 3.0.

[7] Baringer, M. O., and J. C. Larsen (2001), Sixteen years of Florida Current transport at 27˚N, *Geophys. Res. Lett.*, 28, 3179–3182, doi:10.1029/ 2001GL013246.

[8] Barnier B., L. Siefridt, and P. Marchesiello (1995), Thermal forcing for a global ocean circulation model using a three-year climatology of ECMWF analyses, *J. Mar.* Syst., 6, 363-380, doi:10.1016/09247963(94)00034-9.

[9] Beal, L.M., J.M. Hummon, E. Williams, O.T. Brown, W. Baringer and E.J. Kearns (2008), Five years of Florida Current structure and transport from the Royal Caribbean cruise ship "Explorer of the Seas", *J. Geophys. Res.*, 113, C06001, doi:10.1029/2007JC004154.

[10] Brooks, I. H. (1979), Fluctuations in the transport of the Florida Current at periods between tidal and two weeks. *J. Phys. Oceanogr.*, 9, 1048-1053.

[11] Bunge, L., J. Ochoa, A. Badan, J. Candela, and J. Sheinbaum (2002), Deep flows in the Yucatan Channel and their relation to changes in the Loop Current extension, *J. Geophys. Res.*, 107(C12), 3233, doi: 10.1029/2001JC001256.

[12] Candela, J., S. Tanahara, M. Crepon, B. Barnier, and J. Sheinbaum (2003), Yucatan Channel flow: Observations versus CLIPPER ATL6 and MERCATOR PAM models, *J. Geophys. Res.*, 108(C12), 3385, doi: 10.1029/2003JC001961.

[13] Carton, J. A., and Y. Chao (1999), Caribbean Sea eddies inferred from TOPEX/POSEIDON altimetry and a 1/6° Atlantic Ocean model simulation, *J. Geophys. Res.*, 104 (C4), 7743–7752.

[14] Cherubin, L. M., and P. L. Richardson (2007), Caribbean current variability and the influence of the Amazon and Orinoco freshwater plumes, *Deep Sea Res.*, 54, 1451-1473.

[15] Cherubin, L. M., Y. Morel, and E. P. Chassignet (2006), Loop Current Ring shedding: formation of cyclones and interaction with topography. *J. Phys. Oceanogr.*, 36, 569-591.

[16] Cherubin, L. M., W. Sturges, and E. P. Chassignet (2005), Deep flow variability in the vicinity of the Yucatan Straits from a high-resolution numerical simulation, *J. Geophys. Res.*, 110, C04009, doi: 10.1029/2004JC002280.

[17] Coats, D. A. (1992), The Loop Current, in *Physical oceanography of the U.S. Atlantic and Eastern Gulf of Mexico*, J. D. Milliman and E. Imamura, Eds., Atlantic OCS Region, Mineral Management Service, U.S. Dept. of the Interior.

[18] Cooper, M., and K. Haines (1996), Altimetric assimilation with water property conservation, *J. Geophys. Res.*, 101, 1059–1077.

[19] Cunningham, S. A., T. Kanzow, D. Rayner, et al. (2007), Temporal variability of the Atlantic Meridional Overturning Circulation at 26.5°N, S*cience*, 317, 935–938, doi:10.1126/science. 1141304.

[20] da Silva, A. M., C. C. Young-Molling, and S. Levitus (Eds.) (1994), *Atlas of Surface Marine Data 1994*, vol. 3, *Anomalies of Heat and Momentum Fluxes, NOAA Atlas NESDIS 8*, vol. 3, 413 pp., NOAA, Silver Spring, Md.

[21] Dietrich, D. E. (1998), Application of a modified Arakawa "a" grid ocean model having reduced numerical dispersion to the Gulf of Mexico circulation, *Dyn. Atmos. Oceans*, 27, 201– 217, doi:10.1016/S03770265(97)00009-2.

[22] Dietrich, D. E., C. A. Lin, A. Mestas-Nunez1, and D. S. Ko (1997), A high resolution numerical study of Gulf of Mexico fronts and eddies, *Meteorol. Atmos. Phys.*, 64, 187 –201, doi:10.1007/BF01029692.

[23] DiNezio P. N., A. C. Clement, G. A. Vecchi, B. J. Soden, B. P. Kirtman, et al. (2009), Climate response of the Equatorial Pacific to global warming, *J. Clim.*, 22, 4873-4892.

[24] Eden, C., R. J. Greatbatch, and C. W. Boning (2004), Adiabatically correcting an eddy-permitting model of the North Atlantic using large-scale hydrographic data, *J. Phys. Oceanogr.*, 34, 701–719.

[25] Eden, C., R. J. Greatbatch, and J. Willebrand (2007), A diagnosis of thickness fluxes in an eddy-resolving model, *J. Phys. Oceanogr.*, 37(S.): 727–742, doi:10.1175/JPO 2987.1.

[26] Elliott, B. A. (1982), Anticyclonic rings in the Gulf of Mexico, *J. Phys. Oceanogr.*, 12, 1292-1309.

[27] Etter, P. C. (1983), Heat and freshwater budgets of the Gulf of Mexico, *J. Phys. Oceanogr.*, 13, 2058–2069.

[28] Ezer, T., L.-Y. Oey, W. Sturges, and H.-C. Lee (2003), The variability of currents in the Yucatan Channel: Analysis of results from a numerical ocean model, *J. Geophys. Res.*, 108(C1), 3012, doi: 10.1029/2002JC001509.

[29] Ezer, T, D. V. Thattai, B. Kjerfve, and W. D. Heyman (2005), On the variability of the flow along the Meso-American Barrier Reef system: a numerical model study of the influence of the Caribbean current and eddies, *Ocean Dyn.*, 55, 458-475, doi: 10.1007/s10236-005-0033-2.

[30] Fanning, A. F., R. J. Greatbatch, A. M. Da Silva, and S. Levitus (1994), Model-calculated seasonal transport variations through the Florida Straits: A comparison using different wind-stress climatologies, *J. Phys. Oceanogr.*, 24, 30–45.

[31] Gill, A. E. (1982), *Atmosphere-ocean dynamics*, Academic, San Diego, p. 662.

[32] Gill, A. E., and P. P. Niiler (1973), The theory of the seasonal variability in the ocean, *Deep Sea Res.*, 20, 141–177.

[33] Greatbatch R. J., and A. Goulding (1989), Seasonal variations in a linear barotropic model of the North Atlantic driven by the Hellerman and Rosenstein wind stress field, *J. Phys. Oceanogr.*, 94, 12645-12665.

[34] Greatbatch, R. J., Y. Lu, B. deYoung, and J. Larsen (1995), The variation of transport through the Straits of Florida: A barotropic model study, *J. Phys. Oceanogr.*, 25, 2726 – 2740..

[35] Greatbatch, R. J., J. Sheng, C. Eden, L. Tang, X. Zhai, and J. Zhao (2004), The semi-prognostic method, *Cont. Shelf Res.*, 24, 2149–2165.

[36] Hamilton, P., G. S. Fargion, and D. C. Biggs (1998), Loop Current eddy paths in the western Gulf of Mexico, *J. Phys. Oceanogr.*, 29, 1180-1207.

[37] Hamilton, P., J. C. Larsen, K. D. Leaman, T. N. Lee, and E. Waddell (2005), Transports through the Straits of Florida, *J. Phys. Oceanogr.*, 35, 308 –322, doi:10.1175/JPO-2688.1.

[38] Hernandez-Guerra, A., and T.M. Joyce (2000), Water masses and circulation in the surface layers of the Caribbean at 66˚W, *Geophys. Res. Lett*., 27, 3497–3500.

[39] Horel, J. D., (1984), Complex principal component analysis: Theory and examples, *J. Climate Appl. Meteor.*, 23, 1660–1673.

[40] Hughes, C. W., and B. A. de Cuevas (2001), Why western boundary currents in realistic oceans are inviscid: A link between form stress and bottom pressure torques, *J. Phys. Oceanogr.*, 31, 2871 – 2885.

[41] Huh, O. K., W. J. Wiseman, and L. J. Rouse (1981), Intrusion of Loop Current waters onto the west Florida continental shelf, *J. Geophys. Res.,* 86, 4186 –4192, doi:10.1029/JC086iC05p04186.

[42] Hurlburt, H. E., and J. D. Thompson (1980), A numerical study of Loop Current intrusions and eddy shedding, *J. Phys. Oceanogr.*, 10, 1611 –1651.

[43] Johns, E., W. D. Wilson, and R. L. Molinari (1999), Direct observations of velocity and transport in the passages between the Intra-Americas Sea and the Atlantic Ocean, 1984-1996, *J. Geophys. Res.,* 104, 25805-25820.

[44] Johns, W. E., R. H. Smith, E. M. Johns, and W. D. Wilson (2008), The Caribbean mass budget revisited, Eos Trans. AGU, 89(23), Jt. Assem. Suppl., Abstract OS34A-03.

[45] Johns, W. E., T. L. Townsend, D. M. Fratantoni, and W. D. Wilson (2002), On the Atlantic inflow to the Caribbean Sea, *Deep Sea Res.* 49, 211-243.

[46] Johns, W. E., T. N. Lee, F. A. Schott, R. J. Zantopp, and R. H. Evans (1990), The North Brazil Current retroflection: seasonal structure and eddy variability, *J. Geophys. Res.*, 95(C12), 22,103–22,120.

[47] Jouanno, J., J. Sheinbaum, B. Barnier, and J. M. Molines (2008a), The mesoscale variability in the Caribbean Sea. Part II: Energy sources, *Ocean Modell.*, 26, 226–239, doi:10.1016/j.ocemod.2008.10.006.

[48] Jouanno, J., J. Sheinbaum, B. Barnier, J.M. Molines, L. Debreu, and F. Lemarie (2008b), The mesoscale variability in the Caribbean Sea. Part I: Simulations and characteristics with an embedded model, *Ocean Modell.*, 23, 82-101, doi:10.1016/j.ocemod.2008.04.002.

[49] Kanzow, T., S. A. Cunningham, D. Rayner, J. J.-M. Hirschi, W. E. Johns, M. O. Baringer, H. L. Bryden, L. M. Beal, C. S. Meinen, and J. Marotzke (2007), Observed flow compensation associated with the MOC at 26.5°N in the Atlantic, *Science,* 317, 938 –941, doi:10.1126/science.1141293.

[50] Large, W. G., and S. Pond (1981), Open ocean momentum flux measurements in moderate to strong winds, *J. Phys. Oceanogr.*, 11, 324 –336.

[51] Large, W. G., J. C. McWilliams, S. C. Doney (1994), Oceanic vertical mixing: a review and a model with a nonlocal boundary layer parameterization, *Rev. Geophys.*, 32, 363 –404, doi:10.1029/94RG01872.

[52] Larsen, J. C. (1992), Transport and heat flux of the Florida Current at 27˚N derived from cross-stream voltages and profiling data: Theory and observations, *Philos. Trans. R. Soc. London*, Ser. A, 338, 169 – 236, doi:10.1098/rsta.1992.0007.

[53] Le Traon, P.Y., F. Nadal, and N. Ducet (1998), An improved mapping method of multi-satellite altimeter data, *J. Atm. Ocean. Techn.*, 25, 522-534.

[54] Leaman, K. D., P. S. Vertes, L. P. Atkinson, T. N. Lee, P. Hamilton, and E. Waddell (1995), Transport, potential vorticity, and current/temperature structure across Northwest Providence and Santaren channels and the Florida Current off Cay Sal Bank, *J. Geophys. Res.,* 100, 8561–8569, doi:10.1029/94JC01436.

[55] Lin, Y., R. J. Greatbatch, and J. Sheng (2009), A model study of the vertically integrated transport variability through the Yucatan Channel: Role of Loop Current evolution and flow compensation around Cuba, *J. Geophys. Res.*, 114, C08003, doi:10.1029/2008JC005199.

[56] Lin, Y., R. Greatbatch, and J. Sheng (2010a), The influence of Gulf of Mexico Loop Current intrusion on the transport of the Florida Current. *Ocean Dyn.*, in press.

[57] Lin, Y., J. Sheng, and R. Greatbatch (2010b), A numerical study of circulation and associated variability in the Intra-Americas Sea, *Proceedings of the Eleventh International on Estuarine and Coastal Modelling*, Seattle, WA, November 5-7, 2009. Editor: M. L. Spaulding, published by American Society of Civil Engineers, Reston, VA, in press.

[58] Marchesiello, P., J. C. McWilliams, and A. Shchepetkin (2001), Open boundary conditions for long-term integration of regional oceanic models, *Ocean Modell.*, 3, 1–20, doi:10.1016/S1463-5003(00)00013-5.

[59] Maul, G. A., and F. M. Vukovich (1993), The relationship between variations in the Gulf of Mexico Loop Current and Straits of Florida volume transport, *J. Phys. Oceanogr.*, 23, 785–796.

[60] Maul, G. A., D. A. Mayer, and S. R. Baig (1985), Comparisons between a continuous 3-year current-meter observation at the sill of the Yucatan Strait, satellite measurements of gulf Loop Current area, and regional sea level, *J. Geophys. Res.*, 90, 9089 – 9096, doi:10.1029/ JC090iC05p09089.

[61] Merrifield, M. A., and R. T. Guza (1990), Detecting propagating signals with complex empirical orthogonal functions: A cautionary note, *J. Phys. Oceanogr.*, 20, 1628–1633.

[62] Molinari, R. L. (1980), Current variability and its relation to sea-surface topography in the Caribbean Sea and the Gulf of Mexico, *Mar. Geodesy*, 3, 409-436.

[63] Molinari, R. L., M. Spillane, I. Brooks, D. Atwood, and C. Duckett (1981), Surface currents in the Caribbean Sea as deduced from Lagrangian observations, *J. Geophys. Res.*, 86 (C7), 6537–6542.

[64] Mooers, C., and G.A. Maul (1998), Intra-Americas Sea Coastal Ocean Circulation, In: *Global Coastal Ocean*, A.R. Robinson and K.H. Brink, Eds., *The Sea*, V. 11, John Wiley & Sons, NY, 183-208.

[65] Morrison, J. M., and W. D. Nowlin, Jr. (1982), General distribution of water masses within the eastern Caribbean Sea during the winter of 1972 and fall of 1973, *J. Geophys. Res.*, 87, 4207-4229.

[66] Murphy, S. J., H. E. Hurlburt, and J. J. O'Brien (1999), The connectivity of eddy variability in the Caribbean Sea, the Gulf of Mexico, and the Atlantic Ocean, *J. Geophys. Res.*, 104, 1431–1454, doi:10.1029/ 1998JC900010.

[67] Niiler, P. P., and W. S. Richardson (1973), Seasonal variability of the Florida Current, *J. Mar. Res.*, 31, 144-166.

[68] Nof, D. (2005), The momentum imbalance paradox revisited, *J. Phys. Oceanogr.*, 35, 1928–1939, doi:10.1175/JPO2772.1.

[69] Nof, D., and T. Pichevin (2001), The ballooning of outflows*, J. Phys. Oceanogr*., 31, 3045– 3058.

[70] Ochoa, J., J. Sheinbaum, A. Badan, J. Candela, and D. Wilson (2001), Geostrophy via potential vorticity inversion in the Yucatan Channel, *J. Mar. Res.*, 59, 725 –747, doi:10.1357/002224001762674917.

[71] Oey, L-Y. (1996), Simulation of mesoscale variability in the Gulf of Mexico, *J. Phys. Oceanogr.*, 26, 145-175.

[72] Oey, L.-Y. (2004), Vorticity flux in the Yucatan Channel and Loop Current eddy shedding in the Gulf of Mexico, *J. Geophys. Res.*, 109, C10004, doi: 10.1029/2004JC002400.

[73] Oey, L.-Y., H. Lee, and W. J. Schmitz Jr. (2003), Effects of winds and Caribbean eddies on the frequency of Loop Current eddy shedding: A numerical model study, *J. Geophys. Res.*, 108(C10), 3324, doi: 10.1029/2002JC001698.

[74] Oey, L.-Y., T. Ezer, and H.-C. Lee (2005), Loop Current, rings and related circulation in the Gulf of Mexico: A review of numerical models and future challenges, in *Circulation in the Gulf of Mexico: Observations and Models*, *Geophys. Monograph Ser.*, 161, W. Sturges and A. Lugo-Fernandez, Eds., 360 pp., AGU, Washington, D. C.

[75] Orlanski, I. (1976), A simple boundary condition for unbounded hyperbolic flows, *J. Comput. Phys.*, 21, 251–269, doi:10.1016/0021-9991(76) 90023-1.

[76] Pichevin, T., and D. Nof (1997), The momentum imbalance paradox, *Tellus, Ser.* A, 49, 298–319, doi:10.1034/j.1600-0870.1997.t01-100009.x.

[77] Redler, R., C. W. Boning, J. Dengg, C. Dieterich, C. Eden, U. Ernst, and J. Kroger (1999), FLAME - A Model Hierarchy for the Atlantic Ocean, European Geophysical Society, XXIV General Assembly.

[78] Richardson, P. (2005), Caribbean Current and eddies as observed by surface drifters, *Deep Sea Res.* II 52, 429–463.

[79] Rivas, D., A. Badan, and J. Ochoa (2005), The ventilation of the deep Gulf of Mexico, *J. Phys. Oceanogr.*, 35, 763–1781.

[80] Schmitz, W. J., and P. L. Richardson (1991), On the sources of the Florida Current, *Deep Sea Res.*, Part A, 32, S379 –S409.

[81] Schmitz, W. J., J. D. Thompson, and J. R. Luyten (1992), Sverdrup circulation for the Atlantic along 24˚N, *J. Geophys. Res.*, 97, 7251–7256, doi:10.1029/92JC00417.

[82] Schott, F., and R. Zantopp (1985), Florida Current: Seasonal and interannual variability, *Science,* 227, 308–311, doi:10.1126/science.227. 4684.308.

[83] Schott, F., T. N. Lee, and R. Zantopp (1988), Variability of structure and transport of the Florida Current in the period range of days to seasonal, *J. Phys. Oceanogr.*, 18, 1209-1230.

[84] Sheinbaum, J., J. Candela, A. Badan, and J. Ochoa (2002), Flow structure and transport in the Yucatan Channel, *Geophys. Res. Lett.*, 29(3), 1040, doi: 10.1029/2001GL013990.

[85] Sheng, J., and L. Tang (2003), A numerical study of circulation in the western Caribbean Sea, *J. Phys. Oceanogr.*, 33, 2049–2069.

[86] Sheng, J., and L. Tang (2004), A two-way nested-grid ocean-circulation model for the Meso-American Barrier Reef system, *Ocean Dyn.*, 54, 232–242, doi:10.1007/s10236-003-0074-3.

[87] Sheng, J., D. G. Wright, R. J. Greatbatch, and D. E. Dietrich (1998), CANDIE: A new version of the DieCAST ocean circulation model, *J. Atmos. Oceanic Technol.,* 15, 1414–1432.

[88] Sheng, J., R. J. Greatbatch, and D. G. Wright (2001), Improving the utility of ocean circulation models through adjustment of the momentum balance, *J. Geophys. Res.*, 106, 16,711 – 16,728, doi:10.1029/ 2000JC000680.

[89] Smagorinsky, J. (1963), General circulation experiments with the primitive equations. I. The basic experiment, *Mon. Weather Rev.*, 91, 99–164.

[90] Smith, R. D., M. E. Maltrud, F. O. Bryan, and M. W. Hecht (2000), Numerical simulation of the North Atlantic Ocean at 1/10°, *J. Phys. Oceanogr.*, 30, 1532–1561.

[91] Sturges, W. (1992), The spectrum of Loop Current variability from gappy data, *J. Phys. Oceanogr.*, 22, 1245-1256.

[92] Sturges, W., and R. Leben (2000), Frequency of ring separations from the Loop Current in the Gulf of Mexico: A revised estimate, *J. Phys. Oceanogr.*, 30, 1814-1819.

[93] Tang, L., J. Sheng, B. G. Hatcher, and P. F. Sale (2006), Numerical study of circulation, dispersion, and hydrodynamic connectivity of surface waters on the Belize shelf, *J. Geophys. Res.*, 111, C01003, doi: 10.1029/2005JC002930.

[94] Thuburn, J. (1996), Multidimensional flux-limited advection schemes, *J. Comput. Phys.*, 123, 74 –83, doi:10.1006/jcph.1996.0006.

[95] Treguier, A. M., S. Theetten, E. P. Chassignet, T. Penduff, R. Smith, L. Talley, J. O. Beismann, and C. W. Boning, (2005), The North Atlantic subpolar gyre in four high-resolution models, *J. Phys. Oceanogr.*, 35, 757–774.

[96] Vukovich, F. M. (1995), An updated evaluation of the Loop Current's eddy-shedding frequency, *J. Geophys. Res.*, 100, 8655–8659, doi:10.1029/ 95JC00141.

[97] Vukovich, F. M., and G. A. Maul (1985), Cyclonic eddies in the eastern Gulf of Mexico, *J. Phys. Oceanogr.*, 15, 105–117.

[98] Wang, C., and D. B. Enfield (2001), the tropical western Hemisphere warm pool, Geophys. Res. Lett., 28, 1635–1638.

[99] Wiseman, Jr. W. J., and S. P. Dinnel (1988), Shelf currents near the mouth of the Mississippi River, *J. Phys. Oceanogr.*, 18, 1287–1291.

[100] Zhai, L., and J. Sheng (2008), Improve the utility of a coastal circulation model by assimilating hydrographic observations into the model momentum equation, *Geophys. Res. Lett.*, 35, L24603, doi:10.1029/2008GL035640.